CONCEPTUAL DESIGN TOOL TO ANALYZE ELECTROCHEMICALLY-POWERED MICRO AIR VEHICLES

THESIS

Douglas J. Pederson, 2d Lt, USAF

AFIT/GAE/ENY/11-M25

DEPARTMENT OF THE AIR FORCE
AIR UNIVERSITY

AIR FORCE INSTITUTE OF TECHNOLOGY

Wright-Patterson Air Force Base, Ohio

AFIT/GAE/ENY/11-M25

CONCEPTUAL DESIGN TOOL TO ANALYZE ELECTROCHEMICALLY-POWERED MICRO AIR VEHICLES

THESIS

Presented to the Faculty

Department of Aeronautics and Astronautics

Graduate School of Engineering and Management

Air Force Institute of Technology

Air University

Air Education and Training Command

In Partial Fulfillment of the Requirements for the

Degree of Master of Science in Aeronautical Engineering

Douglas J. Pederson

2d Lt, USAF

March 2011

AFIT/GAE/ENY/11-M25

CONCEPTUAL DESIGN TOOL TO ANALYZE ELECTROCHEMICALLY-POWERED MICRO AIR VEHICLES

Douglas J. Pederson

2d Lt, USAF

Approved:

_____	_____
Frederick G. Harmon, Lt Col, USAF (Chairman)	Date
_____	_____
Christopher D. Shearer, Lt Col, USAF (Member)	Date
_____	_____
Dr. Mark F. Reeder (Member)	Date

Abstract

A multi-fidelity conceptual design tool was developed to assess electrochemically-powered micro air vehicles (MAVs). The tool utilizes four areas of contributing analyses (CAs): aerodynamics, propulsion, power management, and power sources to determine the endurance duration of a given mission. The low-fidelity aerodynamic CA consisted of drag polar calculations and the high-level CA used a vortex theory code called Athena Vortex Lattice (AVL). The propulsion CA employed QPROP and a MATLAB code that used experimental propeller data and motor constants to predict propeller-motor combination performance for the low- and high-fidelity tracks, respectively. The power management CA determined the percentage of required power the power sources needed to provide by a user-defined split or an optimization to maximize endurance duration for the two fidelity options. The power source CA used specific energy and specific power calculations for the low-fidelity track and polarization curves and Ragone plots for the high-fidelity track. Model Center software allowed for integration of each of these CAs into one model. Based on the current state of the art battery and fuel cell technology, the model predicted endurance durations ranging from 88.5 to 107.3 min. The mission simulations that led to these durations used a generic MAV (GenMAV) configuration and the complete spectrum of fidelity combinations.

Acknowledgments

First and foremost, I would like to thank my family and friends for their love and support that made each day a joy. Specifically, I would like to thank my amazing girlfriend and my loving parents and sister. For the initial idea of the work and constant help along the way, I would like to thank Lt. Col. Frederick Harmon. For his work before me and his help in getting my work started, I would like to thank Capt. Paul Hrad. For his support as a sponsor and help in electrochemical analysis, I would like to thank Dr. Ryan Miller. For his genius and generous support on Model Center, I would like to thank J Simmons. I would like to thank my fellow students for their academic help but more importantly, for the good times had outside of class to renew and refresh the soul. Finally, I would like to thank God for such a wonderful opportunity to study at AFIT surrounded by the people mentioned above.

Douglas J. Pederson

Table of Contents

Page

List of Figures

Page

List of Tables

Page

Nomenclature

AC	Alternating Current
AFC	Alkaline Fuel Cell
AFIT	Air Force Institute of Technology
AFRL	Air Force Research Laboratory
AV	AeroVironment
AVL	Athena Vortex Lattice
BDC	Brushed Direct Current Motor
BLDC	Brushless Direct Current Motor
BOP	Balance of Plant
CA	Contributing Analysis
CAD	Computer Aided Design
CONOPS	Concept of Operations
CFD	Computational Fluid Dynamics
CG	Center of Gravity
DARPA	Defense Advanced Research Projects Agency
DC	Direct Current
DFAFC	Direct Formic Acid Fuel Cell
DMFC	Direct Methanol Fuel Cell
DNS	Direct Numerical Solver
DoD	Department of Defense
DOE	Design of Experiments
DSM	Design Structure Matrix
DYMORE	A Structural Analysis Code
EDLC	Electric Double-Layer Capacitor
EPMAV	Electrochemically Powered Micro Air Vehicle
ESC	Electric Speed Controller
ESD	Energy Storage Device
FOM	Figures of Merit
GenMAV	Generic Micro Air Vehicle

GT	Georgia Institute of Technology
HHV	Higher Heating Value
ICE	Internal Combustion Engine
ISR	Intelligence, Surveillance, and Reconnaissance
LAR	Low Aspect Ratio
L/D	Lift to Drag Ratio
LiPo	Lithium-ion Polymer Battery
LLT	Lifting Line Theory
MATLAB	A Numerical Computing Environment
MAV	Micro Air Vehicle
MC	Model Center
MCFC	Molten Carbonate Fuel Cells
MDO	Multi-disciplinary Design Optimization
MIT	Massachusetts Institute of Technology
NACA	National Advisory Committee for Aeronautics
NAV	Nano Air Vehicle
NRL	Naval Research Laboratory
OEF	Operation Enduring Freedom
OIF	Operation Iraqi Freedom
PABLO	Potential flow around Airfoils with Boundary Layer
PAFC	Phosphoric Acid Fuel Cell
PEMFC	Proton Exchange Membrane or Polymer Electrolyte Membrane
QPROP	A Motor and Propeller Matching Program
RC	Radio Controlled
ROC	Rate of Climb
RPA	Remotely Piloted Aircraft
RWAV	Munitions Directorate of AFRL, Assessments and Demonstration Division
RZPS	Electrochemical Branch of AFRL
SOC	State Of Charge
SOFC	Solid Oxide Fuel Cell

UAV	Unmanned Air Vehicle
UIUC	University of Illinois at Urbana-Champaign
USAF	United States Air Force
VBScript	Visual Basic Scripting Edition
VORLAX	A Vortex Lattice Program
VLM	Vortex Lattice Method
VSP	Vehicle Sketch Pad
WSU	Wichita State University
XFOIL	An Airfoil Flow Code
XWING	A Wing Flow Code

List of Symbols

J	advance ratio
ω	angular velocity
AR	aspect ratio
F	balance of plant and fuel tank weight factor
β	blade angle
$\overline{X}_{cg}$	center of gravity, normalized by chord length
α	charge transfer coefficient
Γ	circulation
θ	climb angle
C_D	coefficient of drag
$C_{D,0}$	coefficient of drag, zero lift
C_L	coefficient of lift
C_P	coefficient of power
c_p	coefficient of pressure, compressible
$c_{p,0}$	coefficient of pressure, incompressible
C_T	coefficient of thrust
C_Q	coefficient of torque
C_Y	coefficient of side force
σ	conductivity
K	constant, drag polar
F	constant, Faraday
K_V	constant, motor
i	current density
i_o	exchange current density
i_L	limiting current density
I	current
I_0	current, no load
ρ	density, air
D	diameter or drag
Δ	difference
q	dynamic pressure
η	efficiency
$\Delta\overline{g}_f$	Gibbs free energy

L	lift
c_L	local lift coefficient
M	Mach number
m	mass
$\overline{X}_{np}$	neutral point, normalized by chord length
N	number of cells in the stack
$\%P_{fc,end}$	percent of endurance power taken by the fuel cell
P	power
r	radius
r_1	radius of curvature relative to vertical plane, local
r_2	radius of curvature relative to horizontal plane, local
ROC	rate of climb
R	resistance, or universal gas constant
E	reversible electromotive force, energy, theoretical voltage
RPM	revolutions per minute
Re	Reynolds number
φ	roll angle
n	rotational speed in revolutions per second, or number of moles
ϖ	rotational speed, QPROP
e	span efficiency factor
SE	specific energy
SP	specific power
T	thrust, or temperature
ε	thrust angle relative to flight path
t	time
Q	torque
$C_{D,i}$	Trefftz plane drag coefficient
U	velocity
V	voltage
$W\text{-}hr/kg$	watt-hours per kilogram
W/kg	watts per kilogram
W	weight
c	wing chord, local
W/S	wing loading
S	wing planform area

b	wing span

CONCEPTUAL DESIGN TOOL FOR FUEL-CELL POWERED MICRO AIR VEHICLES

I. Introduction

I.1. Motivation and Background

The United States' military currently finds itself heavily involved in numerous operations around the globe. Most recently, Operation Enduring Freedom (OEF) and Operation Iraqi Freedom (OIF) demanded a great deal of troops and resources, but other involvements including relief efforts and counterdrug operations further stretch the burden placed on today's military. The United States (U.S.) military has helped meet this increased tasking with unmanned systems both on the ground and in the air. P.W. Singer's "Wired for War" articulates this exponential increase in unmanned systems and argues that it is critical to the future of military operations.[1] Looking at unmanned systems in the air, a wide variety of remotely-piloted aircraft (RPA) can greatly advance the capabilities of the military by providing unmatched Intelligence, Reconnaissance, and Surveillance (ISR). By providing ISR as well as other Air and Space Functions outlined in the Air Force Doctrine Document, RPA can be seen as essential to the Air Force's mission success.[2] RPA innovation is therefore crucial to furthering the strength of the U.S. Air Force and ultimately the entire military. In addition to military applications, RPA can provide numerous solutions to civilian organizations.

The civilian use of RPA provides an increased demand for innovation both during conflicts and peacetime. Similar to military applications, ISR is the main task that RPA perform in civilian sectors. In addition, RPA uses include scientific observation

missions, weather data, relaying communications, placing sensors, securing borders, crop dusting, and aerial photography.[3, 4, 5] Altogether, the RPA market is a multi-billion dollar industry with defense spending leading the way. In 2010 alone, Department of Defense (DoD) spending on RPA was estimated to be $5.4 billion and in 2011, defense officials plan to double the production of RPA.[6, 7] In the next five years, the entire RPA market is predicted to generate revenues of over $60 billion, making it a lucrative area of research and development around the globe.[7] With motivation coming from both national security and financial backgrounds, innovation leading to increased RPA capabilities is necessary. Different advances could increase RPA utility, but reduced size and increased endurance are arguably two of the most important aspects to address. The idea of an electrochemically-powered Micro Air Vehicle (MAV) addresses both of these concerns.

I.1.1. Electrochemically-Powered Micro Air Vehicles

The concept of an electrochemically-powered RPA replaces the traditional internal combustion engine with some type of electrochemical energy storage device (ESD), namely a fuel cell, battery, or fuel cell-battery hybrid system. The exact size and weight of a MAV varies by source. Smaller estimates suggest a MAV measures less than 20 cm (8 in) in any one direction and weighs under 0.5 kg (1.1 lbs).[8, 9] AFRL's generic MAV (GenMAV) falls on the larger end of MAV sizes with a wingspan of roughly 60 cm (24 in) and a mass of 1kg (2.2 lbs). By either definition, the small size of MAVs allows them to be carried by soldiers on the battlefield and launched by hand.[4] These capabilities are crucial to protecting the lives of soldiers on the ground. Furthermore, it makes them harder to be detected by opposing forces. Since the utility of MAVs depends on the quality of its payload (sensors and cameras), the concept of a MAV first became

feasible when the required equipment carried by a MAV reached a mass of less than 18 g (0.04 lbs) in the mid-1990s.[10]

The idea of fuel cells in RPA is not a new one. Inherent benefits of a fuel cell include low acoustic and heat signatures, less environmental impact, and the potential for increased endurance.[11] Since the beginning of OIF and OEF, numerous fuel cell-powered RPA have had success with a polymer electrolyte membrane fuel cell (PEMFC), but also a solid oxide fuel cell (SOFC). As technology continues to grow, their application in MAVs is becoming more apparent due to a reduction in fuel cell size and mass. Of all fuel cell types, the PEMFC is the most attractive, as shown in Table 1.[12]

Table 1. Chronological list of fuel cell-powered RPA

Name	Date	Fuel Cell Type	Wing Span/Mass	Endurance Duration
Hornet[13] (AeroVironment)	2003	PEMFC	38 cm (15 in)	0.2 hr
Global Observer[14] (AeroVironment)	2005	PEMFC	15 m (50 ft)	24 hr
Hy-Fly[12] (FH Wiesbaden)	2005	PEMFC	Unknown	90 s
Spider-Lion[15] (NRL)	2005	PEMFC	2.5 kg (5.5 lbs)	3.33 hr
Adaptive[16] Materials Inc.	2006	SOFC	1.9 kg (4.3 lbs)	4.33 hr
Pterosoar[17] (CSULA)	2006	PEMFC	5.5 m (18 ft)	0.75 hr
Georgia Inst. of Technology[18]	2006	PEMFC	6.7 m (22 ft)	0.75 hr
HyFish[19] (DRL)	2007	PEMFC	1 m (3.3 ft)	0.25 hr
CSULA/OSU[17]	2007	PEMFC	4.4 m (14.4 ft) / 5 kg (11.0 lbs)	12 hr
KAIST[20]	2007	PEMFC	1.2 m (3.9 ft) / 2 kg (4.4 lbs)	10 hr
Fuel Cell Puma[21] (AeroVironment)	2007	PEMFC	6.35 kg (14 lbs)	9 hr
Ion-Tiger[22] (NRL)	2009	PEMFC	16.8 (37 lbs)	23.3 hr

Powered by hydrogen, a PEMFC has high specific energy, but low specific power. For this reason, a hybrid fuel cell-battery system can be used to increase the specific power of the overall MAV. A fuel cell also operates most efficiently under constant power demands and a hybrid system allows the battery to take the fluctuations in power demands. A hybrid system has the advantage over an all battery configuration because of its added endurance potential and the ability to use fuel cartridges instead of waiting hours for a battery to recharge.[4] Similar to the payload of a MAV, the fuel cell and its subsystems need to be of a reasonable mass. While fuel cells have had success operating in reduced sizes, further advancements in technology will continue to solidify the fuel cell as the best option for long endurance applications with a low power demand.[23]

Recognizing the potential and importance of MAV technology, the Air Force's Research Laboratory (AFRL) has established a group to direct and define the goals of development for MAVs in terms of their propulsion, power, payload, CONOPS, and integration.[24] The number of tasks that fall under this group are immense and decision making tools are imperative to aid leaders in selecting what tasks to put time and money into. Focusing on a MAVs power, conceptual design tools can be created to assist decision makers involved in the future of MAV technology.

I.1.2. A Conceptual Design Tool

A conceptual design tool that examines the endurance duration of a MAV would be helpful to leaders making decisions about MAV spending and research. An area of particular interest within the realm of MAV design is the development of an electrochemically-powered MAV (EPMAV) due to its ability to take advantage of new,

reusable technologies and the capabilities electrochemical devices provide for small-scale applications. Full-blown conceptual design would determine MAV aspects including the shape of the wings (swept, straight, etc.) and the tail (T-tail, V-tail, etc.), their location on the fuselage, and propulsion requirements. Conceptual design can also focus on one of the many parts of the overall design.[25] In some cases, cost and time are major reasons for choosing to concentrate on limited aspects of an aircraft's design in a conceptual design model. Additionally, the overall goals of the model affect the level of fidelity that should be utilized to solve the problem for which it was designed. For example, the fuel cell is the most important aspect of an EPMAV and should therefore be a large part of the design.[26] A conceptual design tool that examines the use of a fuel cell-battery hybrid system in existing MAV platforms will provide initial insight into their feasibility and allow for validation without the costs of development. By performing mission simulations with an existing configuration, the scope of the results can be narrowed and flight-tests can be conducted quicker than waiting for the creation of a new MAV configuration.

I.2. Problem Statement and Research Objectives

Currently, organizations such as the propulsion directorate at the AFRL (AFRL/RZ) have no decision making tool as to where to invest time and dollars in MAV design. Specifically, the thermal and electrochemical branch (AFRL/RZPS) has interest in learning EPMAVs are capable of in terms of endurance. The objectives of this research are therefore as follows:

- Create a conceptual design tool that calculates an EPMAV's endurance duration with emphasis on the power source analysis
- Validate and verify the different components of the conceptual design tool
- Use the model to conduct mission simulations on a MAV configuration

With this tool, the decision making process becomes easier when comparing different MAVs and their ESDs. While the focus of this research is on the power source of ESD portion of the model, system-level analysis in the areas of aerodynamics, propulsion, and power management will make it a more involved tool than just comparing ESD statistics.

I.3. Scope and Assumptions

The model is not designed to take into account certain disciplines of aircraft design including structural integrity, aeroelasticity, material selection, spatial requirements, or navigational control. Each of these disciplines could be added to the model, but the sponsor's immediate need called for endurance optimization on existing airframes. A MAVs mode of flight could be either fixed wing (e.g. a Boeing 747), rotary wing (e.g. a UH-60 Black Hawk), or a flapping wing (e.g. an ornithopter). Each of these configurations has distinct advantages and disadvantages, given the requirements of the mission. A study by Sibilski et. al. examined the energy and power requirements of these different configurations and it showed that the fixed wing aircraft was the most efficient form of flight when no hovering was required.[30] Therefore, this model looks at fixed wing geometries and could be modified if a flapping wing configuration was desired due to the recent interest in this configuration.[28, 29, 30] Furthermore, only existing configurations are examined upon the request of the sponsor. The ESD performance in

terms of specific energy and specific power values are assumed to scale with the size of the device. Additionally, the analysis looks at specific energy and specific power on a mass basis. A mass basis is used over a volume basis due to the request of the sponsor and because it was assumed mass constraints were greater than volume constraints for MAV design. While capacitors and ultracapacitors are also ESDs, this research focuses on the use of fuel cells and batteries due to the extremely short discharge duration of capacitors. The approach taken for the high-fidelity power source CA is a novel strategy to account for the efficiencies of fuel cells and batteries. It is assumed that the methodology for this option provided an acceptable projection for ESD efficiency and ultimately the MAV's endurance time. The final assumption is that the variable fidelity built into the model will provide an increasingly accurate projection for the actual endurance duration of a MAV.

I.4. Hypothesis

Given mission requirements, MAV geometry, a motor-propeller combination, and ESD data, a variable-fidelity conceptual design tool can be created for fixed-wing EPMAVs to determine their optimum duration. This tool is referred to as a model with a rubber endurance segment or simply, "model." Here, a rubber endurance segment implies an endurance segment within a mission that does not have a fixed duration. The design for such a model can be broken down into four areas of focus or contributing analyses (CAs) to include aerodynamics, propulsion, power management, and power sources. The CAs can then be put into a data flow automation program such as Model Center (MC) to manipulate the data for optimized results. MC can also assist in the

process of validating the model and run mission simulations to learn more about the capabilities of MAVs and how to improve their design.

I.5. Methodology

The work on a tool of this nature at the Air Force Institute of Technology (AFIT) began with the work of Mustafa Turan when he established a model for MAV design by utilizing a statistical database of MAV designs in look-up tables.[27] Turan's work focused on the aerodynamics of a MAV and laid the groundwork for MAV design. Paul Hrad followed this work and directed the model towards an optimal power system using lump calculations for the ESDs (specific energy and specific power).[24] The product of Hrad's research gave the user the required masses of ESDs to complete a given mission. Both efforts set the stage for a variable fidelity model to meet the sponsor's need and justify future flight-testing. The goals and expansions from the previous research efforts are as follows:

- Create a conceptual design tool to determine an EPMAV's endurance duration
- Utilize Model Center's new process modeling features to take advantage of more powerful and current data flow automation
- Expand the fidelity of each part of the model to create a model with variable fidelity for both low- and high-level analysis
- Focus on the power source portion of the model's analysis while still examining the areas of aerodynamics, propulsion, and power management
- Account for the mass change from the fuel burnt during the fuel cell's operation

- Determine the ideal hybridization for an endurance-based EPMAV
- Determine the ideal operating points on a polarization curve and a Ragone plot to optimize endurance
- Determine the current and near-term feasibility of an EPMAV

The creation of the model began by creating a flow chart of data from user inputs to the calculation of endurance duration. This flow chart included the levels of fidelity planned for each area of CA. Each CA was either created or identified from existing resources. Each level of fidelity within a CA was designed to operate independently if the proper inputs were provided. Once completed, the CAs were integrated into the MC environment. This integration called for additional coding and extensive variable linkage to ensure that the data flow through each component occurred as planned. Once programmed into MC, optimization routines could be set in place to ensure the best result for endurance duration. The completed model then required a validation platform and mission profile to get results from a variety of mission simulations. The result of the simulations could then be used to make decisions that surround the use and development of EPMAVs. The platform chosen was AFRL's GenMAV or generic MAV from Eglin Air Force Base's munitions directorate (AFRL/RWAV). This platform provided results that MC could run trade studies on for validation and verification. Comparisons to available literature and similar conceptual design tool efforts were also made to validate the model's accuracy.

I.6. Outline of Chapters

Chapter 1 discussed the background and motivation behind this research. The scope of the work conducted as well as the assumptions moving forward were established. Next, the hypothesis was defined before presenting a brief outline of the methods used to complete the research. Chapter 2 next reviews the existing literature that relates to this research. A conceptual design tool utilizes many different disciplines, and therefore only a brief overview is presented on some of the topics related to its creation. The literature review does take an in-depth look into state of the art MAV and ESD technology as well as the key software utilized for the model's design. Chapter 3 focuses on an examination of the steps taken to create the model. It first looks at each area of CA and then covers how they were integrated into the MC environment. This chapter also introduces the validation platform used for the mission simulations discussed in Chapter 4. Chapter 4 presents the results and analysis of the research as well as model validation. Validation for the model comes from areas including MC trade studies, published references, and previous efforts on the same topic. Finally, Chapter 5 discusses the conclusions gathered by the research effort. Both the successes and limitations of the model are presented, and recommendations for future examinations are suggested.

II. Literature Review

Being a conceptual design effort, the model involved ideas from a number of different topics, especially those related to each area of CA. The bulk of this review seeks to provide a basic understanding of each of these areas. The review also presents the state of the art information on MAVs and ESDs as well as a summary of similar conceptual design efforts to date. The chapter ends by discussing the software that will integrate the four CAs.

II.1. State of the Art

The creation and improvement of an electrochemically-powered MAV required the combination of the most advanced MAV and ESD technology. Knowing the capabilities and limitations of each affected the approach chosen to reach the best solution.

II.1.1. MAVs

The past 15 years has seen the creation of a wide range of RPA and MAVs from various research programs around the world. The Unmanned Vehicle Systems Website and Yearbook in their 2009-2010 data stated that 1,190 RPA were developed in 51 countries, with approximately 11% of them around the MAV size.[31] This number increased 22% from the previous year and did not include projects purposely kept secret around the globe. Some of these attempts are very well documented, while others are less known. The most readily available information is found from projects funded by the Defense Advanced Research Projects Agency (DARPA).[3] Two of the best MAV

examples of DARPA funded research are AeroVironment's (AV) Black Widow and Wasp III (Figure 1).

Figure 1. The Black Widow (left) and Wasp III (right)

The Black Widow is an important MAV and arguably helped spur widespread MAV research.[32, 33] Capable of 30-minute flight durations at velocities up to 13.4 m/s (30 mph), this fixed wing aircraft has a 15.25 cm (6 in) wingspan with a mass less than 0.1 kg (0.22 lbs).[34, 3] The development of the Black Widow relied heavily on the multi-disciplinary design optimization (MDO) that consisted of five different components that roughly parallel the CAs: vehicle and propeller aerodynamics, battery and motor performance, and a weight buildup.[34] Another result of the partnership between DARPA and AV was the Wasp III. The Wasp III (Figure 1) is currently the smallest aircraft in the United States Air Force's (USAF) arsenal with a wingspan of 72.4 cm (28.5 in), a length of 25.4 cm (10 in), and a total mass of 0.453 kg (1 lb).[35] Used for night and day surveillance and reconnaissance, it is capable of reaching velocities of 17.9 m/s (40 mph) and an endurance of 45 min through rechargeable lithium ion batteries.

One final example of MAV technology is the GenMAV. The GenMAV (Figure 2), is the baseline configuration for AFRL and AFRL sponsored research.[36] The GenMAV has a wingspan of 60.0 cm (24 in) and a length of 43.2 cm (17 in) and is

designed for a velocity of 13.4 m/s (30 mph).[36] The GenMAV falls into state of the art because it is well positioned for near-term research and unlike other MAV examples, data for validation purposes is readily available.

Figure 2. GenMAV configuration

II.1.2. Electrochemical Storage Devices

ESDs are simply devices that take advantage of electrochemical energy or the conversion of chemicals directly to electricity. Systems that utilize electrochemical energy include fuel cells, batteries (both primary and secondary), and capacitors. One way to view advancement in electrochemical devices is by the energy and power that they provide in terms of specific energy (W-hr/kg) and specific power (W/kg). In the literature, these values are also referred to as energy density and power density, but these terms create ambiguity in terms of whether mass density or volume density is being referenced.

Beginning with the basics, a Ragone plot displays specific energy vs. specific power and shows where each category of ESD typically operated (Figure 3).[38] This plot quickly communicates that the "holy grail" of electrochemical devices would be one lying in the top-right of the plot with high specific energy. As such, this is the direction advancements in state of the art technology move. The plot also shows typical discharge (device life during use) lines that range from one hour to less than a second. Unlike

capacitors, fuel cells and batteries have a discharge time on the order of magnitude required for MAV flight.

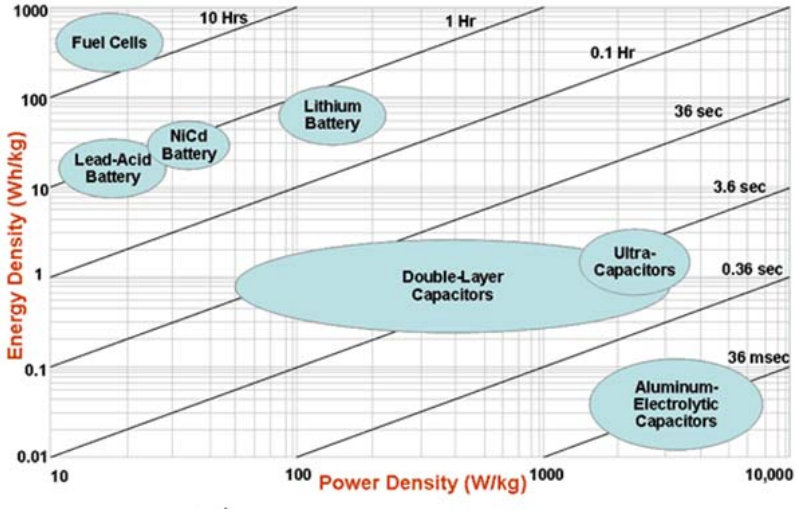

Figure 3. Ragone plot for various electrochemical devices

In general, batteries have high specific power but lower specific energy. Therefore, innovative battery technology seeks to maximize specific energy while still providing adequate specific power. Three of the leading battery chemistries include the lithium thionyl chloride battery ($Li/SOCl_2$), the zinc-air battery, and the lithium-ion polymer battery. Compared to other lithium anode batteries, a lithium thionyl chloride system has the highest energy density.[39] With a theoretical specific energy of 1,450 W-hr/kg, current practical specific energy ranges from 100 to 520 W-hr/kg, with the majority of values falling around 420 W-hr/kg.[40, 41] In addition, Li-$SOCl_2$ cells produce 3.6 V per cell. The zinc-air battery is a unique cell that only contains the zinc powder anode. The theoretical and practical specific energy of a zinc-air cell is similar to that of the lithium-thionyl chloride cell with a theoretical specific energy of 1,350 W-hr/kg.[42] The zinc-air cell's practical specific energy falls between 100 and 470 W-hr/kg, most

commonly around 450 W-hr/kg.[42, 43, 44, 45] The cell voltage for a zinc-air battery is only 1.65 V. Lithium-ion polymer batteries (LiPo) are rechargeable batteries with a practical specific energy between 95-190 W-hr/kg and a nominal voltage of approximately 4 V.[39, 46] LiPo batteries have great flexibility in terms of their shape, making them extremely attractive to applications that have constraints in terms of where mass is located such as aircraft. Compared to batteries, fuel cells have high specific energy but lack specific power.

Fuel cells are best viewed as power plants that convert a fuel such as hydrogen into energy, similar to an ICE and gasoline. Two key companies that make top of the line fuel cells for RPA and MAV applications are Protonex and UltraCell. Metrics such as specific energy and specific power can be misleading for fuel cells because these values depend on the fuel used and how that fuel is stored. Specific energy and specific power values still provides a method for fuel cells to be compared and state of the art examples to be identified. The hydrogen powered PEMFC and two subcategories of the PEMFC, the direct methanol fuel cell (DMFC) and the direct formic acid fuel cell (DFAFC), stand out as the most promising fuel cell technologies due to their high specific power.

PEMFCs fueled by hydrogen have the highest specific power of all types of fuel cells and also have an open circuit voltage of 1.23 V.[47] They have robust start-stop capabilities with a short warm up time that is crucial to MAVs carried around by troops used often. PEMFCs operate best at temperatures from room temperature to about 80° C. This temperature range also reduces the amount of subsystems needed for operation.[48] Finally, PEMFCs scale down in size much more efficiently than ICEs and other types of fuel cells.

The DMFC is a subcategory of the PEMFC that runs on methanol (CH_3OH). The DMFC currently has a maximum specific power of 15.1 W/kg and a maximum specific energy of 805.1 W-hr/kg while providing 1.21 V.[49, 50] One key advantage DMFCs have over the hydrogen powered PEMFC revolves around the use of methanol. Methanol is much easier to acquire, transport, and store than hydrogen. DFAFCs are a relatively new fuel cell technology with much of the research related to efforts of Dr. Masel et. al. at the University of Illinois. Overall, they have roughly the same specific energy as DMFCs, but three to six times the specific power.[51] Finally, DFAFCs operate more effectively at room temperature than DMFCs.

A final type of ESD worthy of mention is capacitors. Capacitors are devices that consist of two conductors separated by an insulator (dielectric). They store energy via an electric field in the dielectric when a voltage exists between the conductors. There is no chemical reaction to release energy, but instead a charge rearrangement. Electrochemical capacitors are referred to by several different names including supercapacitors, ultracapacitors, and hybrid capacitors. Supercapacitors and ultracapacitors are terms used to signify a type of capacitor that forms an electric double layer and can be grouped as electric, double-layer capacitors. Unfortunately, capacitors have a very short discharge duration as shown on the Ragone plot in Figure 3. Being that they can only provide power for a matter of seconds, they are not included in the scope of this research.

II.1.3. Electrochemically-Powered MAVs

The combination of current MAV platforms and leading ESD technology presents an opportunity to utilize the best aspects of the state of the art examples presented above. Successful examples of fuel cell powered flight were outlined in Table 1, but several

specific examples stand out due to their proximity to a MAV's size. The first of those followed an approach similar to what this research aims to do by retrofitting AV's Wasp I (a precursor to the Wasp III) into a fuel cell-powered MAV called the Hornet (Figure 4).[52, 13] The Hornet is another DARPA initiative with a goal of exploring innovative propulsion and structural concepts. Slightly heavier than the Wasp, the Hornet weighs 0.38 kg (0.84 lbs) and utilizes a 10 W PEMFC that is integrated into the wing to provide structural support and reduce overall MAV mass.[24] While not improving the endurance duration or adding to operational capabilities the Wasp had with batteries alone, the Hornet did provide proof of concept for MAVs powered from a fuel cell when it became the first of its kind to fly in March 2003.[13]

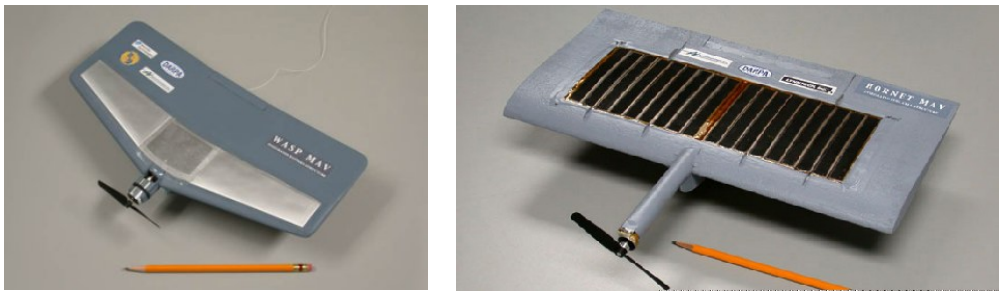

Figure 4. AV's Wasp I (left) and Hornet (right)

Another slightly larger example is the Spider-Lion developed by the Naval Research Laboratory. Using a 100 W PEMFC and having a total mass of 2.5 kg (5.5 lbs), the Spider-Lion demonstrated an endurance duration of 3 hrs and 19 min.[15] A joint AFRL and AV electrochemically-powered RPA is the Fuel Cell Puma. The Fuel Cell Puma weighs 6.35 kg (14 lbs) and therefore falls outside of the MAV size this research focuses on; however, the Fuel Cell Puma is interesting because it employs a hybrid setup with a PEMFC and a lithium-ion battery.[21] Since this is the configuration that this

research investigates, the Fuel Cell Puma's successful demonstration is relevant. The Fuel Cell Puma achieved over a 9-hr endurance flight, which was roughly 3-4 times the endurance achieved by batteries alone.[53] This final example goes beyond proof of concept and shows that fuel cells can improve the capabilities of RPA. As ESD technology continues to improve and scale down in size, MAVs will continue to increase their endurance capabilities.

II.2. Aerodynamics

The wing planform and airfoil section of a MAV are critical to it being a stable and controllable vehicle. MAVs have several attributes that present challenges to aerodynamic analysis. Compared to other aircraft, MAVs fly at low airspeeds, have small dimensions, and therefore fall into low Reynolds number regimes. They also have low aspect ratios, thin airfoils, and limited experimental data and published research. While there are various aerodynamic techniques for the design of aircraft, two main categories of computational tools stand out: viscous and inviscid simulations. Viscous tools include techniques such as the direct numerical simulations (DNS) of Navier-Stokes equations.[54] This approach has a high computational cost that can be prohibitive to an aircraft in the conceptual design stage. Inviscid solvers include methods such as lifting-line theory (LLT), the vortex lattice method (VLM), and the panel method. These approaches are computationally cheaper and even though they do not resolve the effects of the viscous boundary layer, they are prime candidates for simulations where inviscid effects are vital.[54]

II.2.1. Low Reynolds Numbers and Aspect Ratios

Though it has been over 100 years since the Wright Brothers' historic flight, MAV development has followed a similar path in which fundamental aerodynamic relationships have been identified emperically.[55] One of the most important measurements of aerodynamic relationships to study is the Reynolds number. The typical Reynolds number of a MAV is on the order of 10^4 and 10^5, due to reasons mentioned above.[56, 57, 58] According to Mueller, a conventional fixed-wing MAV flies in a Reynolds number regime between $4.5x10^4$ to $1.8x10^5$, which is less than what other RPA and conventional aircraft fly at (Figure 5). [8, 59]

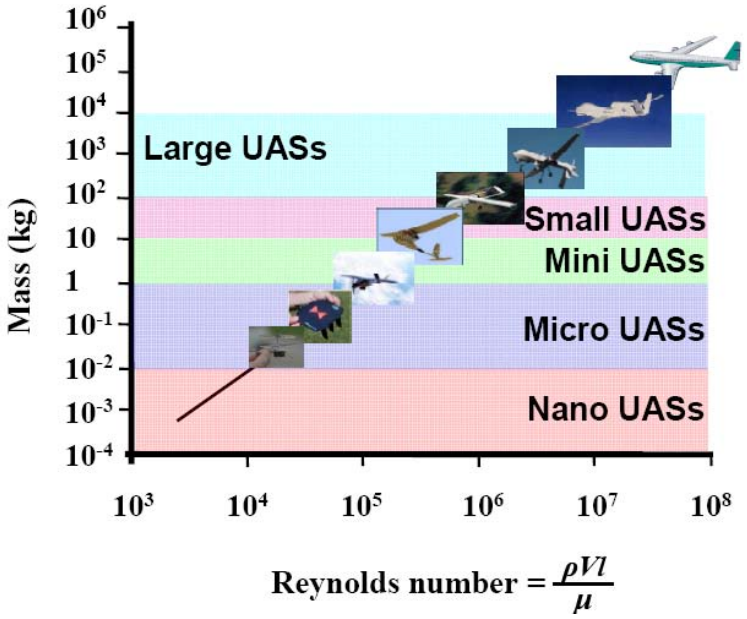

Figure 5. Typical Reynolds number regimes for various aircraft

The implications of low Reynolds number are numerous. Separation issues represent the first and most explored problem of low Reynolds number regimes. Regions near the leading and trailing edge are of concern if transitions from laminar to turbulent flow occur. The Reynolds number regime between 30,000 and 70,000 was found to be of

great interest to MAV designers.[37] Here, thin airfoils exhibited reasonable performance, whereas thicker airfoils have shown laminar separation and transition to turbulent flow. Below Reynolds numbers of 50,000, the free shear layer after laminar separation typically cannot transition to turbulent flow in time to reattach to the airfoil surface. This causes stall if separation reaches the leading edge. To complicate matters, separation is nonlinear and hard to predict.[55]

Another area affected is aerodynamic efficiency, which can be measured by an aircraft's lift-to-drag (L/D) ratio. The L/D ratio is expressed as a non-linear function of Reynolds number. As the Reynolds number is reduced, lift to drag ratios reduce dramatically; however, Reynolds numbers below 10,000 show an increase in lift.[60] Next, profile drag increases as Reynolds number increases as shown in Eq. (1). Finally, camber

$$C^2_{L,\min\ power} = \left(\frac{3 \cdot C_{D_0}}{b}\right)\left(\frac{\mathrm{Re}_{ref}}{\mathrm{Re}}\right)^{0.5} \qquad \textbf{(1)}$$

plays a role in a wing's performance at low Reynolds numbers. Cambered-plate wings with a 4% camber section offer better aerodynamic characteristics (maximum L/D) as compared to flat-plate wings for a given aspect ratio and Reynolds number.[60, 61]

Low aspect ratio (LAR) wings, or wings with an aspect ratio below 2.0, have also received very little attention in aerodynamic research; however, several studies have been performed that discovered notable properties. As LAR wings generate lift, counter-rotating vertical structures form near the wingtips (wingtip vortices) that strengthen as the angle of attack increases.[62] These wingtip vortices can be present over the majority of the wing and as a result, the aerodynamic characteristics are greatly affected. LAR wings with an aspect ratio of less than 1.5 can be described as having both linear and nonlinear

sources of lift.[62] Circulation around the airfoil, as with higher AR wings, causes linear lift. Tip vortices forming low-pressure areas on top of the wing create nonlinear lift. The nonlinear effect increases with angle of attack and leads to a steeper angle of attack at which stall occurs.

II.2.2. XWING

XWING seeks to solve the problems that exist in analyzing the aerodynamics of a MAV by addressing the 2D viscous boundary layer effects and combining it with a 3D potential flow matching technique. XWING performs analysis by first dividing the 3D flow into 2D elements that run parallel to the wing's plane. Next, the tool calculates the incoming flow for each element using a 3D inviscid technique (e.g. VLM) and proceeds to add viscous effects to each element with a 2D boundary layer solver. Displacement thickness is then added to each 2D element and a new 3D wing is constructed. Iterations of this process are performed until a desired level of convergence is achieved. Being computationally cheap and inclusive of MAV intricacies, it is a perfect match for preliminary MAV design.[54] The software, unfortunately, is currently undergoing validation and not available for public use.

II.2.3. Athena Vortex Lattice

The Athena Vortex Lattice (AVL) software presents another solution for dealing with low Reynolds number flow. AVL is a product of Dr. Mark Drela and Dr. Harold Youngren at the Massachusetts Institute of Technology (MIT) and falls into the category of a VLM. The program has yielded accurate and robust results for various applications including the stability of a design for the DARPA MAV competition.[63, 64] The creators of AVL recommend using it for low to moderate angles of attack. AVL transforms thin

lifting surfaces into single-layer vortex sheets and discretizes them into horseshoe vortex filaments.[65] While the fuselage of an aircraft typically is left out of calculations such as these, it can be added in via source-doublet filaments. Using this method, AVL outputs measurements and coefficients associated with lift and drag, stability and control derivatives, and eigenmode analysis. Wind tunnel testing is currently being performed on the GenMAV to provide further validation for AVL.

II.3. Propulsion

One of the most important elements of a aircraft's performance is its propulsion system.[66, 67] The two major subcomponents to an electrically-propelled propulsion system are the electric motor and the propeller. Because the propulsion system (motor, propeller, and the ESD to power it) of MAVs account for 60-70% of their total weight, optimization of these components is critical.[37] This section provides some basic background on these two systems and introduces QPROP, a software program that models their behavior.

II.3.1. Electric Motors

Electric motors use electric energy to produce mechanical energy with magnetic fields and current-carrying conductors. While motors can operate on direct current (DC) or alternating current (AC), only DC motors are examined for this research. The two most common kinds of DC motors are brushed (BDC) and brushless (BLDC) motors (Figure 6).[68]

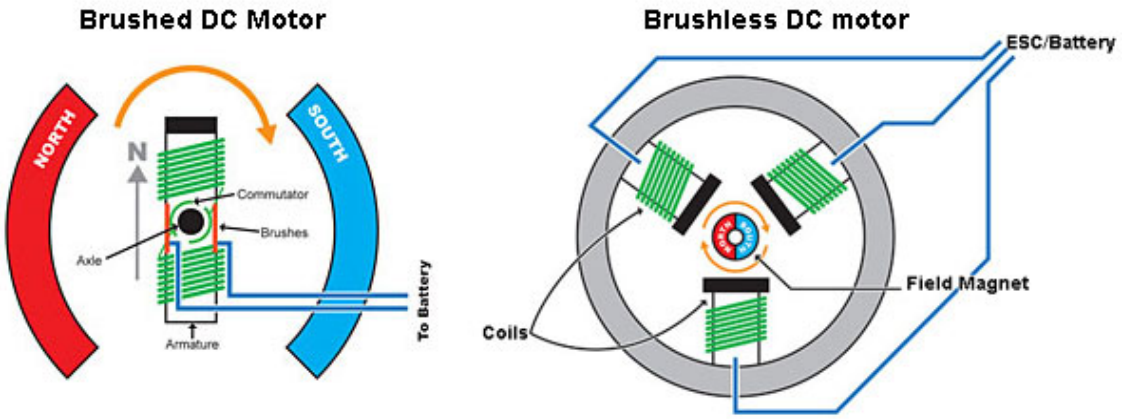

Figure 6. Brushed vs. brushless motors

While brushed motors have been in use much longer than brushless, brushless motors now provide more power at higher efficiencies. Furthermore, the difference in weights between the two types of motors is often negligible even when considering the added weight of the electronic speed controller of the brushless motor.[3] The performance characteristics of motors are often exaggerated by manufactures and to obtain accurate data they should be subjected to a series of testing.[69] For the purposes of this study, the manufacturer's data still provides results that will allow for accurate system-level analysis.

II.3.2. Propellers

The recent boom of MAV development has created an increasing demand for small-diameter propellers. Currently, a large number of small-diameter propellers exist largely due to the radio controlled (RC) airplane enthusiast community, but their performance data is unknown. To remedy this problem, Wichita State University (WSU) began an effort to test and create a database of these propellers.[70] According to WSU, small-diameter propellers range from 15 cm to 56 cm (6 in to 22 in) and operate at

Reynolds numbers between 30,000 and 300,000. A similar study at the University of Illinois at Urbana-Champaign (UIUC) has initiated testing of micro propellers with diameters ranging from 5.7 cm to 12.7 cm (2.25 in to 5 in) operating at Reynolds numbers less than 50,000.[71] Even with performance data on a propeller, simply selecting the best propeller without consideration of the other subsystems in the propulsion system will not yield optimum results.

With MDO that addresses characteristics of the entire airframe, especially its propulsion system to include the motor and gearbox, an optimal design can be obtained.[66] The propeller has an advantage over the other subsystems of the aircraft because swapping it out for a different propeller is much easier than replacing an internal component. A successful conceptual design tool would ideally even avoid the extra cost of replacing a propeller that was poorly matched with the rest of the propulsion system. AFRL has recently explored an alternative method to MDO that simply creates a large look up table of similar propellers.[72] A table such as this would help determine performance characteristics including efficiency and thrust given different diameters or degrees of pitch. Their research found fits for propeller performance that were from "mediocre to very good" and discovered that results were very sensitive to twist distribution.

II.3.3. QPROP

QPROP is another product of Mark Drela at MIT and it seeks to find the performance of motor and propeller combinations. For the propulsion system to operate at peak efficiency, the motor and propeller must be properly matched. This occurs when

the efficiency curves of both the propeller and the motor have their peaks at roughly the same speed and required thrust (Figure 7).[73]

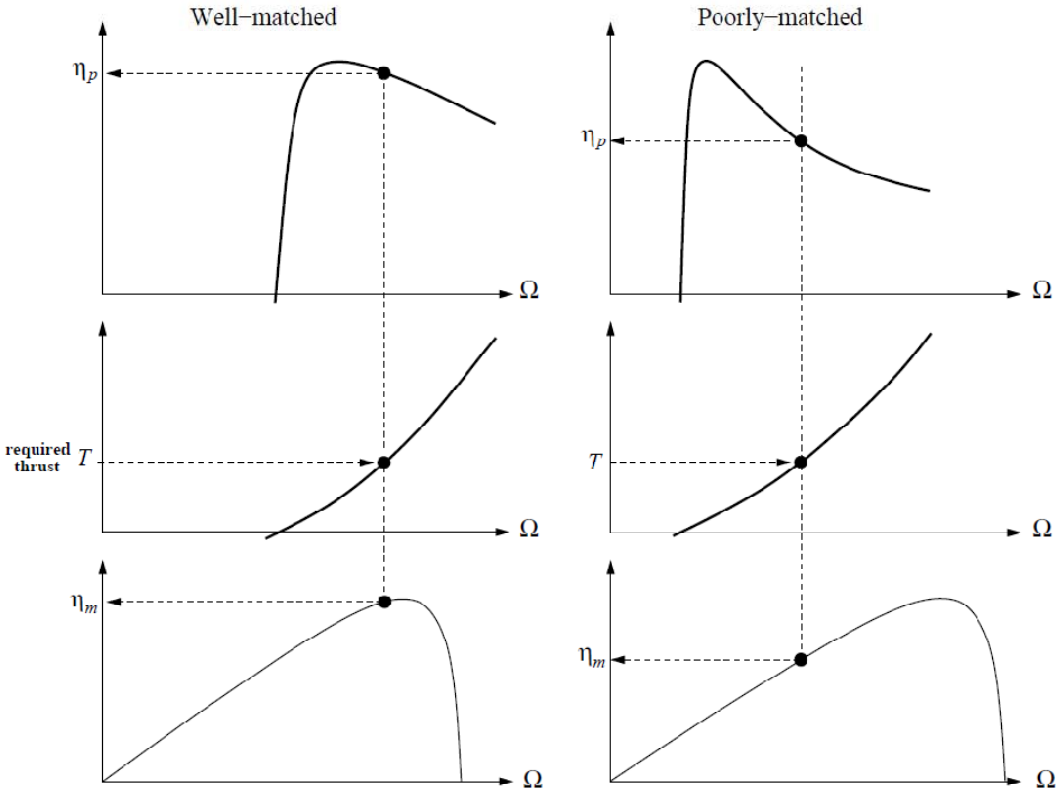

Figure 7. Well-matched and poorly-matched motor and propeller pairs

QPROP predicts the performance of these propeller-motor combinations. It does so by extending upon classical blade-element and vortex simulation by adding radially varying self-induction velocity.[74] In general, QPROP employs a sophisticated aerodynamic propeller model and a generalized motor model. Given flight conditions, propeller geometry, and basic motor parameters, QPROP outputs a multitude of parameters to include velocity, RPM, pitch rate change, thrust, torque, shaft power, voltage, current, motor efficiency, propeller efficiency, advance ratio, thrust coefficient, torque coefficient, slipstream velocity increment, electrical power, propeller power,

power weighted average of local C_L, and power weighted average of local C_D. Theory and further specifics of QPROP will be discussed in Chapter 3.

II.4. Energy Storage Devices

All aircraft depend on some type of ESD or power source for their propulsion systems to be able to get an aircraft moving. For larger aircraft and RPA in the USAF, JP-8, a kerosene-based fuel, is the solution of choice.[75] For MAVs, ICEs are less efficient because they do not scale well to a size desirable for MAVs; however, electric motors have proven to be more effective. Electricity must be provided to the motor of a MAV and two of the best solutions are batteries and fuel cells, both of which are electrochemical storage devices.

II.4.1. Batteries

Batteries convert stored chemical energy into electrical energy through an electrochemical reaction and are divided into two main categories: primary and secondary. Primary batteries or batteries that are disposable (non-rechargeable) have an electrochemical reaction that is non-reversible. When primary batteries discharge, the chemical compounds inside them are permanently changed and energy is released until the original compounds are depleted. As such, primary batteries are referred to as closed systems. Two electrodes (an anode and cathode) and an electrolyte compose the structure of a battery (Figure 8).[39]

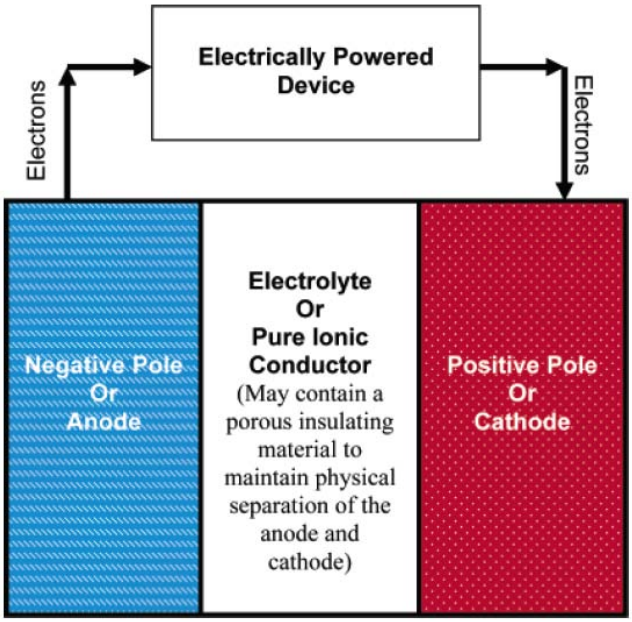

Figure 8. Battery block diagram

There are many kinds of primary batteries, but two of the most common categories are alkaline batteries and lithium batteries. Alkaline batteries utilize an electrochemical reaction with an alkaline metal such as zinc and manganese dioxide. Lithium batteries, as their name suggests, utilize lithium as the anode. Typical voltages for lithium batteries are around 3-4 V, whereas alkaline batteries are at 1.5 V.[39] Various primary batteries have certain advantages and disadvantages, but generally speaking, the advantages of primary batteries are their high specific energy (compared to secondary batteries), comparative low cost to other electrochemical systems, convenience, scalability, and high performance in low drain applications. Disadvantages of primary batteries include the large amount of waste they create, poor performance in high drain applications, and low energy efficiency.[38]

Secondary batteries are multi-use (rechargeable) batteries that use reversible electrochemical reactions. Secondary batteries discharge similarly to primary batteries and return to their charged state by reversing the electrochemical reactions and applying an electrical current. Secondary batteries have the same setup as primary batteries or two electrodes with an electrolyte between them. In general, the requirements to meet rechargeablity typically result in secondary batteries having lower storage capabilities than primary batteries, as well as fewer chemicals for electricity conversion.[39] There are many types of secondary batteries. The main types include lead acid, nickel-cadmium, nickel-metal hydrides, and lithium-ion batteries. Taken as a whole, the advantages of secondary batteries include low cost over the batteries life time (with higher initial costs), good performance in high drain applications, and less waste materials compared to primary batteries. Disadvantages include the cost of a charging system, lower specific energy than primary batteries, lack of standards and compatibility between types, and downtime during recharge.[38]

II.4.1.1. Figures of Merit: Batteries

Selecting the best battery is unfortunately not as easy as picking the one with the highest specific energy or specific power. Examining various other figures of merit (FOM) provides a holistic view of which battery to select. After specific energy and specific power, the next FOM is the theoretical voltage of a battery. This indicates the maximum voltage a singular cell can provide with higher voltages being superior. The theoretical specific capacity of a battery tells the total charge (electrical energy or current) of the battery's active materials on a mass basis. Once again, higher capacities are desirable. Another FOM is capacitance.

Capacitance is different than capacity and is the ability of a battery to hold an electric charge. Capacitance can also be expressed as the amount of charge for a given electric potential. The last three FOM each represent different forms of a battery's life: service life, shelf life, and cycle life. Service life is how long a battery can operate and is directly related to specific power and theoretical specific capacity. Cycle life is how many times a battery (secondary only) can be charged and recharged before it loses 80% of its initial rated capacity.[76] Finally, shelf life is how long a battery can hold its charge. This FOM is important for military applications where batteries can sit in storage for years before being called upon to operate in a moment's notice with lives depending on its reliability.

Many of the FOM depend on one another or even external factors such as temperature. For example, the theoretical voltage of a battery is reduced based upon the battery's state of charge (SOC) or percent of the battery that has been discharged (Figure 9).[77] Voltage also depends on the "C-Rate" or discharge rate of a battery. A C-Rate of 1.0 (1C) represents the current the battery can provide for an hour before the voltage drops to an unusable value. Two examples help illustrate the concept of a C-Rate. A C-Rate of 0.05C would represent the current the battery could provide for a 20-hour discharge. On the other hand, a C-Rate of two (2C) would represent the current the battery could provide for 30 minutes. The effect of different C-Rates is displayed in Figure 10. The battery for these curves is the LiPo curve shown in Figure 9 as the green curve at the top of the plot.[77]

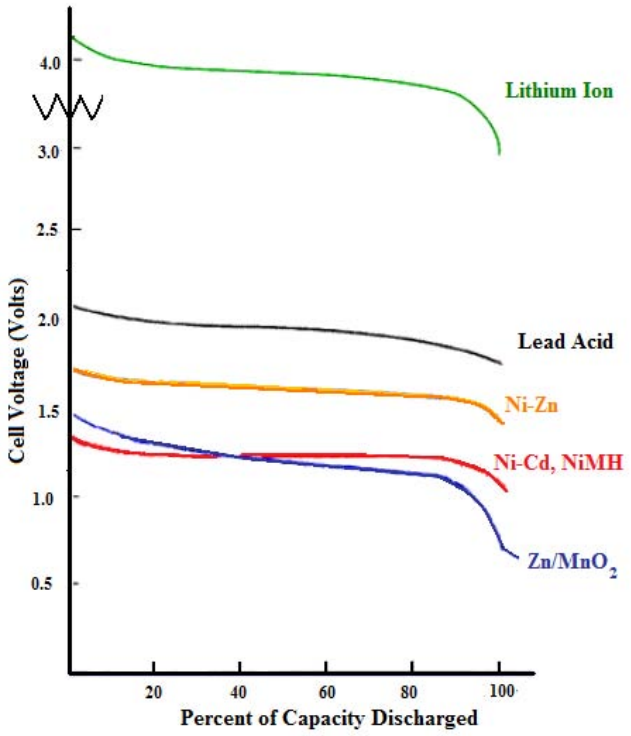

Figure 9. Voltage change due to state of charge

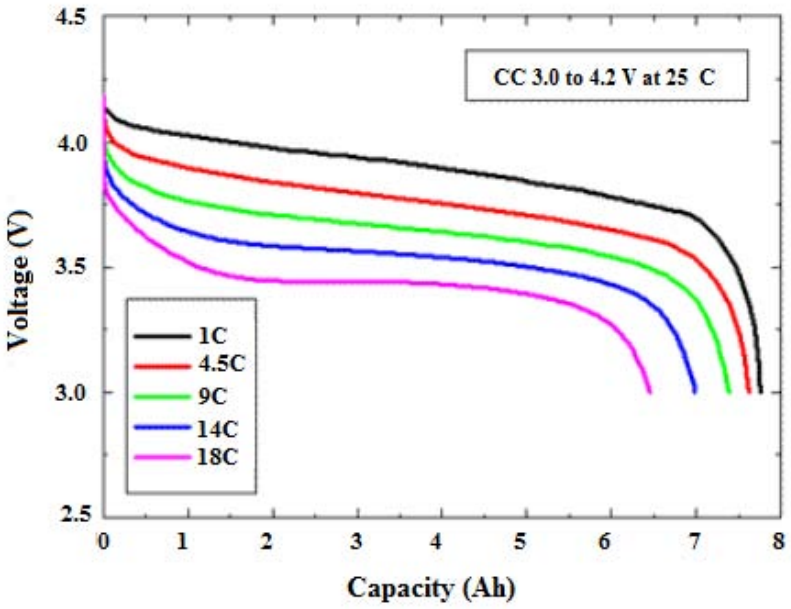

Figure 10. Voltage change due to discharge rate

While manufacturers provide data on these FOM, the values cannot always be trusted until verified by neutral sources through experimental analysis. A 2007 study by the Naval Research Laboratory (NRL) examined the lithium-ion polymer batteries on the market that would be useful in a NAV or MAV platform. These batteries were commercial-off-the-shelf batteries that varied in mass from 2 to 5 grams. The results of the testing further reflect the effect of discharge rate on a battery's performance for a range of performance characteristics. Figure 11 shows the NRL's results for an Atomic Workshop 200 mAh, 4.7-gram LiPo battery.[78] The experimental data shown here reflects the expected results of changing C-Rates shown in Figure 10. A full range of performance characteristics for this battery reinforces the effects of C-Rate on a battery's other FOM (Table 2).[78]

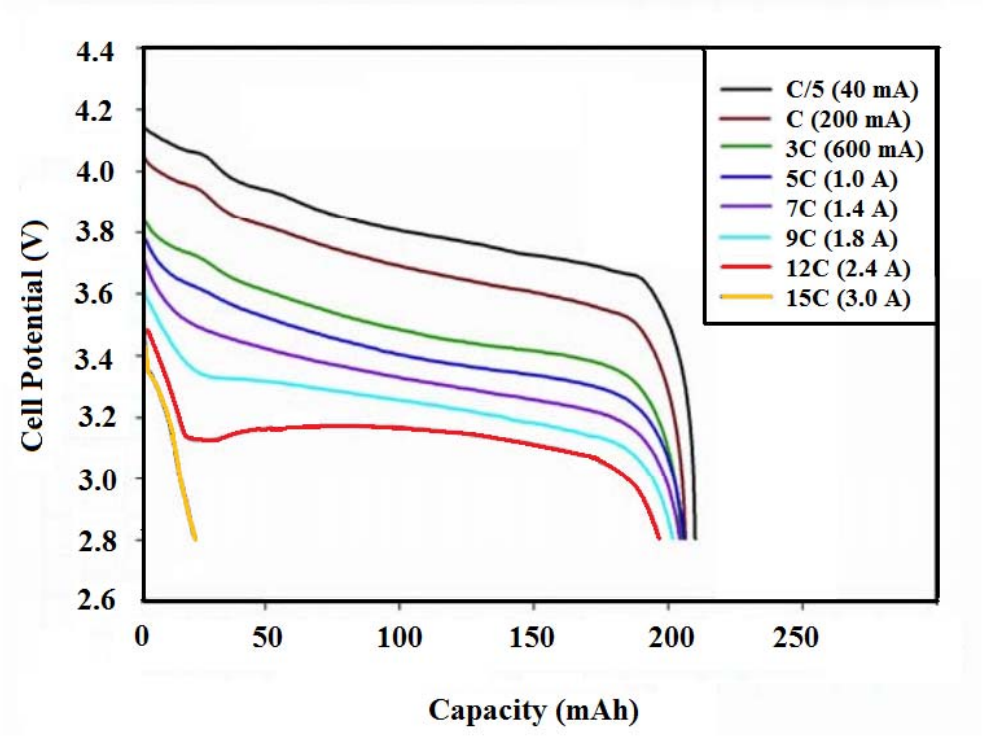

Figure 11. Atomic Workshop 200mAh battery

Table 2. Atomic Workshop 200mAh battery discharge data

C-rate	Current	Voltage	Capacity	Power	Energy	Energy	Sp. Energy	Sp. Power
	(A)	(V)	(mAh)	(W)	(mWh)	(J)	(W-hr/kg)	(W/kg)
1	0.2	3.7	202	0.7	747	2741	159	157
3	0.6	3.48	201	2.1	699	2532	149	443
5	1	3.4	201	3.4	683	2460	145	722
7	1.4	3.3	200	4.6	660	2426	140	981
9	1.8	3.26	197	5.9	642	2333	136	1246
12	2.4	3.2	192	7.7	614	2211	130	1631
15	3	0	0	0	0	0	0	0

II.4.1.2. Ragone Plots and Discharge Curves

A Ragone plot is one of the more useful tools for examining the performance of any ESD, including batteries. By adding discharge curves to a Ragone plot, further information can be obtained. Figure 12 shows this kind of Ragone plot for five LiPo cells that could be used in a MAV platform.[79]

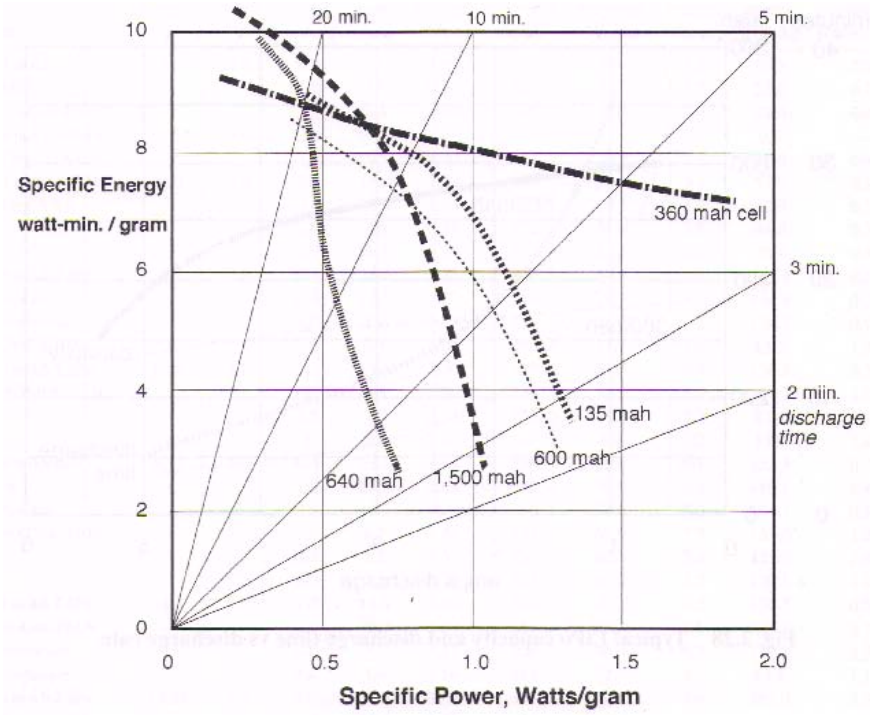

Figure 12. Ragone plot of several small LiPo cells

Several characteristics of Figure 12 are worth mentioning. The further a point is located from the origin, the better the indicated performance. Lines of constant discharge radiate from the origin, with the battery (or "cell") capable of the best energy performance at that discharge rate being the farthest from the origin on that line. When two different cell lines intersect, the cell's line with the flatter curve represents better performance at shorter discharge times and the one with a steeper curve has better performance at long discharge times.[79] If experimental data for a cell is available in this form it can be used in a conceptual design model for high-fidelity analysis.

II.4.2. Fuel Cells

Fuel cells are energy conversion devices that convert the chemical energies stored in various fuels to electricity via electrochemical reactions. These fuels can vary from hydrogen to methanol and are supplied continuously to the cell's surface so that they can react with an oxidant such as oxygen. There are many different kinds of fuel cells, but they all share the same basic structure, consisting of a positive electrode (cathode), a negative electrode (anode), and an electrolyte. The material selected for the electrolyte of the fuel cell plays a major role in classifying the type of fuel cell. The most common types include phosphoric acid fuel cells (PAFC), polymer electrolyte membrane fuel cells (PEMFC), alkaline fuel cells (AFC), molten carbonate fuel cells (MCFC), and solid oxide fuel cells (SOFC). Each kind of fuel cell operates most efficiently at a specific temperature range and has unique properties in terms of the its fuel, electrolyte, and mobile ion (Table 3).[80]

Table 3. List of fuel cells and their properties

Type	Operating Temperature (°C)	Fuel	Electrolyte	Mobile Ion
PEMFC	70-110	H_2, CH_3OH	Sulfonated polymers (Nafion^{TM})	H+
SOFC	700-1000	Hydrocarbons, CO	$(Zr,Y)O_{2-\delta}$	O^{2-}
AFC	100-250	H_2	Aqueous KOH	OH-
PAFC	150-250	H_2	H_3PO_4	H+
MCFC	500-700	Hydrocarbons, CO	$(Na,K)_2CO_3$	CO_3^{2-}

The advantages of fuel cells that make them attractive for use in a MAV are their efficient energy conversion, modular construction, low maintenance, quiet and safe operation, reliability, and high specific energy. The disadvantages of fuel cells are their sensitivities to impurities in the fuel, poor response to pulse demands, low specific power, and their expense.[39]

II.4.2.1. Figures of Merit: Fuel Cells

The FOM of fuel cells are essentially the same as batteries; however, not all of the same FOM apply to fuel cells largely due to fuel cells being an open system. For a fuel cell, theoretical voltage, specific energy, and specific power are the biggest players. The theoretical voltage of a fuel cell is subject to other properties of the ESD that result in losses to the overall theoretical voltage. Theoretical voltage for a fuel cell is given by Eq. (2), where *n* is the number of moles of electrons transferred, *E* is the theoretical

$$E = \frac{-\Delta\overline{g_f}}{n \cdot F} \qquad \textbf{(2)}$$

voltage or reversible open circuit voltage, $\Delta\overline{g_f}$ is the molar specific Gibbs free energy, and *F* is the Faraday constant. The electrochemical reaction for a PEMFC is shown in Eq. (3).[47] A PEMFC's theoretical voltage is equal to 1.23 V, which is significantly less

voltage than LiPo batteries. For this reason, fuel cells typically come in stacks of individual fuel cells connected in parallel to increase the overall voltage.

$$\begin{gathered} \textit{Anode Reaction: } H_2 \rightarrow 2H^+ + 2e^- \\ \textit{Cathode Reaction: } \frac{1}{2}O_2 + 2H^+ + 2e^- \rightarrow H_2 0 \\ \textit{Overall Reaction: } H_2 + \frac{1}{2}O_2 \rightarrow H_2O, \quad \overline{\Delta G_f} = -237.17\ kJ\ /\ mol \end{gathered} \tag{3}$$

Fuel cell voltage is reduced from its theoretical voltage due to activation polarization (reaction rate losses), ohmic polarization (resistance losses), and concentration polarization (transport losses) seen in Eqs. (4), (5), and (6), respectively.

$$\eta_{activation} = \frac{RT}{n\alpha F} \ln \frac{i}{i_0} \tag{4}$$

$$\eta_{ohmic} = iR = \frac{iL}{\sigma A} \tag{5}$$

$$\eta_{conc} = \frac{RT}{nF}\left(1 + \frac{1}{\alpha}\right) \ln \frac{i_L}{i_L - i} \tag{6}$$

The charge transfer coefficient, α, is dependent on the type of reaction and electrode material. Exchange current density, i_o, depends on electrode material. Conductivity is σ, area is A, L is length, and R is the area specific resistance in kΩ/cm^2. The limiting current density is $i_{L.}$ These losses can be minimized with better designs, materials, and certain operating conditions including temperature and pressure. Taking all the losses into account, the operating voltage of the fuel can be found using Eq. (7). Overall, a fuel cell's voltage and losses are easiest to visualize and most useful when they are plotted in a polarization curve.

$$V = E - \eta_{act} - \eta_{ohmic} - \eta_{conc} \quad \textbf{(7)}$$

II.4.2.2. Polarization Curves

A polarization curve plots the fuel cell's voltage versus its current according to Eq. (7). It consists of three different "loss regions" which represent the three polarization losses. An example polarization curve is shown in Figure 13.[81] The first region or "activation region" is the activation voltage lost due to the speed of the electrochemical reactions on the electrode surfaces. Factors that affect the width of this region are temperature, pressure, type of electrode, and type of catalyst used. The ohmic region consists of the losses due to the ionic and electronic conduction.[47] Finally, the third region represents the "mass transport" or concentration losses that come from losses associated with the transport of the reactants.

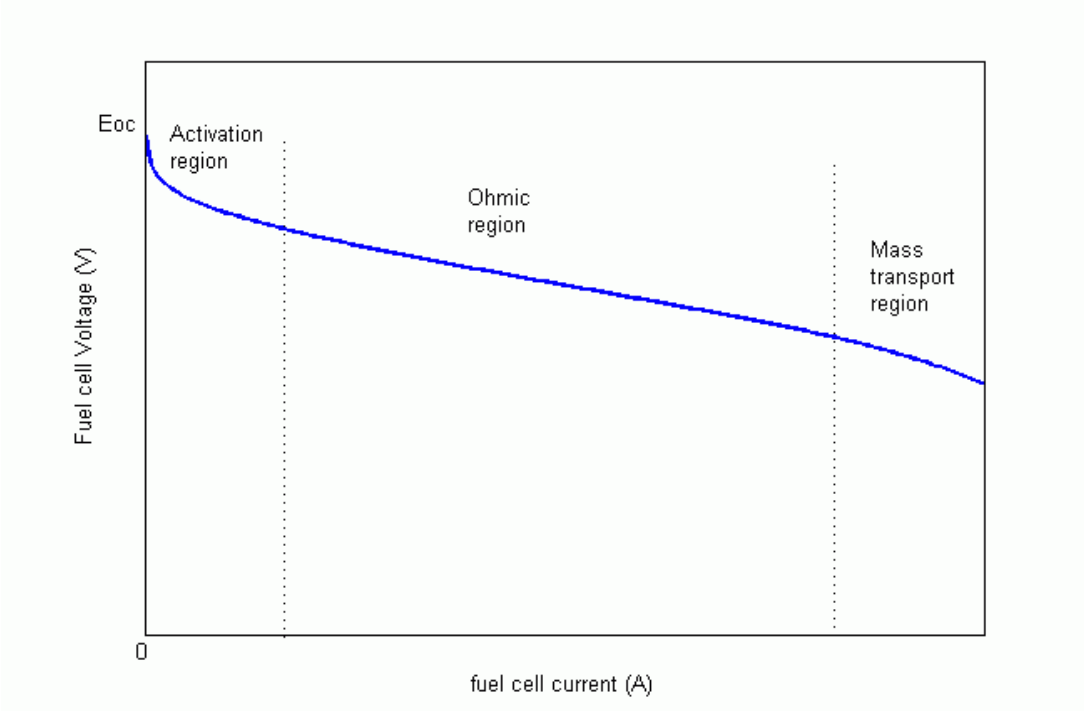

Figure 13. Generic polarization curve

II.4.2.3. Balance of Plant

The fuel cell balance of plant (BOP) are the subsystems that allow the fuel cell to generate power. The BOP often includes air and fuel delivery and regulation, thermal and humidity management, and power management and distribution. Ensuring that the BOP functions properly is critical to the efficiency of the fuel cell. Properly designing and sizing a fuel cell's BOP requires MDO and is beyond the scope of this model; however, the weight of the BOP affects the overall mass of the MAV and is therefore accounted for in the high-fidelity power source CA.

II.4.2.4. Fuel Storage

Of all fuel cell types, the PEMFC stands out as the best option for near-term use in a MAV due to the recent research interest and number of successes of PEMFCs in RPA flight (Table 1). All fuel cells require fuel and therefore storage of hydrogen in a PEMFC is important to address. There are many different methods for the storage of hydrogen, but three of the methods stand out as having the most potential for use in a MAV: metal hydrides, hydrogen as a compressed gas or cryogenic liquid, and by using another chemical such as formic acid or methanol that contain hydrogen. Metal hydride examples include LiD, $NaAlH_4$, $TiFeH_2$, and $NaBH_4$. Upon heating, these hydrides release hydrogen. Waste heat from the fuel cell can be used to maximize efficiency for this process. While metal hydrides do offer high energy density by volume, they do not offer high energy density by weight, possessing only 1.3% hydrogen by weight.[82]

Containing hydrogen in a tank can be done either by storing it as a compressed gas or as a liquid. The main problem with this method is the weight of the tank itself as well as the large volume it occupies. The last method of storage is formic acid or

methanol for use in a PEMFC. Formic acid (HCOOH) or methanol is broken down into hydrogen (H_2) and carbon dioxide (CO_2) with the help of a water-soluble ruthenium catalyst.[83] Formic acid contains 4.3% hydrogen by weight, making it a viable storage method for a MAV. Methanol must also be refined before being used by a PEMFC fuel cell, and being a liquid at room temperature, methanol allows for easier transportation and storage.[11] The storage of hydrogen is an important consideration for the final design of a MAV, but at the conceptual design phase, only the mass of the hydrogen storage tank is taken into account in the high-fidelity power source CA.

II.4.3. Energy Management of a Hybrid System

Control strategies have been created and proven effective for minimum fuel consumption in hybrid systems containing ICEs, but less research efforts have been directed at fuel cell-battery hybrid systems.[84] Some aspects of energy management are intuitive from the traits of fuel cells and batteries. Having a high specific power, batteries are capable of providing power for high demand mission segments such as takeoff. A fuel cell can utilize its high specific energy and need for constant power demands on longer endurance segments such as cruise or loiter. Taking these traits, the overall efficiency of the hybrid system can improve if batteries are used for peak power requirements.[24] This can be done by assigning the fuel cell a constant power for the entire mission. The battery would then be used to provide the additional power required for segments requiring more than that assigned power. The optimal degree of hybridization differs based upon mission requirements, the ESDs the aircraft utilizes, and the size of the aircraft. An investigation of a 700 W fuel cell-battery hybrid aircraft system found that endurance was optimized when the fuel cell was sized to provide

between 60-80% of the total system power.[85] This number is similar to the results from Hrad's conceptual design tool that showed that ideal split occurred when the fuel cell took 93% of the average power.[24] It is important to point out that the first investigation looked at hybridization percentage based on total power, whereas Hrad's findings were based on average system power. Therefore, the values could actually be closer than the numbers suggest. The research described here provided more insight into optimizing the energy management system.

II.5. Existing Conceptual Design Efforts

Aircraft design requires considerations in aerodynamics, thermodynamics, propulsion, structures, stability and control, and others must come together to meet system level objectives. New technology comes forth every day that has potential to change the process. For example, advances in fuel cell technology could dramatically change the propulsion systems of an EPMAV. According to Anderson, the conceptual design process "is an act of creativity, and like all creative endeavors, there is no one correct and absolute method to carry it out."[25]

Some examples exist for conceptual design tools that specifically look at electrochemically-powered RPA, though they focus on aircraft much larger than the MAV size. The Georgia Institute of Technology (GT) has put considerable effort into one such tool over the past decade.[23, 86, 87, 88, 89, 90] GT breaks down the aircraft design process into areas called Contributing Analyses, a term which this research adopts. Each of these CAs requires global input variables and adds intermediate variables that are shared with other CAs. A design structure matrix (DSM) is created with all of the

intermediate variables that are linked together throughout the various CAs.[89] Fixed-point iteration then converges on the aircraft's performance metrics by tweaking the intermediate variables until conversion is reached. Finally, optimization on the design space identifies the best design. The University of Colorado has also created a tool similar to GT.[24] Since the tools have similar properties, this investigation will focus on GT's efforts. Even though their research focuses on RPA larger than the size of a MAV, insight can be gained by examining their efforts.

GT has developed a variable-fidelity tool that allows a user to specify the complexity and therefore fidelity of the model. Choices in this area will directly affect computational costs, the accuracy of results, and methods used for convergence. To perform this analysis, GT utilized the power of MC to integrate an assortment of sub tools that add different levels of fidelity to the model while still providing an environment that gives flexibility to the user. The specific tools used in MC provided an example for creating a similar conceptual design tool.[87]

Once the input variables are initialized, a user selects which airfoil analysis software to use. In order of increasing fidelity, options include PABLO, XFOIL, or experimental data. Step two then models the geometry of the aircraft using a computer-assisted design (CAD) software technique developed by NASA known as vehicle sketchpad (VSP). VSP also moves into step three and calculates lift, induced drag, and aerodynamic moments using VORLAX, a vortex lattice solver. Because VORLAX calculations are time demanding, GT added a numerical lifting code in MATLAB for quick wing aerodynamics.[87] Structural analysis of the aircraft is examined in step four with either regressed equations for low-fidelity or finite element software called

DYMORE for a medium fidelity. At this point, the user can choose to iterate back with the structurally-deflected geometry to update the overall geometry and aerodynamic characteristics. Finally, step five examines the propulsion of the aircraft using various propulsion architects modeled in MATLAB Simulink. Architects include combinations of solar cells, fuel cells, and hydrogen ICEs. Once the model has completed the various disciplines, it takes the initial propulsion sizing from step five and simulates a mission, checking requirements or "sizes" along the way. If a requirement is not met, the model iterates back through the disciplines until all requirements are met and performance outputs are finalized. A flow chart that illustrates the different steps in GT's analysis is shown in Figure 14. In addition to the fidelity options that currently exist, GT has plans to continue adding levels of fidelity to the model. The full range of existing and planned fidelities for the model can be found in Table 4.[87]

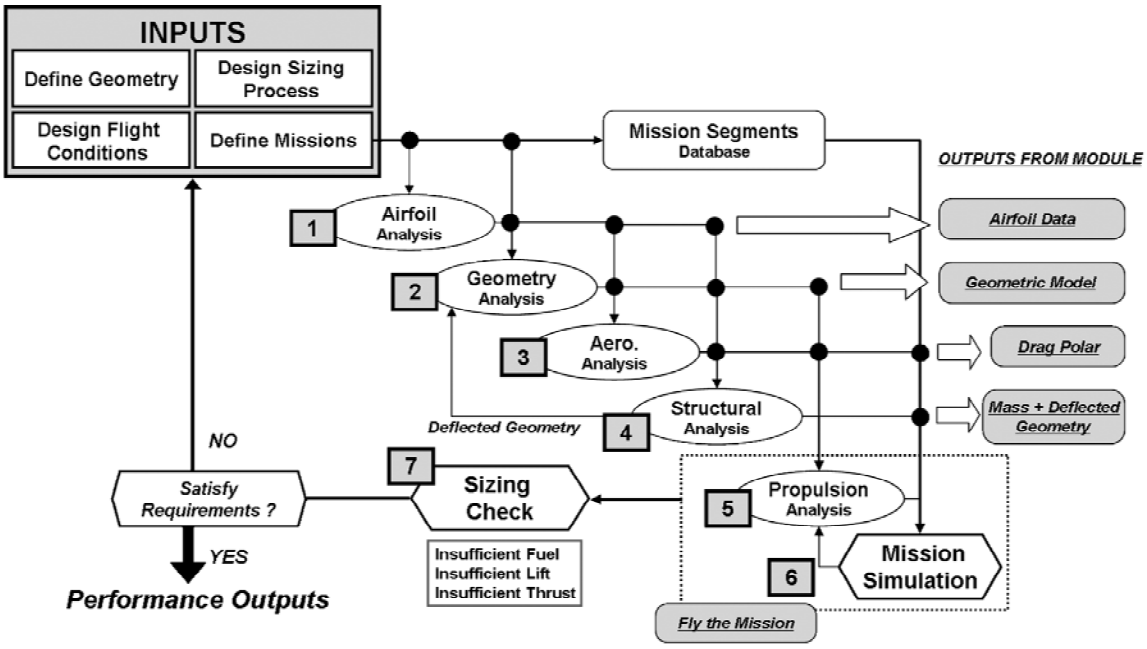

Figure 14. Flow chart of GT's variable-fidelity model for MC

Table 4. GT existing and planned levels of fidelity for design

	Discipline		
Fidelity	**Geometry**	**Airfoil**	**Aerodynamics: friction drag**
Low	*2-D model*	*Inviscid (PABLO)*	*Empirical method (form factor)*
Medium	*Vehicle sketch pad (VSP): 3-D*	*Inviscid–viscous (XFOIL)*	*Airfoil numerical integration*
High	*CATIA V5®*	*Experimental data*	*CFD–Fluent*
High	*offline*	——	*CFD–Fluent*
	Discipline		
Fidelity	**Aerodynamics: lift and induced drag**	**Structures**	**Propulsion**
Low	*Lifting line*	*Regressed equations*	*Table lookup*
Medium	*Vortex lattice (VORLAX)*	*Finite element (DYMORE)*	*MATLAB/Simulink modules*
High	*CFD–Fluent*	*FEM-ANSIS*	*Experimental engine data*
High	——	*CFD–Fluent*	*FEM-ANSIS*

II.6. Software Synthesis (Model Center)

The design of an aircraft has changed a great deal since the Wright Brothers' historic flight more than a hundred years ago. One tool that has arguably ushered in the most change is the computer. Computers today have no problem crunching through calculation after calculation and numerous software applications have been created to simplify the process. To take advantage of these tools for aircraft design, integration on a grand scale must occur. MC, a workflow automation program, was selected to handle this task.

MC allows any number and kinds of programs or pieces of information to be linked together with existing plug-ins or user-created file wrappers. Existing plug-ins found in MC handle a range of programs from Microsoft Excel to Mathwork's

MATLAB. Software that does not have an existing plug-in requires file wrappers, which can be created by code written in VBScript. Once software has been integrated into the MC environment and proper linkage between inputs and outputs of each piece has been finalized, a number of built in analysis tools are available. Using these, models can be manipulated with relative ease to run trade studies, parametric studies, Design of Experiments (DOE), and optimization routines. Additional information on MC will be discussed in Chapter 3.

II.7. Chapter Two Summary

The literature review discovered that the innovative technology for both MAVs and ESDs provide motivation for the development of an EPMAV and suggest that its creation is feasible. Several efforts currently exist for larger RPAs that are powered by ESDs. These efforts began with conceptual design work that continues to be refined to add fidelity and corrections based upon flight-tests. Moving to the MAV size range, there were no examples found for flight-tested EPMAVs or conceptual design tools for EPMAVs outside of the work that this effort follows. Therefore, the development of a multi-fidelity conceptual design tool for an EPMAV would be a first step to getting an EPMAV into the air. A conceptual design tool of this kind would have to examine the areas of aerodynamics, propulsion, power management, and the ESDs used. Several tools for aerodynamics and propulsion are readily available for EPMAV design; however, tools for the power management and the capabilities of ESDs given power demands were limited. Chapter 3 examines the methodology for creating a multi-fidelity conceptual

design tool for an EPMAV that uses both existing tools and develops new tools for the areas of analysis that have received less attention by previous efforts.

III. Methodology

The process to create a conceptual design tool to determine the maximum endurance duration of an EPMAV began by outlining a flow chart that illustrated the flow of data all the way from user-specified inputs to the resulting endurance duration using only one level of fidelity. The outline was then expanded to include multiple levels of fidelity as well as the optimization and convergence loops that yielded the maximum endurance duration. The flow chart shown in Figure 15 shows the four areas of CA that are the foundation of the model: aerodynamic, propulsion, power management, and power source. It also describes the most important input and output variables of each of the components within the CAs. After the CAs were created, they were combined into a data flow automation program (MC) to pass information between each other. MC also provided tools to aid in iterative solutions such as convergence loops and optimizations. Chapter 3 examines each of these CAs in detail and then describes their synthesis into the MC environment.

III.1. Contributing Analyses

The CAs of the model were created first. Data flow into and out of each of these components could be determined with a given set of user inputs and an end goal. Even though each CA depended on user inputs and preceding CA calculations, each CA was able to run independently if initial estimates were provided for the variables that were needed for analysis. This was useful for testing and debugging the various CAs. The theories behind the methodology of each CA assists the understanding of the inner-workings of the model.

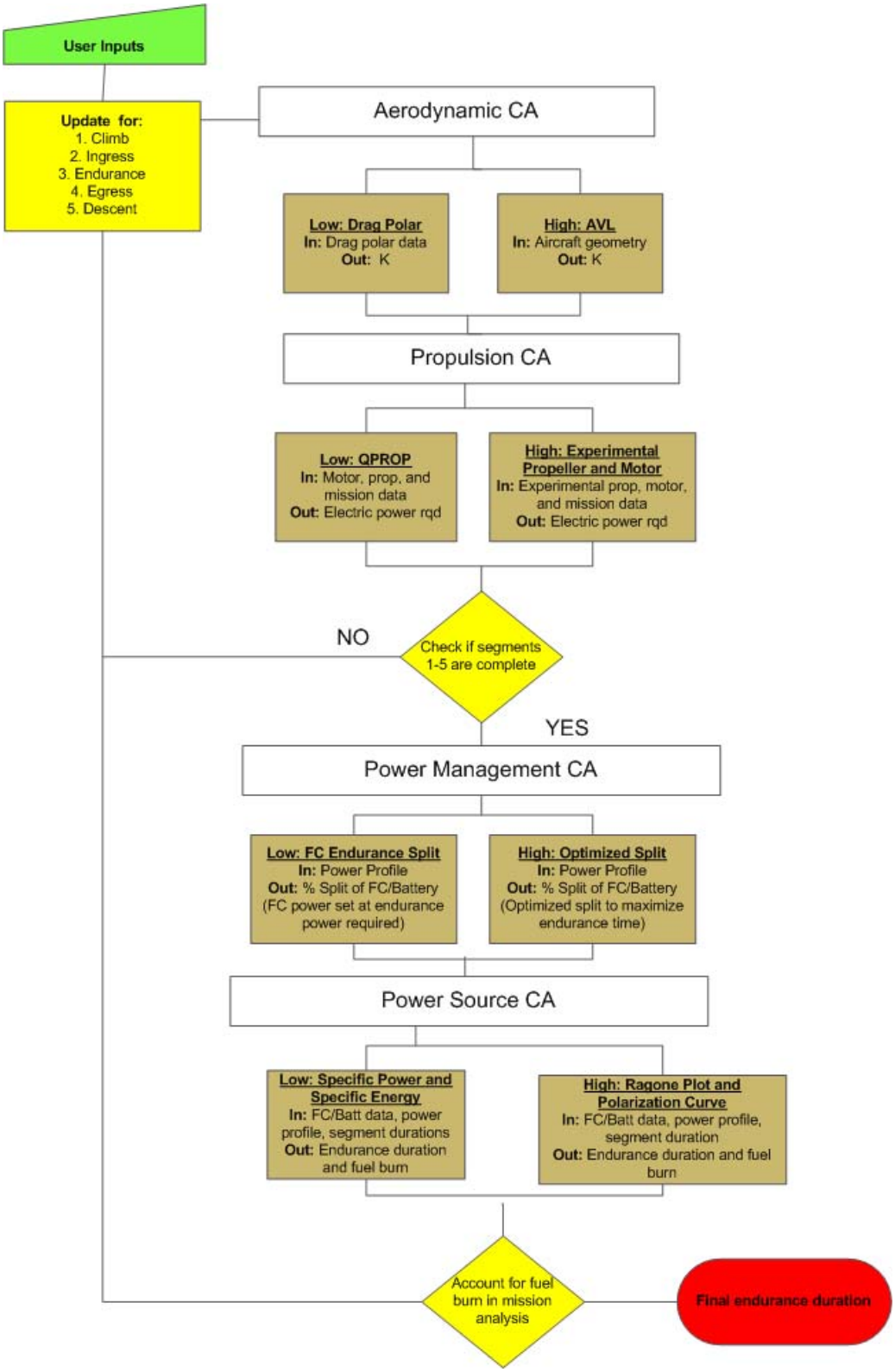

Figure 15. Rubber endurance segment flow chart

III.1.1. Aerodynamic CA

The aerodynamic CA's main goal was to determine the span efficiency factor, *e*, which was related to the drag polar coefficient, *K*, through Eq. (8). This value was needed to determine power required in the propulsion CA. The aerodynamic CA can be used to get *K* by calculations coming from a drag polar (low-fidelity) or from AVL (high-fidelity).

$$e = \frac{1}{K \cdot \pi \cdot AR} \tag{8}$$

III.1.1.1. Low-Fidelity: Drag Polar

The drag polar summarizes the aerodynamics of an aircraft and since it was commonly available, the drag polar provided a useful tool to conduct low fidelity calculations. The most important things to take from a drag polar were the zero-lift drag coefficient, $C_{D,0}$, and any additional point along a curve, such as the one shown in Figure 16. The zero-lift drag coefficient represented the combination of the zero-lift parasite drag and wave drag coefficients. Any point along the curve showed the relationship between the lift and drag of the aircraft. Given these two pieces of data, the value for K was found with Eq. (9). A publication on the Unicorn MAV, a MAV of similar size to the GenMAV, confirmed that this form of the drag polar was sufficient for accurate aerodynamic analysis.[93]

$$C_D = C_{D,0} + K \cdot C_L{}^2 \tag{9}$$

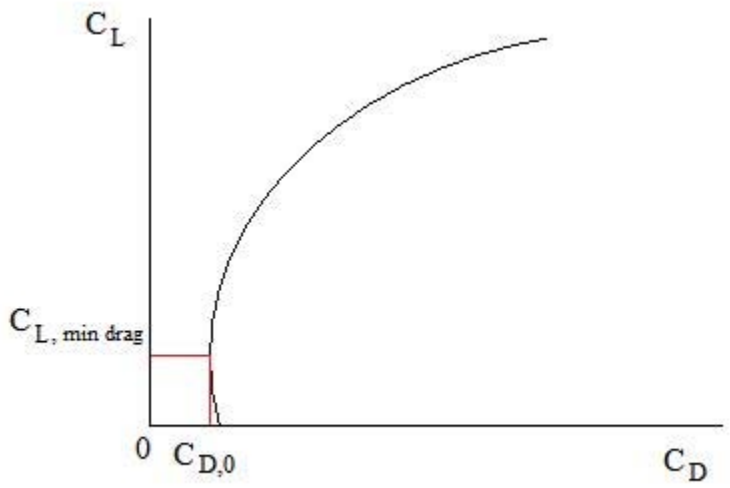

Figure 16. Drag polar plot

III.1.1.2. High-Fidelity: AVL

A vortex lattice method of analysis called AVL was used to achieve a higher level of fidelity for aerodynamic analysis. As highlighted in Chapter 2, AVL provided an acceptable tool for in-depth aerodynamic analysis. Further, it has also been proven accurate for slightly larger MAVs and a wide range of aircraft configurations, including configurations that are atypical.[27] While the MAV examined in this analysis did not have an atypical configuration, future configurations of interest might require a robust tool of this kind.

III.1.1.2.1. AVL Modeling Principles

Vortex lattice methods similar to AVL provided the best results when used on aerodynamic configurations that consisted of thin lifting surfaces at small angles of attack and sideslip. As such, the user was notified in AVL's documentation to use small angles of attack in mission analysis.[65] The surfaces of such configurations and their trailing

wakes were modeled as vortex sheets that were discretized into horseshoe vortex filaments. AVL also modeled slender bodies such as fuselages with a source-doublet filament. The integration of the forces of each vortex resulted in the lift and induced drag of an aircraft.

AVL assumed a quasi-unsteady flow and as such, vorticity shedding was neglected. This ultimately meant that oscillatory motions must occur at low frequencies so that the resulting flow angles were small. Typical aircraft motions fit well within the range of frequencies that AVL can handle. Compressibility was treated using the Prandtl-Glauert transformation seen in Eq. (10). This transformation allowed AVL to handle Mach numbers up to 0.6 with accuracy, which was far higher than MAV speeds.

$$c_p = \frac{c_{p,0}}{\sqrt{1-M^2}} \tag{10}$$

III.1.1.2.2. AVL Theory of Operations

The goal of AVL was to calculate the span efficiency factor found with Eq. (11). Here, $C_{D,i}$ is the Trefftz Plane drag coefficient calculated within AVL from the wake

$$e = \frac{C_L{}^2 + C_Y{}^2}{\pi \cdot C_{D,i} \cdot AR} \tag{11}$$

trace in the Y-Z plane far downstream. The coefficients of side force and lift, C_L and C_Y, respectively, came from the resultant of the forces in the Y and Z directions from the integration of the vortices. The forces were then normalized by dynamic pressure and planform area. While AVL was capable of additional calculations such as eigenmode

analysis, the model did not focus on these areas. Further details on AVL's theory of operations can be found in the user documentation.[65]

III.1.1.2.3. AVL Inputs and Outputs

AVL required a geometry, mass, and run-case file to conduct analysis. The geometry file must include the aerodynamic section properties and the vortex lattice geometry. Default values for velocity and air density were stored in this file. This file also included the user-specified zero-lift drag coefficient or else AVL set it to zero. Airfoil data was included in this file and came from a specific airfoil stored in AVL (NACA airfoils) or calculated using XFOIL. XFOIL was created by MIT and calculates aerodynamic airfoil coefficients for atypical airfoils.[94] The mass file contained the mass, moment of inertia, and center of gravity details of the aircraft and was an optional file. A mass file also served the purpose of setting the units and magnitude of the numbers used. If a mass file was not specified, the run-case mass was utilized as described below. The final file was the run-case file. Running AVL in MC made this file necessary due to it being an executable. The run-case file overrode inputs in both the geometry and mass file for parameters including velocity, density, and overall mass. The run-case file also included any desired constraints such as trimmed flight.

Upon execution, AVL took these three files and determined trim conditions, aerodynamic coefficients, control surface deflections, and stability derivatives. While the focus of the analysis was to obtain *e*, the additional results were used for validation purposes. For example, Eq. (12) shows how a positive static margin indicated an aircraft that was longitudinally stable and therefore able to fly. The distance measured from the

nose of the aircraft to its neutral point, X_{np}, must be greater than the distance from the nose to the center of gravity, X_{cg}.

$$\bar{X}_{np} - \bar{X}_{cg} > 0 \tag{12}$$

III.1.1.2.4. Velocity Calculations for AVL

Since AVL required velocity as an input, it is important to discuss what velocities AVL utilized for its calculations. The model required the user to input a velocity for each mission segment other than endurance. These velocities were checked to ensure they were not below the stall velocity (U_{stall}), which would drop the aircraft from the sky. The stall velocity was calculated with Eq. (13), where W is weight, S is wing area, and $C_{L,\max}$ is the maximum coefficient of lift. If there was an endurance segment in the mission analysis, the endurance velocity (U_{end}) was calculated using Eq. (14).[25] The use of Eq. (14) depended on knowledge of *K*. Since AVL required velocity to get *K* and *K* was needed to get endurance velocity, a converging routine was necessary to ensure the two variables satisfied both sets of calculations.

$$U_{stall} = \sqrt{\frac{2W}{\rho_\infty S C_{L,\max}}} \tag{13}$$

$$U_{end} = \left(\frac{2}{\rho_\infty} \sqrt{\frac{K}{3C_{D,0}}} \frac{W}{S} \right)^{1/2} \tag{14}$$

III.1.2. Propulsion CA

The overall goal of the propulsion CA was to calculate the electric power

required. QPROP, a program that predicted the performance of propeller-motor combinations provided the low-fidelity solution. The high-fidelity solution came from experimental data obtained by Wichita State University (WSU) and a propeller-motor code written by AFIT's Todd Rotramel.[97] In both cases, the propulsion CA took in power required, velocity, atmospheric data, and motor and propeller data to calculate electric power required. While most of that information was readily available without manipulation, an intermediary step was necessary to get power required.

III.1.2.1. Aircraft Power Required

The aircraft power required is directly related to the thrust required by the aircraft's velocity (U), as shown in Eq. (15). Velocity was either an input to the model or equal to the stall or endurance velocity, and therefore thrust required $\left(T_{req}\right)$ needed to be calculated. Thrust required was calculated by using the equations of motion as discussed by Anderson.[25] Anderson used Newton's second law parallel to the flight path for the basic form of the equation of motion in Eq. (16). Here *m* is mass, U_∞ is the free-stream velocity, ε is the angle of thrust relative to the flight path, *D* is drag, *W* is weight, and θ is the local climb angle. A similar expression, shown in Eq. (17), exists for flight perpendicular to the flight path in the vertical plane, where r_1 is the local radius of curvature in the vertical plane and ϕ is the roll angle. A third and final equation describes motion perpendicular to the flight path in the horizontal plane and is shown in Eq. (18). Here, r_2 is the local radius of curvature in the horizontal plane. Looking at steady, unaccelerated flight, the left hand side of Eqs. (16)-(18) change to zero. If the

thrust line is assumed to be in the direction of flight so that ε = 0, the equations of motion simplify to Eq. (19) and Eq. (20).

$$\mathrm{P}_{req} = T_{req} * U \tag{15}$$

$$m\frac{dU_{\infty}}{dt} = T_{req}\cos\varepsilon - D - W\sin\theta \tag{16}$$

$$m\frac{U_{\infty}^{\ 2}}{r_1} = L\cos\varphi + T\sin\varepsilon\cos\varphi - W\cos\theta \tag{17}$$

$$m\frac{\left(U_{\infty}\cos\theta\right)^2}{r_2} = L\sin\varphi + T\sin\varepsilon\sin\varphi \tag{18}$$

$$T - D - W\sin\theta = 0 \tag{19}$$

$$L - W\cos\theta = 0 \tag{20}$$

The equation for the rate of climb (ROC) of an aircraft can be gleaned from a free-body diagram of an aircraft and is shown in different forms in Eq. (21). The power-available, P_A, is what the power plant can produce and the power-required, P_R, is the power the airframe requires to overcome drag. By utilizing aerodynamic coefficients and drag polar theory discussed previously, Eq. (21) can be manipulated into the form shown in Eq. (22). Here, q_{∞} is dynamic pressure and S is wing area. Furthermore, if the aircraft is at low climb angles, the small angle assumption can be used. This assumption made the $\cos\theta = 1$ and turned Eq. (22) into Eq. (23). Finally, Eq. (23) can be solved for thrust, which then becomes thrust-required as shown in Eq. (24). The latter provided an option for a mission that had climbing, descending, or non-climbing segments by setting the *ROC* = 0.

$$ROC = U_\infty \sin\theta = \frac{T_A U_\infty - DU_\infty}{W} = \frac{P_A - P_R}{W} \quad \textbf{(21)}$$

$$ROC = \frac{T_A U_\infty - \left(q_\infty S C_{D,0} + \frac{KW^2 \cos^2\theta}{q_\infty S} \right) U_\infty}{W} \quad \textbf{(22)}$$

$$ROC = U_\infty \left[\frac{T_A}{W} - q_\infty \left(\frac{W}{S} \right)^{-1} C_{D,0} - \frac{W}{S} \frac{4K}{q_\infty} \right] \quad \textbf{(23)}$$

$$T_R = W \left[\frac{ROC}{U_\infty} + q_\infty \left(\frac{W}{S} \right)^{-1} C_{D,0} + \frac{W}{S} \frac{4K}{q_\infty} \right] \quad \textbf{(24)}$$

III.1.2.2. Low-Fidelity: QPROP

QPROP operations were based on classical blade element and vortex formulation theory. QPROP modeled the propeller with an advanced blade-element/vortex method that improved upon other codes by including the propeller's self-induction. The propeller analysis assumed that the blade airfoil's lift curve slope $\left(C_{L,\alpha}\right)$ was linear with $C_{L,\max}$ and $C_{L,\min}$ at its limits. The motor analysis used basic motor parameters including the motor constant $\left(K_v\right)$, electrical resistance $\left(R\right)$, and a constant rotational friction or zero-load current $\left(I_o\right)$. Newton's method started the process to solve for electric power required by determining circulation. Circulation was then used to determine torque and thrust. QPROP required that no more than three design variables be specified (i.e. velocity, thrust or power required, and pitch) and then attempted to satisfy the following equations:

$$\varpi_{prop} = RPM \cdot \frac{\pi}{30} \quad \textbf{(25)}$$

$$J = \frac{U}{\varpi_{prop} r} \tag{26}$$

$$Q = \frac{\left(I - I_0\right)}{K_V} \tag{27}$$

$$C_T = \frac{T}{\left(1/2\right)\rho\left(\varpi_{prop} r\right)^2 \pi r^2} \tag{28}$$

$$C_P = \frac{Q}{\left(1/2\right)\rho\left(\varpi_{prop} r\right)^2 \pi r^3} \tag{29}$$

$$P_{prop} = UT \tag{30}$$

$$\varpi_{prop} = \varpi_m = \left(V - IR\right) K_V \tag{31}$$

$$P_{shaft} = P_m = \varpi_m Q = \left(V - IR\right)\left(I - I_0\right) \tag{32}$$

$$\eta_{prop} = \frac{P_{prop}}{P_{shaft}} = J\frac{C_T}{C_P} \tag{33}$$

$$P_{elec} = VI \tag{34}$$

$$\eta_m = \frac{P_{shaft}}{P_{elec}} = \left(1 - I\frac{R}{V}\right)\left(1 - \frac{I_0}{I}\right) \tag{35}$$

$$\eta_{overall} = \eta_m \eta_{prop} \tag{36}$$

For Eqs. (25)-(36) radius is r, advance ratio is J, velocity is U, current is I, voltage is V, torque is Q, thrust is T, power is P, efficiency is η, and C_T and C_P are the coefficients of thrust and power, respectively. With a gear ratio of one-to-one, the rotational speed (ϖ) of the motor and propeller were equal. QPROP required all variables to be in SI units. In satisfying the above equations, QPROP sought to optimize four different parameters: RPM, pitch rate change, thrust, and velocity. As previously mentioned, up to three of these were specified prior to the analysis and held static during

calculations. The QPROP users guide provides additional information on how the equations are used in QPROP operations.[95]

III.1.2.2.1. QPROP Inputs and Outputs

QPROP required three input files to run. The first of these files was the fluid constants file that contained density, dynamic viscosity, and speed of sound. The next file was the propeller file, which included information about the propeller such as chord and blade angle (β) measurements at several positions along the blade, the number of blades, and propeller-specific aerodynamic coefficients. Last, a motor file included values for K_v, R, and I_o. QPROP used these input files to create a range of outputs of which P_{elec} was the most desired; however, other useful results included η, V, I, J, C_T, and C_P. For example, efficiency (η) was used to determine if the motor and propeller were well matched.

III.1.2.2.2. QPROP Propeller File: XFOIL and xflr5

QPROP's analysis required the creation of a propeller file. Drela, the creator of QPROP, provided a guide that described the operations to characterize a propeller blade for QPROP.[96] These directions were modified by making use of a 3D-scanner to obtain a SolidWorks model of the entire propeller. The airfoil shape, chord length, and blade angle were then found using this file. The radial distance, chord length, and blade angle were direct inputs to the propeller file. The airfoil shape required further analysis to obtain aerodynamic coefficients. These coefficients were found using xflr5, a user-friendly GUI that harnessed XFOIL's code.

III.1.2.3. High-Fidelity: Experimental Propeller and Motor Code

The high-fidelity propulsion CA used data collected by WSU specifically to address the issue of the low Reynolds numbers at which MAVs fly. WSU compiled a large database of performance data from small propellers that provided high-fidelity analysis when paired with motor data. In particular, the performance data helped account for propellers that had irregular shape and pitch angles and were therefore hard to model analytically. More information on WSU's propeller database is found in Merchant's paper.[70]

The experimental propeller and motor code took WSU's results, added basic motor constants, and used standard propulsion equations to determine the performance of a given motor and propeller combination. The propeller analysis used Eqs. (37)–(42),

$$C_T = \frac{T}{\rho \cdot n^2 \cdot D^4} \tag{37}$$

$$C_P = \frac{P_p}{\rho \cdot n^3 \cdot D^5} \tag{38}$$

$$C_Q = \frac{Q}{\rho \cdot n^2 \cdot D^5} \tag{39}$$

$$P_P = \Omega \cdot Q \tag{40}$$

$$\eta_P = J \frac{C_T}{C_P} = \frac{T \cdot U'}{P_P} \tag{41}$$

$$J = \frac{U'}{n \cdot D} \tag{42}$$

where n and Ω are rotational velocity (revolutions per second and radians per second, respectively), D is diameter, and C_Q is the coefficient of torque. The set of equations for the experimental propeller and motor code differed from similar equations in QPROP.

For example, QPROP used the radius and the experimental data code used diameter to non-dimensionalize the coefficients and advance ratio. The importance of this difference was to ensure that the inputs into each program aligned to the convention utilized by the software.

The motor equations used in the experimental propeller and motor code were similar to the equations used by QPROP and are shown in Eqs. (43)-(47). More information on how the experimental propeller and motor code worked can be found in Todd Rotramel's thesis.[97]

$$Q = \frac{\left(I - I_0\right)}{K_V} \tag{43}$$

$$Q = \frac{\left(v - I \cdot R\right)}{K_V} \tag{44}$$

$$P_{shaft} = \Omega \cdot Q = \left(V - I \cdot R\right)\left(I - I_0\right) \tag{45}$$

$$P_{elec} = V \cdot I \tag{46}$$

$$\eta_m = \frac{P_{shaft}}{P_{elec}} = \left(1 - I\frac{R}{V}\right)\left(1 - \frac{I_0}{I}\right) \tag{47}$$

III.1.3. Power Management CA

The power management CA determined the amount power that the fuel cell and battery each had to provide. The literature review revealed that fuel cells operated most efficiently when power demands were constant, whereas batteries were capable of handling variable power demands. As a result, each segment had the same power provided by the fuel cell and the remaining power required came from the battery as

expressed in Eq. (48). The power provided by the fuel cell was determined by taking a percentage of the power required for the endurance segment $\left(\%P_{fc,end}\right)$. Since the fuel cell was the energy dense power source, it was helpful to see what percentage of the endurance power it took. With this definition of power management, Eq. (48) changed into the form seen in Eq. (49).

$$\overline{P}_{batt} = \overline{P}_{segment} - P_{fc(const)} \quad \textbf{(48)}$$

$$\overline{P}_{batt} = \overline{P}_{segment} - P_{end} \cdot \%P_{fc,end} \quad \textbf{(49)}$$

The low-fidelity power management CA assumed that the fuel cell took the entire power load during endurance $\left(\%P_{fc,end} = 1\right)$ and the battery was off. The high-fidelity CA left $\%P_{fc,end}$ variable and optimized it based upon the results of the power source CA. In this optimization, the design variable was $\%P_{fc,end}$ and the objective was to maximize endurance duration. The optimization was constrained by both the fuel cell and battery having to have endurance duration greater than or equal to zero. Furthermore, each of the power sources had to have enough energy and power to complete all mission segments based upon what the power management CA assigned.

III.1.4. Power Source CA

The power source CA was the last step in determining the endurance duration. User-specified data on the battery and fuel cell, as well as the segment durations other than endurance, were required for this analysis. Additionally, the segment power was needed from the propulsion CA and the endurance power percentage split from the power management CA. Both levels of fidelity utilized a PEMFC fueled by compressed

hydrogen gas. The low-fidelity CA was a MATLAB script that used specific energy and specific power to determine the endurance duration. The high-fidelity CA was also a MATLAB script that used a polarization curve from a fuel cell and a Ragone plot from a battery to determine the endurance duration.

III.1.4.1. Low-Fidelity: Specific Power and Specific Energy

The process for calculating endurance duration began by determining the power that the fuel cell and the battery needed to provide for each mission segment. This was done by using Eqs. (50) and (51). If any element of $\overline{P}_{batt}$ was less than zero, the battery power was reset to zero, representing a battery that was not in operation.

$$\overline{P}_{fc} = P_{end} \cdot \%P_{fc,end} \tag{50}$$

$$\overline{P}_{batt} = \overline{P}_{segment} - \overline{P}_{fc} \tag{51}$$

The next step was to size the battery to satisfy both power and energy requirements. To size the battery for energy, the energy required from each mission segment was found using Eq. (52) with $\bar{t}_{segment}$ as the duration of each segment and $\overline{P}_{segment}$ as the power of each segment. An initial guess was provided for the endurance duration that would later be iteratively converged to ensure it was the correct duration for endurance and the battery was sized correctly. The mass of the battery was found using Eq. (55) once the battery mass for power and energy were first found using Eqs. (53) and (54), respectively.

$$E_{batt} = \sum \overline{P}_{segment} \cdot \bar{t}_{segment} \tag{52}$$

$$m_{batt,P} = \frac{\max\left(\overline{P}_{segment}\right)}{SP_{batt}} \quad \textbf{(53)}$$

$$m_{batt,E} = \frac{E_{batt}}{SE_{batt}} \quad \textbf{(54)}$$

$$m_{batt} = \max\left(m_{batt,P}, m_{batt,E}\right) \quad \textbf{(55)}$$

The fuel cell mass was determined next. Fuel cells found in the literature review were listed as either "dry" or "wet." The dry mass of a fuel cell implied the mass of the fuel cell stack alone and the wet mass implied the weight of the stack plus the fuel. For lump calculations that used specific energy and power, the wet and dry fuel cell had the same mass. The fuel cell mass depended on the overall power source mass that was determined based on the decision for the percentage of total aircraft weight the power sources could be $\left(\%_{ps,allowable}\right)$ as shown in Eq. (56). With the total mass of the power sources, m_{ps}, the mass of the fuel cell was determined with Eq. (57).

$$m_{ps} = m_{aircraft} \cdot \%_{ps,allowable} \quad \textbf{(56)}$$

$$m_{fc} = m_{ps} - m_{batt} \quad \textbf{(57)}$$

The next step was to determine how much energy was left in the battery and fuel cell after each of the mission segments (with the exception of endurance) were completed. The energy of the battery and the fuel cell were first found with Eq. (52) using the numbers specific to each power source; however, this time the energy was found assuming an endurance duration of zero. The remaining energy in both the battery and the fuel cell were found using Eqs. (58) and (59), respectively. Finally, the total

excess energy $\left(E_{excess}\right)$ found in Eq. (60) was used to determine the endurance time in Eq. (61).

$$E_{batt,excess} = m_{batt} \cdot SE_{batt} - E_{batt,non-end} \quad \textbf{(58)}$$

$$E_{fc,excess} = m_{fc} \cdot SE_{fc} - E_{fc,non-end} \quad \textbf{(59)}$$

$$E_{excess} = E_{batt,excess} + E_{fc,excess} \quad \textbf{(60)}$$

$$t_{end} = \frac{E_{excess}}{P_{end}} \quad \textbf{(61)}$$

The endurance duration was then inserted as the initial guess to size the battery with Eqs. (52)-(55). The code was repeated until the guessed endurance duration and the final endurance duration converged. Once converged, several additional items had to be examined. With lump sum calculations, there was no fuel burn associated with fuel cell operation. As such, the fuel mass was set to zero for the low-fidelity power source CA. Next, the battery and fuel cell had to be checked to ensure they were of adequate size to meet the demands placed on them by the power management CA. The battery size check required only that the battery's mass be smaller than the mass of the power source. Since the fuel cell was not sized in the same manner as the battery, the fuel cell had to be checked to ensure it met energy and power demands. Altogether, Eqs. (62)-(64) each had to be true for the mission to be completed successfully.

$$m_{batt} < m_{powersource} \quad \textbf{(62)}$$

$$E_{fc,excess} > 0 \quad \textbf{(63)}$$

$$m_{fc} \cdot SP_{fc} > \overline{P}_{fc} \quad \textbf{(64)}$$

III.1.4.2. High-Fidelity: Ragone Plot and Polarization Curve

The high-fidelity power source CA began the same way as the low-fidelity analysis: determining the power requirements for both the battery and fuel cell by using Eqs. (50) and (51). A Ragone plot and polarization curve were next created for the battery and fuel cell, respectively (Figure 17). The remainder of the high-fidelity CA sought to find the operating points of the battery and fuel cell or the points on the two curves where the power sources operated during each mission segment to optimize endurance duration. Example operating points are shown as red circles in Figure 17.

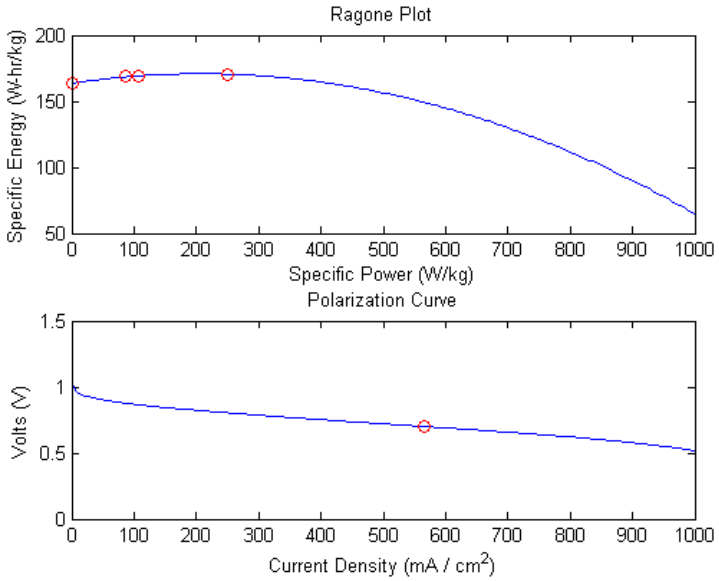

Figure 17. Ragone plot and polarization curve

Finding operating points began with the Ragone plot of the battery. Again, the battery was sized based upon power and energy; however, this time the assumption of the battery operating at peak specific energy and specific power at the same time was removed. The mass of the battery due to power was determined by an initial guess of the battery's specific power and Eq. (65). The energy of the battery for all segments of the

mission, with an initial estimate for endurance duration, was again found using Eq. (52). The mass of the battery from energy requirements was calculated in Eq. (66) using the specific energy that corresponded to the initial guess for specific power on the Ragone plot. The greater of the two masses was then assigned to the battery mass.

$$m_{batt,P} = \frac{\max\left(\overline{P}_{segment}\right)}{SP_{batt,initial}} \tag{65}$$

$$m_{batt,E} = \frac{E_{batt,non-end}}{SE_{batt,inital}} \tag{66}$$

The operating point for each segment was found by determining the specific power of each segment through Eq. (67). The specific energy $\left(\overline{SE}_{Ragone}\right)$ of each point came directly from the corresponding specific power values on the Ragone curve. Based upon the location of the operating point, the efficiency of the battery was found using Eq. (68). The efficiency in Eq. (68) came from seeing how far away the operating point's specific energy was from the maximum specific energy on the Ragone plot

$$\overline{SP}_{Ragone} = \frac{\overline{P}_{batt}}{m_{batt}} \tag{67}$$

$$\eta_{batt} = \frac{\overline{SE}_{Ragone}}{\max\left(\overline{SE}\right)} \tag{68}$$

The endurance duration was reset to zero to determine the correct amount of energy used. The battery energy burn $\left(\Delta\overline{E}\right)$ was determined using Eq. (69). The excess energy in the battery and the endurance duration provided by the battery was calculated using Eqs. (70) and (71), respectively.

$$\Delta\overline{E}_{batt,non-end} = \frac{\overline{E}_{batt,non-end}}{\eta_{batt}} \tag{69}$$

$$E_{batt,excess} = m_{batt} \cdot \max\left(\overline{SE}\right) - \sum \Delta\overline{E}_{batt,non-end} \tag{70}$$

$$t_{batt,end} = \frac{E_{batt,excess}}{P_{end}} \tag{71}$$

The fuel cell calculations began with an estimate for the operating voltage $\left(V_{inital}\right)$ of the fuel cell. From this estimate, a corresponding current density $\left(i\right)$ was taken from the polarization curve. These two values were used to calculate the power per area of the fuel cell in Eq. (72). Knowing the power per area of the fuel cell, the total number of cells in the fuel cell stack was determined with a user-specified area per cell $\left(A_{fc}\right)$ and Eq. (73). The number of cells, *N*, in the fuel cell stack, along with information on the fuel cell's mass specifics, provided an estimate for the fuel cell's dry mass in Eq. (74). Here, m_{cell} is the mass of each cell, m_{casing} is the mass of the casing around the fuel cell, and $f_{bop,tank}$ is a weight factor to account for the mass of the compressed hydrogen tank and BOP.

$$P_{fc,area} = V_{inital} \cdot i \tag{72}$$

$$N = \frac{P_{fc} / P_{fc,area}}{A_{fc}} \tag{73}$$

$$m_{fc,dry} = f_{bop,tank}\left(N \cdot m_{cell} + m_{casing}\right) \tag{74}$$

The total mass of the power source described in Eq. (56) along with the mass of the battery and the dry mass of the fuel cell were used with Eq. (75) to calculate the mass

of compressed hydrogen. The energy the fuel cell provided from the stored hydrogen was found by first calculating the efficiency of the fuel cell $\left(\eta_{fc}\right)$ in Eq. (76), where *V* was the voltage at which the fuel cell was operating and *E* was the voltage of a perfectly efficient system in reference to the higher heating value (HHV). The value of 0.95 for fuel efficiency came from a published value for a PEMFC.[98] The fuel burn of the fuel cell could then be found using Eq. (77), where $SE_{hydrogen}$ is the specific energy of hydrogen gas. Finally, the endurance duration provided by the fuel cell was calculated using Eq. (78) and the total endurance energy of the aircraft was found using Eq. (79).

$$m_{fuel} = m_{powersource} - m_{batt} - m_{fc,dry} \tag{75}$$

$$\eta_{fc} = \eta_{fuel} \cdot \eta_{voltage} = 0.95 \cdot \frac{V}{E} \tag{76}$$

$$\Delta\overline{E}_{fc,non-end} = \frac{\overline{E}_{fc,non-end}}{SE_{hydrogen} \cdot \eta_{fc}} \tag{77}$$

$$t_{fc,end} = \frac{\eta_{fc}\left[\left(m_{fuel} - \sum \Delta\overline{E}_{fc,non-end}\right) SE_{fuel}\right]}{P_{end}} \tag{78}$$

$$t_{end} = t_{batt,end} + t_{fc,end} \tag{79}$$

The endurance duration was then inserted as the initial guess to size the battery in Eqs. (52)-(55). The code was repeated until the guessed endurance duration and the final endurance duration converged. Furthermore, the initial guesses for the specific power of the battery and the operating voltage of the fuel cell were iterated until the endurance duration was at a maximum. Once endurance duration was maximized, several additional items had to be examined. Mass burns for each segment were calculated and then a

convergence loop was used to ensure that earlier mission analysis from the aerodynamic CA and propulsion CA were adjusted to reflect the correct mass of the aircraft. Next, the battery and fuel cell had to be checked to ensure they were of adequate size to meet the demands placed on them by the power management CA. The battery size check was the same as in the low-fidelity power source CA. Since the fuel cell was sized to meet power demands by increasing or decreasing the number of cells, only the energy demands of the battery had to be examined. This requirement was satisfied if the endurance duration provided by the fuel cell found in Eq. (78) was greater than zero.

III.2. Model Center

Model Center (MC) provided the integration of all CAs through a graphical user interface that controlled the data automation and linkage of one piece of software to the next. MC models fell into two categories: process and data models. Both models had strengths and weaknesses, but for data flow automation, the process model was the most helpful. For this reason, the model created in this endeavor utilized a process model. A process model allowed for the use of if-statements and while-loops directly in the MC environment. An example of the MC user environment is shown in Figure 18.

Script files were written in VBScript and placed directly into the MC environment to manipulate data. Before integrating the CAs into MC, it was imperative for all files to be in the same folder that was made known to Analysis Server (AS). AS is a program that came complimentary with MC and ran in the background to assist with the linkage between certain aspects of the model. Since MC referenced files by their location on the

hard drive, keeping them in the same folder removed the need to search for a specific file every time MC was opened on the same or even different machines.

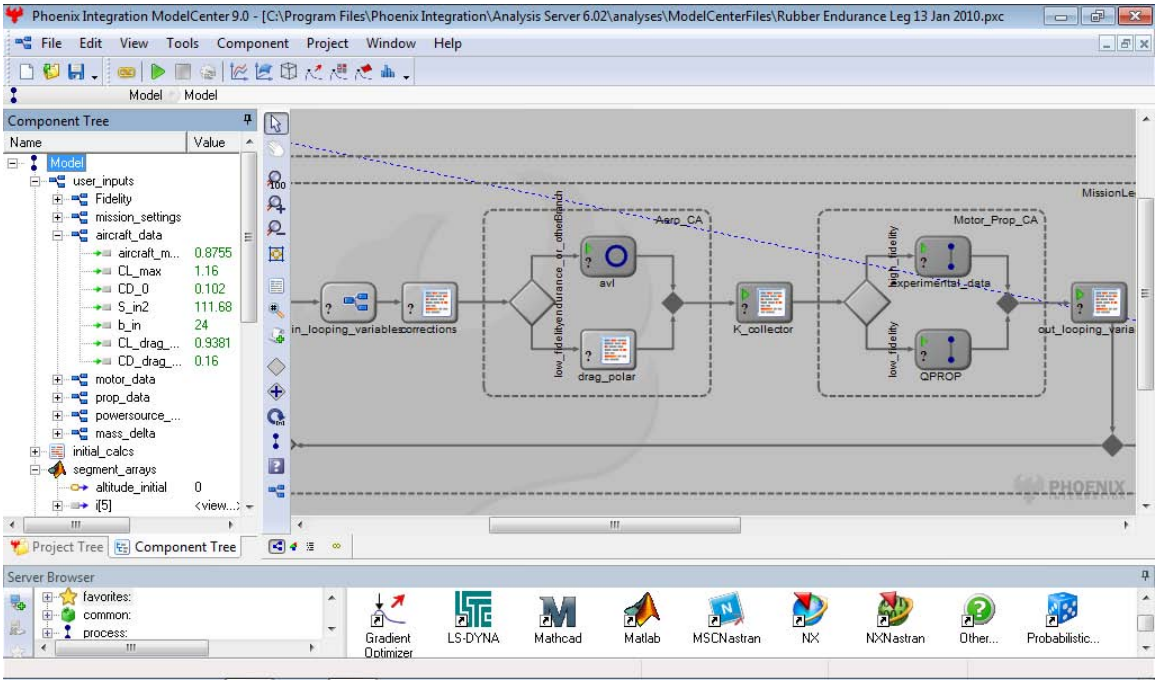

Figure 18. MC user environment

The integration of the CAs into MC depended on the program or software used to create the CA. Popular applications including MATLAB, Microsoft Excel, Mathcad, and various CAD programs had built-in tools within MC called plug-ins that assisted in connecting the inputs and outputs of each program. For other applications and codes, a file-wrapper was required to connect to MC. File-wrappers functioned as a MC plug-in for the software for which it was written. Once all the applications and software pieces were placed into MC, the inputs and outputs of each component were connected using the link editor (Figure 19).

Knowing how MC operates allows for the specifics of the model to be addressed as well as how each CA was integrated into the MC environment. Overall, the entire

model (Figure 20 and Figure 21) closely resembled the flow chart shown at the beginning of this chapter (Figure 15). Due to the size of the model, the layout was broken into two different pieces that connect at the red dot.

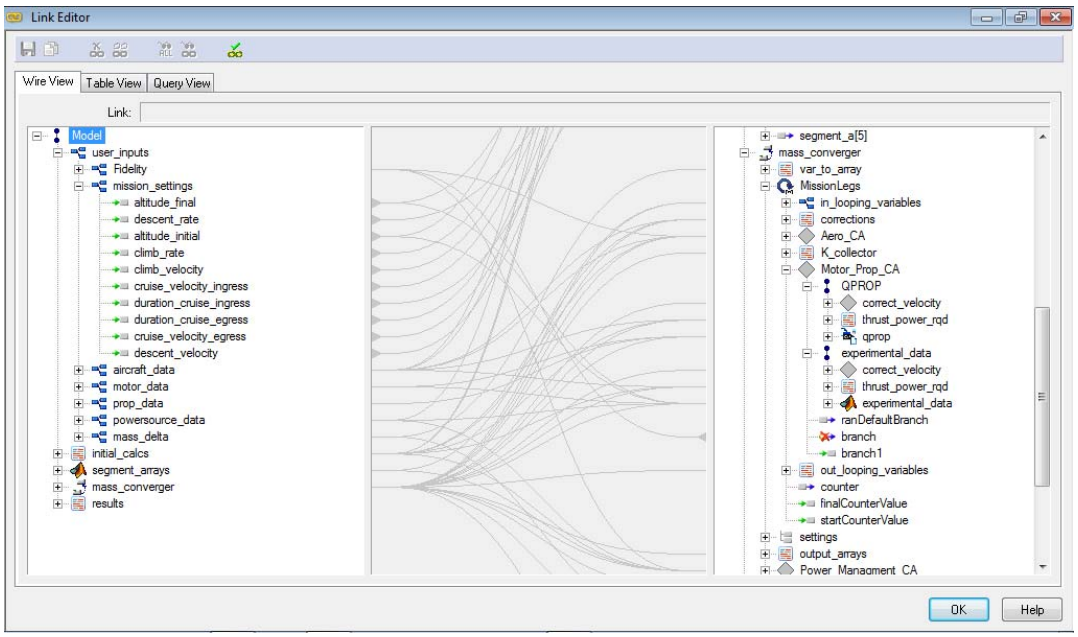

Figure 19. Model Center link editor

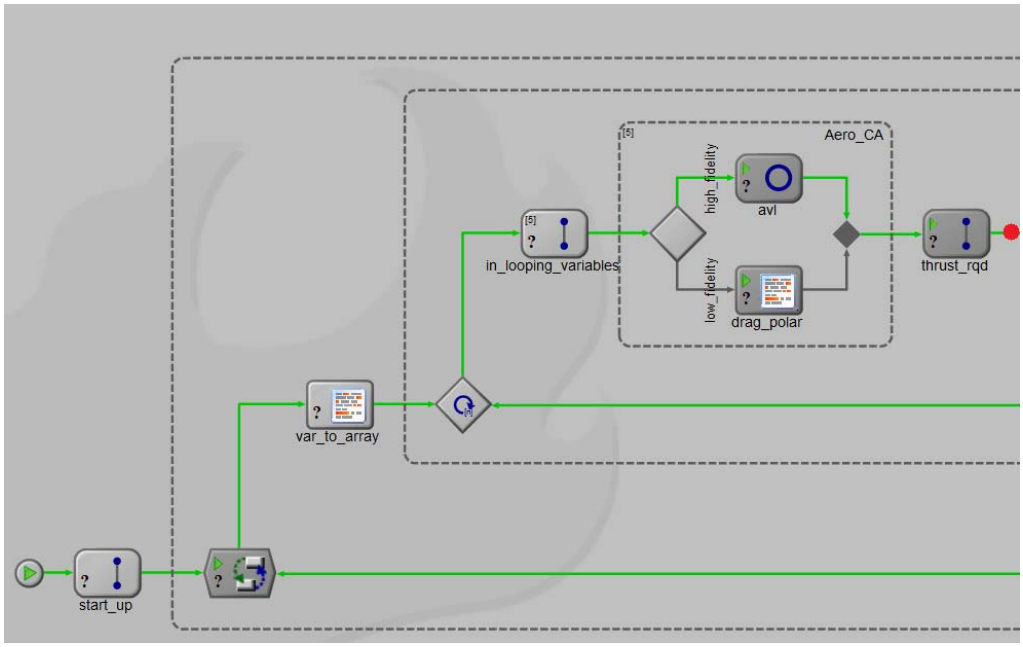

Figure 20. The entire MC model (left side)

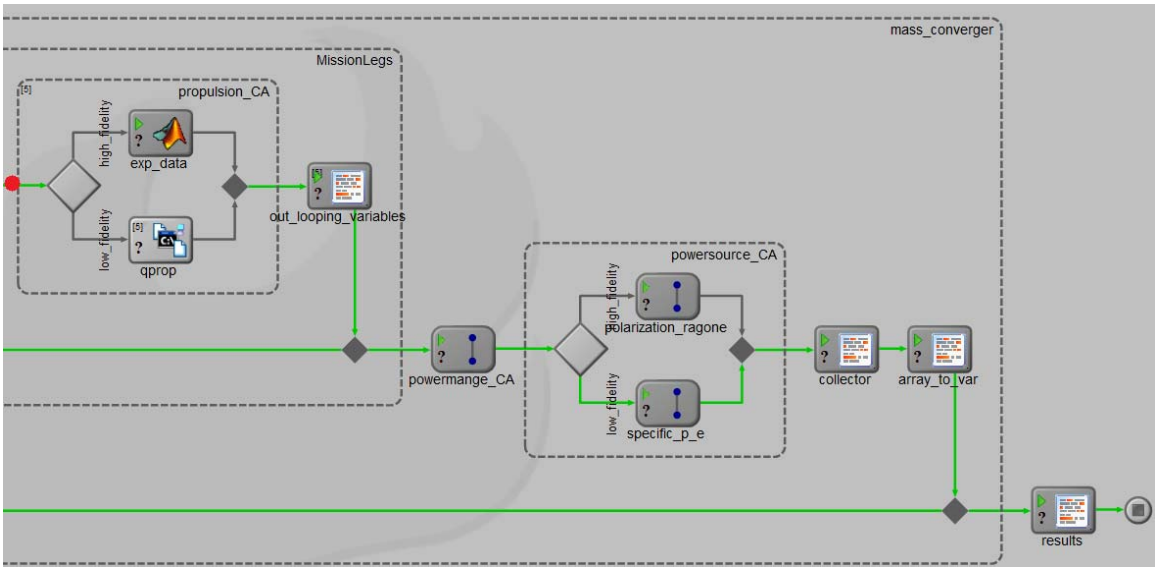

Figure 21. The entire MC model (right side)

III.2.1. Initial Calculations

The model began its analysis in the "start_up" sequence that first called for user inputs stored in blocks called assemblies, as seen in the first component of Figure 22. User inputs included fidelity selection, mission settings, and data about the aircraft, motor, propeller, and power sources. Initial calculations were performed in the script file (second component of Figure 22) by converting variables to the correct units and calculating readily available information such as aspect ratio. Arrays of mission segment data were created using a MATLAB plug-in (third component of Figure 22) to be passed into the model's mission analysis that used a process model for-each loop.

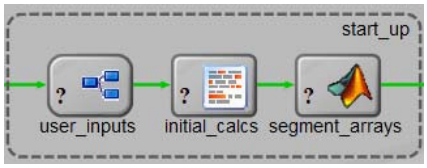

Figure 22. The start up sequence of the model

III.2.2. Integration of the Aerodynamic CA

The aerodynamic CA began the mission analysis. Before going into the low- or high-fidelity analysis, a script file was used to check the stall velocity. An if-block from a MC process model selected the fidelity for the aerodynamic CA (Figure 23). The low-fidelity drag polar calculations were performed completely in a script file, whereas the high-fidelity analysis required significant programming within MC as Figure 24 suggests.

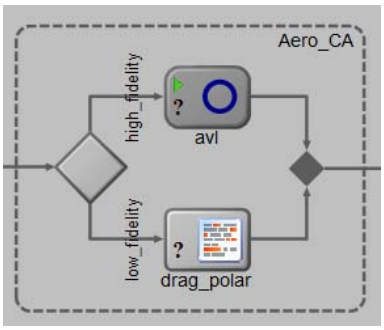

Figure 23. Aerodynamic CA in MC

Within the AVL analysis, an additional if-block determined if the segment was endurance or non-endurance. For non-endurance segments, a file-wrapper was used to execute AVL with AS assistance. The file-wrapper told MC what files AVL required in the form of "bat" files that contained command prompt inputs and "batch" files that dictated the sequence of operations. To assist the process, MC required "template" files, which served as a guide for where to insert the run-case data. The output of AVL for span efficiency factor, *e*, was sent to the "post-processing" component to convert the value to the drag polar coefficient, *K*. The value for *K* was sent to a "collector" script file to allow the model to continue analysis regardless of which fidelity was selected. These components made up the non-endurance, high-level aerodynamic CA.

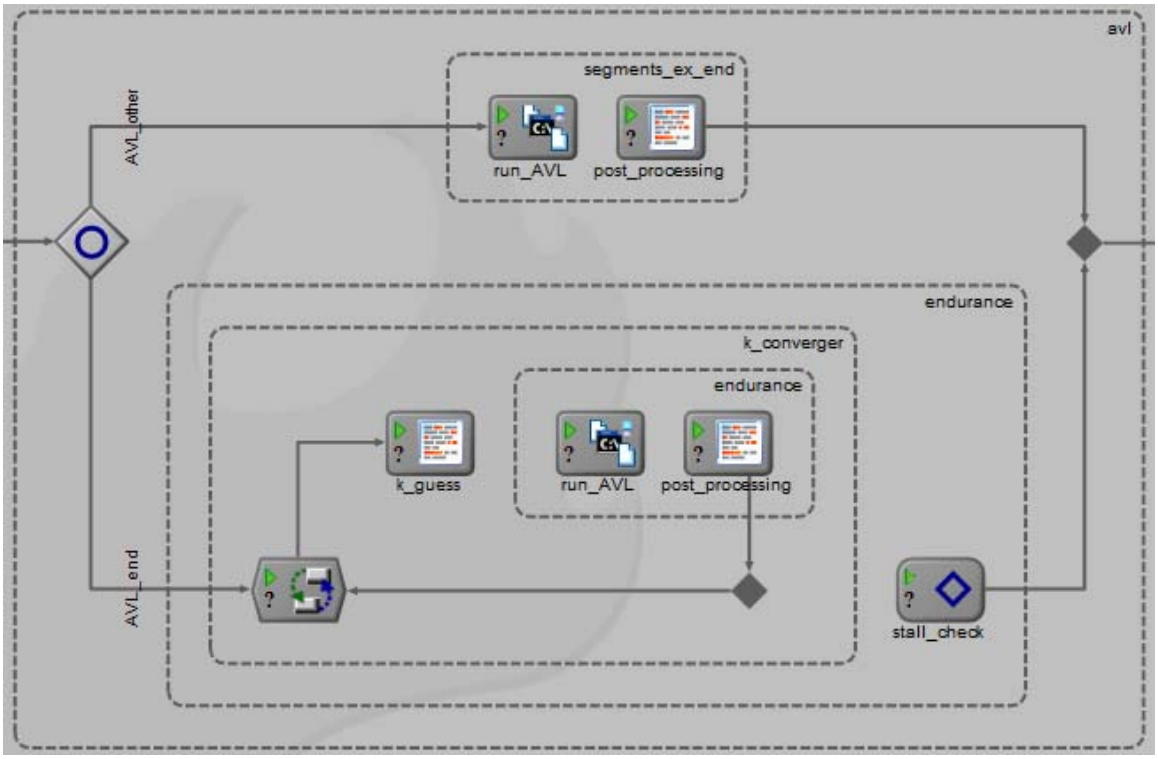

Figure 24. AVL analysis within MC

The same basic components were used for the endurance segment, but additional computation was required because of the interdependence between endurance velocity and the drag polar coefficient. To determine the correct value for each of these variables, MC's "converger" tool was used. This tool assumed an initial *K* value and iterated until the *K* value satisfied both the endurance velocity calculation and AVL's output. A final if-block ("stall check") ensured that the endurance velocity was not below the stall velocity. The final *K* was again stored in the collector script file.

III.2.3. Integration of the Propulsion CA

Before the propulsion CA executed, the aircraft thrust and power required was calculated with a script file (first component of Figure 25). The propulsion CA started with an if-block to execute the level of fidelity specified for the propulsion CA. The low-

fidelity path utilized QPROP with a file-wrapper. The high-fidelity path used a MATLAB plug-in to run the experimental propeller and motor code.

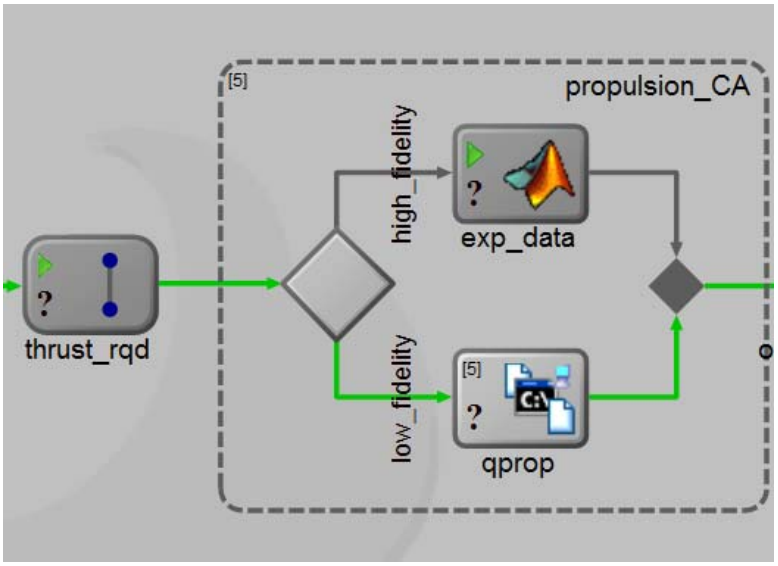

Figure 25. Propulsion CA in MC

III.2.4. Integration of the Power Management CA

The power management CA followed the mission analysis conducted in the aerodynamic and propulsion CAs. First, a script file was used to collect all the necessary data from the mission analysis (first component of Figure 26). The second script file was used to determine the power split based on $\%P_{fc,end}$. This script file left $\%P_{fc,end}$ as an input that either could be set at one for the low-fidelity CA or optimized using a parametric study for the high-fidelity CA.

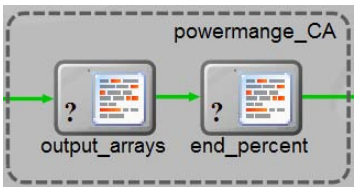

Figure 26. Power management CA in MC

III.2.5. Integration of the Power Source CA

The power source CA began with an if-block to determine the desired fidelity (Figure 27). The low-fidelity track consisted of a MATLAB plug-in that ran the code written for specific power and energy that used a converging routine to ensure the initial guess for endurance duration was correct. After the converging routine completed, the "size-check" script file ensured that the fuel cell and battery were large enough to meet the demands placed on them by the power management CA. The high-fidelity track also used a MATLAB plug-in, but ran the Ragone plot and polarization curve code. A converging routine and a script file to check the size of the battery and fuel cell were also included in the high-fidelity analysis. A DOE was used to vary the initial guesses for specific power of the battery and starting voltage of the fuel cell to optimize endurance duration.

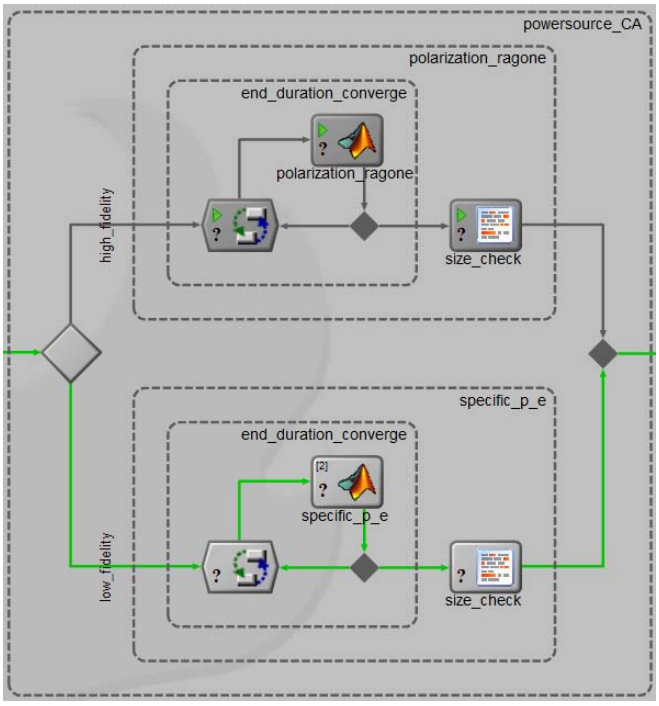

Figure 27. Power Source CA in MC

III.2.6. Model Center Studies

MC provided an environment to validate the results with two main trade study tools: parametric studies and design of experiments (DOE). Both tools provided numerical and visual results that helped interpret the model's findings. The parametric study took one input variable, swept it through a given range, and captured the results of any number of output variables in the form of a parametric plot. This provided a method to identify trends, confirm published trends, and locate areas for optimization. The parametric study turned into a carpet plot or a two-dimensional parametric study if two input variables were used. The carpet plot provided increased detail on variable dependency and constraint effects when compared to the parametric plot. In some scenarios, parametric studies and carpet plots poorly portrayed aspects of the model. In these scenarios, a DOE provided a robust tool to investigate the model's response.

A DOE statistically illustrated the variables that were most important to the model's results. With a DOE, any number of input variables could be tweaked to see the results of any number of output variables. The algorithm that the DOE used was selected by the user and could be chosen from twelve different options. The default and sometimes most effective algorithm was the full-factorial method. The best way to determine if the algorithm was effective or not was to view the results of the DOE. Additionally, some DOE algorithms led to extensive iteration and time management had to be taken into account. A glyph plot was a helpful visualization of the DOE's results. This plot communicated multivariable effects by showing numerous variables on one plot. To validate the model, all three of these studies were examined.

III.3. Validation Platform

Chapter 2 presented a wide variety of MAV platforms of greatly varying traits. The AFRL Munitions Directorate created a test MAV known as the GenMAV to directly deal with the issue of the numerous kinds of MAVs and serve as a baseline for future collaboration. The availability of information on the GenMAV, as well as its potential for further investigation, made it the perfect candidate for model validation in Chapter 4. The GenMAV 2, shown in Figure 28, was the second generation of AFRL's attempt and it added an articulated wing to increase aerodynamic control.[99] The GenMAV 2 had a wingspan of 60.0 cm (23.6 in), a chord length of 12.7 cm (5 in), and a mass of 1.018 kg (2.24 lbs). The GenMAV used an AXI 2808/20 motor and a Graupner CAM 8x4.5" folding propeller (Figure 29).[100,101]

Figure 28. GenMAV 2

Figure 29. Propeller (left) and motor (right) of the GenMAV 2

III.4. Chapter Three Summary

Chapter 3 discussed what tools were used to build the model of an EPMAV and how they were integrated in MC. Chapter 4 examines each of the tools used and provides verification and validation for the results they produced. After each of the tools has been validated, the entire model is used to perform mission simulations that show the capabilities of an electrochemically-powered GenMAV. The mission simulations focus on the endurance capabilities of the GenMAV, but also investigate the results of the CAs other than the power source CA. To conduct mission simulations, inputs detailing mission specifics such as velocities, elevations, and durations are required. A schematic in Figure 30 shows the details of the "rubber endurance" mission that is typical of MAV flight.

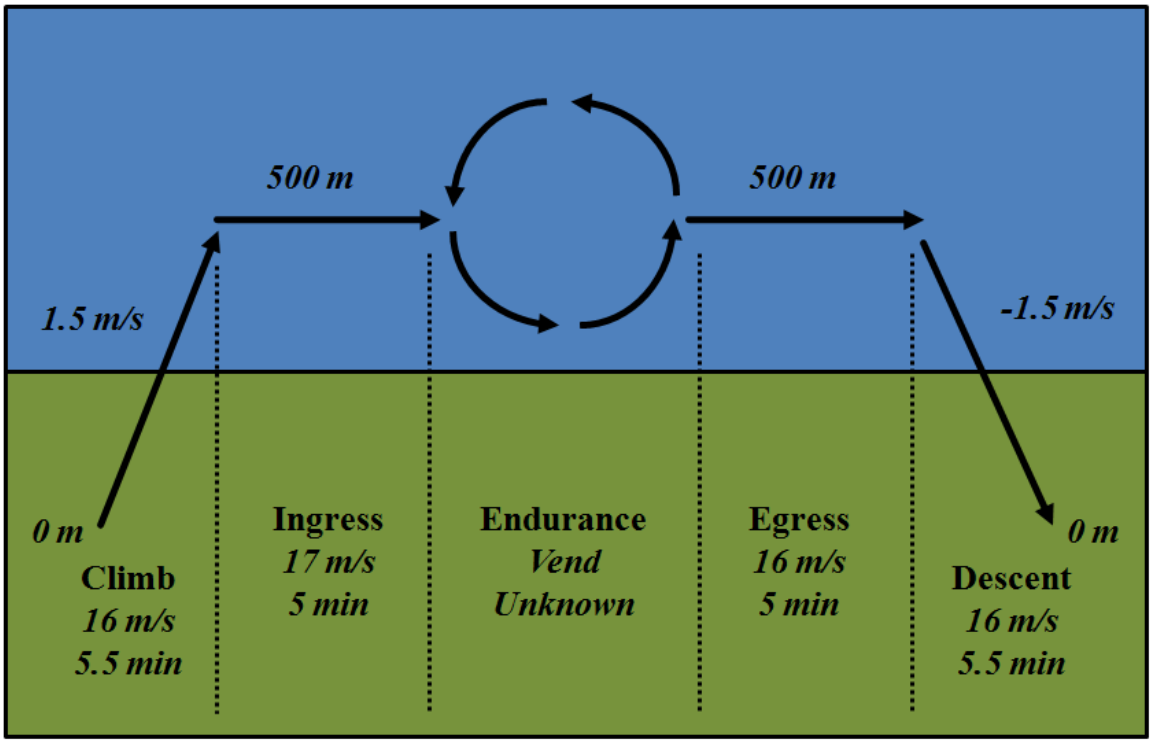

Figure 30. Mission profile for analysis

IV. Analysis and Results

The analysis and results section first looks at each of the four areas of CA and provides validation and verification (V&V) for each level of fidelity in the CA. Mission simulations using the entire model provides V&V for the entire effort and furthermore gives the results that show the capabilities and traits of an EPMAV in flight.

IV.1. Validation and Verification

The outcome of the entire model depended on the successful operation of each CA. Each CA had to be checked that it operated as designed and produced results that matched expectations based upon published data. *Verification* efforts checked that the item of interest operated as designed. *Validation* implied a confirmation that the results were accurate. MC served as the central tool to conduct V&V.

IV.1.1. Aerodynamic CA

For the aerodynamic CA, the most important result was the value for the drag polar coefficient, K. The value for span efficiency factor, e, was directly related to K. Using parametric studies, changes were made to the inputs of the aerodynamic CA to determine the effect on e or K. Verification of these tools came from the changes leading to the predicted trends. Validation for both levels of fidelity came from published data and research conducted by AFRL/RWAV on the GenMAV 2. The inputs used to perform the V&V came from the ingress leg of the mission profile, as well as drag polar data from Hrad's findings and AVL geometry from AFRL/RWAV.

IV.1.1.1. Drag Polar

Drag polar theory was straightforward and allowed for quick verification beginning with a visual inspection of the drag polar created. Essentially, the drag polar should look the exact same as the one used to provide the inputs to the analysis. Drag polar data for verification was available only from the results of Hrad's analysis.[24] The resulting drag polar shown in Figure 31 matched expectations based on findings from Hrad's aerodynamic calculations.

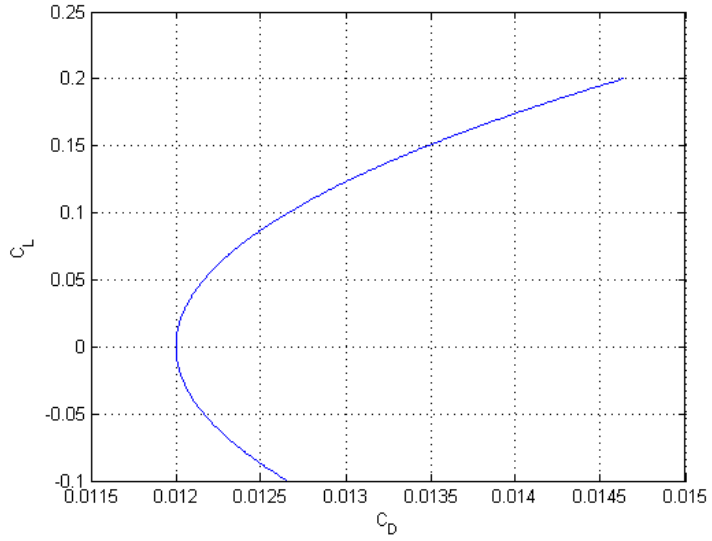

Figure 31. Drag polar from the low-fidelity aerodynamic CA

The curve was created from Eq. (9) with a *K* value of 0.0659 and a zero-lift drag coefficient of 0.0102. The value for zero-lift drag coefficient came from wind tunnel tests at AFRL/RWAV. This corresponded to a span efficiency factor of 0.936 or 93.6%. A span efficiency factor this high indicated the drag polar calculations might be optimistic compared to Raymer's estimation of values between 70% and 85%; however, Raymer also suggested the use of Eq. (80), which provided an empirical estimate for the span

efficiency factor of a straight wing aircraft given an aspect ratio. [102] With an aspect ratio of 5.16, a span efficiency factor of 90.0% was predicted with Eq. (80). Compared to this calculation, which was based on actual aircraft data, the percent error of the span efficiency factor found through drag polar analysis was 4%.

$$e = 1.78\left(1 - 0.045 * AR^{0.68}\right) - 0.64 \quad \textbf{(80)}$$

A parametric study swept a range of drag coefficients to determine the response of span efficiency factor. As predicted, increased drag coefficient values led to reduced span efficiency factors (Figure 32). This examination indicated that the code worked as expected.

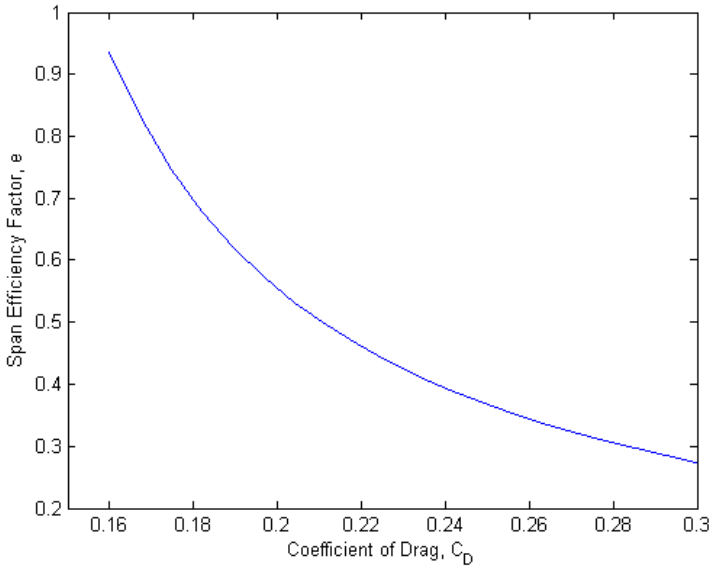

Figure 32. Drag polar parametric study sweeping C_D

IV.1.1.2. AVL

The same general process used for the drag polar V&V was used for AVL. In addition to mission details such as velocity and altitude, AVL called for a maximum lift

coefficient. Wind tunnel tests from AFRL/RWAV predicted this value to be 1.16.[24] The resulting drag polar from AVL's analysis had a *K* value of 0.0665 and the same zero-lift drag coefficient that the low-fidelity CA used (Figure 33).

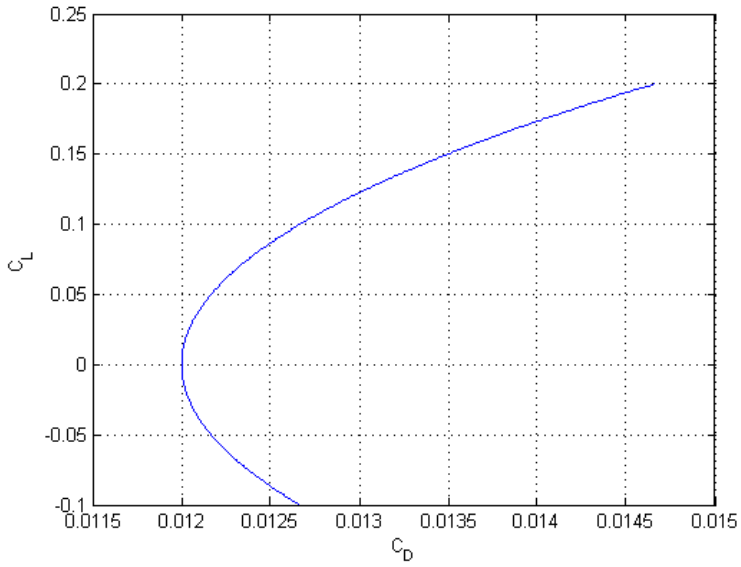

Figure 33. Drag polar from the high-fidelity aerodynamic CA

The drag polar and *K* value matched Hrad's findings, which was expected because the same AVL files were utilized. Furthermore, the percent error in the *K* values between the low-fidelity drag polar calculations and the high-fidelity AVL analysis was less than 0.1%. This was also expected because the drag polar data used in the low-fidelity V&V was only available from the drag polar created by Hrad's efforts in AVL. The span efficiency factor found through AVL was 0.927 or 92.7%. This value was close to suggested values from Raymer and had a percent error of 3% from the result predicted in Eq. (80).

Parametric studies were also conducted on the AVL results. A range of velocities was swept to determine the changes to span efficiency factor and power required (Figure 34).

The velocities ranged from 13.5 m/s (22.4 mph) to 20 m/s (44.74 mph). For velocities less than approximately 13.5 m/s, AVL failed to converge due to the required lift being greater than the maximum coefficient of lift. For MAV flight, speeds higher than 20 m/s were not explored because of the high power demands they required. The parametric studies showed that velocity changed the span efficiency factor found with AVL's analysis, but all of the values were between 92% and 95%. The change in span efficiency factor as well as an increased velocity affected the results for power required. As expected, higher velocities led to greater power required. The flat portion at the beginning of the power required curve was due to the velocity being reset to the stall velocity, which was equal to 15.8 m/s (35.34 mph).

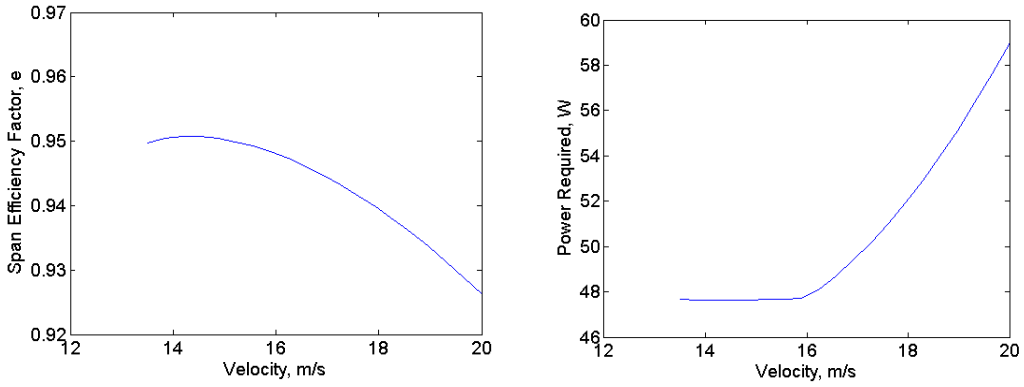

Figure 34. Parametric study results for velocity sweeps in AVL

Validation for AVL was found in the literature for other MAV configurations. AVL provided accurate and robust results for a MAV's aerodynamics from the DARPA MAV competition.[63, 64] Though these findings were not for the GenMAV's geometry, they provided validation for the AVL code. Unfortunately, AFRL/RWAV was still in the process of validating their AVL model for the GenMAV at the time this paper was written.

IV.1.2. Propulsion CA

The most important result from the propulsion CA was the electric power required; however, other findings were important for complete V&V. Various results from both levels of fidelity could checked against calculations from non-derived variables to provide verification. The calculations performed to conduct V&V used the same inputs discussed in the aerodynamic CA. They also utilized a QPROP propeller file made for the Graupner 8x4.5" folding propeller and data from static tests at WSU of the same propeller for the low- and high-fidelity CA, respectively. Additionally, both the low- and high-fidelity tracks used motor constants from the AXI 2808/20.

IV.1.2.1. QPROP

Verification of QPROP came from checking its outputs against calculations from non-derived variables including velocity, power, density, and RPM. Values for parameters including advance ratio, propeller efficiency, and motor efficiency were calculated in MATLAB using Eqs. (25)-(36). Verification would occur if the independent calculations matched the values that QPROP found. The efficiencies of the motor and propeller were key to determining the correct electric power and therefore were examined to verify QPROP's results (Figure 35). The results from these independent calculations in MATLAB aligned perfectly with QPROP outputs. The high correlation between independently calculated results and QPROP showed that QPROP acted as expected. Furthermore, the trends found for the QPROP propeller matched the results presented by Merchant.[70]

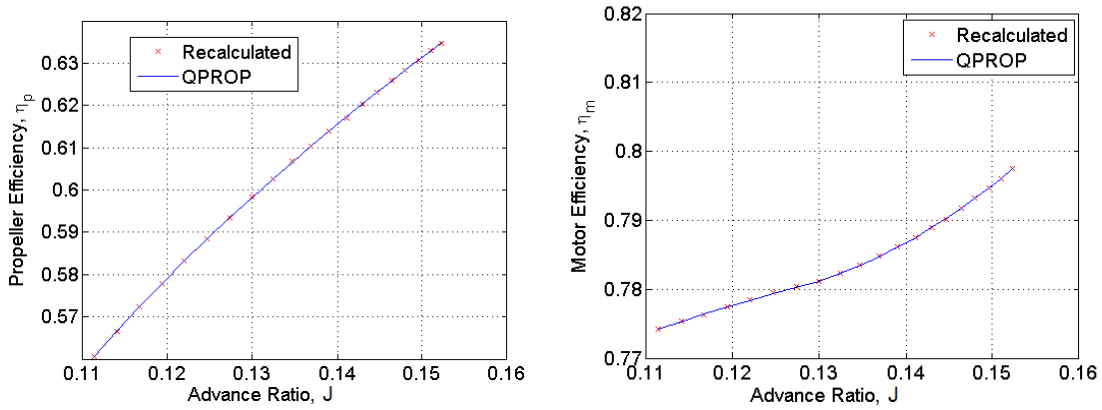

Figure 35. QPROP propeller (left) and motor efficiency (right)

The validation of QPROP began with examples in the literature for the propeller's efficiency. A study examining small RPA at low Reynolds number regimes showed that QPROP over-predicted the efficiencies of propellers by approximately 10-15%.[103] The size of this error was less than ideal, but still allowed for adequate predictions in the conceptual design stage. Finally, the efficiencies found in QPROP were slightly better (2-3%) than Hrad's results.[24] The difference in efficiencies was the result of different propeller files being used in QPROP. It was encouraging to see an increase in propeller efficiency when a propeller file created from the actual propeller was used as opposed to one that was extrapolated from a smaller propeller as was used in previous efforts.

The efficiency of the motor was also important to validate. One previous study created a model for small motors in MAVs and validated it with experimental results. The investigation yielded two relevant pieces of information. First, the experimental results indicated that the maximum motor efficiency was approximately equal to 80%. Second, the model for motor efficiency was the least accurate of all the predictions, which a predicted maximum efficiency of 68-80%.[67] The motor efficiencies found in

QPROP fell between 77% and 80%, which aligned well with the investigation's findings. Furthermore, one manufacturer's webpage listed the efficiency of the AXI 2808/20 at 77%.[101] Overall, QPROP's predictions for propeller and motor efficiency fell well within an acceptable region based upon the results of available investigations.

IV.1.2.2. Experimental Propeller and Motor Code

Similar to QPROP, verification of the experimental propeller and motor code came from comparing its results to calculations from non-derived variables including velocity, power, density, and RPM. Values for advance ratios, coefficients, efficiencies, and power values were calculated using Eqs.(37)-(47) in a separate MATLAB file. The results from these independent calculations matched the findings from the experimental propeller and motor code (Figure 36). The high correlation between the two results confirmed that the code behaved as expected.

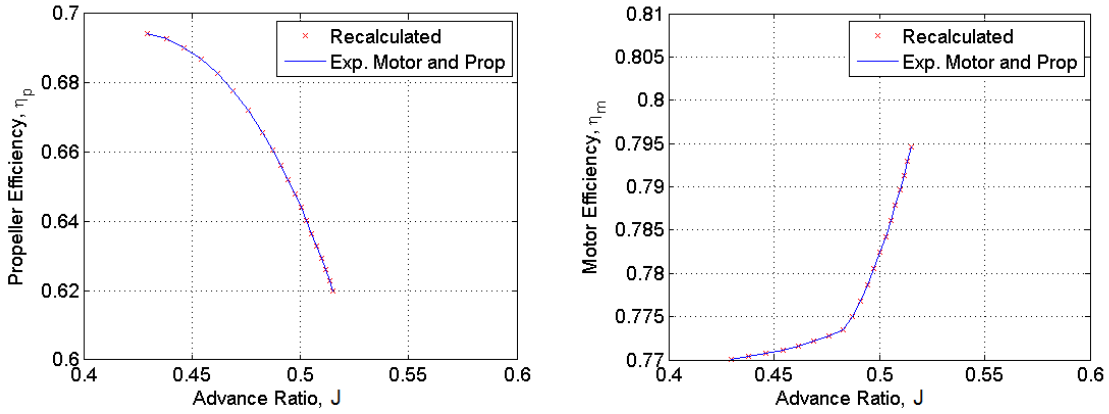

Figure 36. Experimental propeller and motor code efficiency results

The validation of the experimental propeller and motor code began with examples in the literature for propeller efficiency. A study from the University of Illinois at Urbana-Champaign (UIUC) examining 9- to 11-in propellers at low Reynolds numbers

showed propeller efficiencies from approximately 28% to 65%.[104] This study looked at almost 80 propellers and represented the most substantial results for MAV-sized propellers. From the experimental propeller and motor code, propeller efficiency ranged from 62% to 69%. These efficiencies were at the top end and slightly above the best efficiencies found in the MAV propeller study. A comparison between the trends of propeller efficiency found for the Graupner 8x4.5" and a similar propeller from the UIUC study showed that this was a feasible result (Figure 37).[105] Both curves used Reynolds numbers under 10^5, which was typical of MAVs. Overall, this comparison implied that the propeller the GenMAV used was a highly efficient propeller.

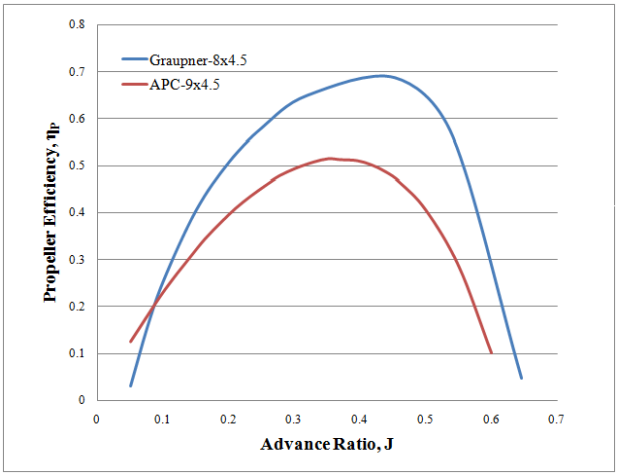

Figure 37. Experimental propeller efficiency comparison

The motor efficiency was compared to the study discussed earlier on MAV motor modeling. The study suggested that the maximum efficiency of a similar sized motor was approximately 80%. This compared to the experimental motor and propeller results which ranged from 77% to 79.5%. The motor efficiency found from the experimental propeller and motor code was also compared to the results from QPROP. QPROP

predicted motor efficiencies between 77% and 80%, which was almost exactly the same range as what the experimental propeller and motor code found (Figure 39).

The last area for validation came from comparing the high-fidelity experimental propeller and motor results to the low-fidelity QPROP results. The most significant areas to examine were the propeller efficiency, motor efficiency, and the resulting electric power (Figure 38-Figure 40). Of these comparisons, the electric power required has the most influence on the analysis that follows the propulsion CA.

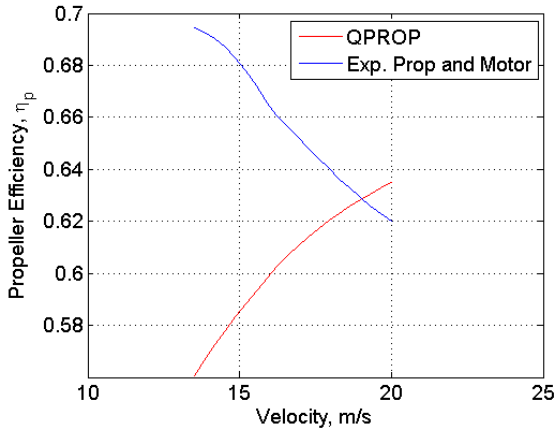

Figure 38. Propulsion CA propeller efficiency comparison

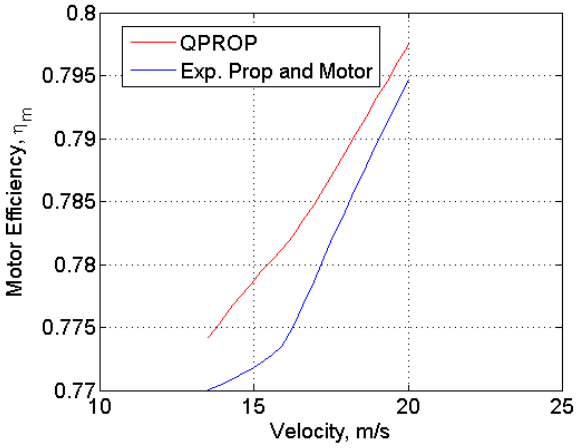

Figure 39. Propulsion CA motor efficiency comparison

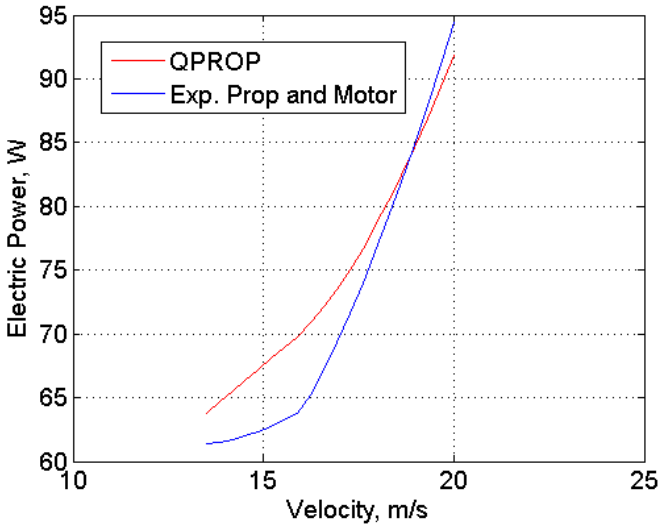

Figure 40. Propulsion CA electric power comparison

The comparisons between the two fidelity options for the propulsion CA showed similar trends for the motor efficiency and electric power results; however, the two propeller efficiency curves showed an inverse relationship over the range of velocities examined. The reason for this effect were the operating points the two different codes utilized on the propeller efficiency curve shown in Figure 37. QPROP operated at lower advance ratios (or the right side of the efficiency curve peak) than the experimental propeller and motor code (left side of the efficiency curve peak), which led to the trends seen in Figure 38. The difference in advance ratio came directly from the difference in the rotational velocity of the propeller (RPM) shown in Figure 41. QPROP's higher rotational velocity led to lower advance ratios and ultimately the different trend seen for propeller efficiency. Overall, the relative closeness of the electric power results in Figure 40, showed the similarity between the two levels of fidelity.

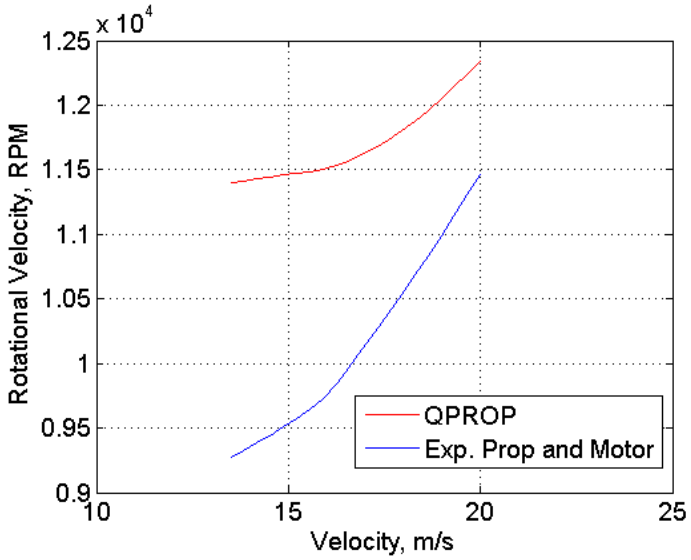

Figure 41. Propulsion CA RPM comparison

IV.1.3. Power Management CA

The V&V of the power management CA was straightforward and did not require outside sources or parametric studies. The low-fidelity power management CA simply turned off the battery so the fuel cell operated alone during the endurance segment. The result was verified by confirming the battery did not provide any assistance to the fuel cell in the endurance segment. Though not replicated here, the low-fidelity power management CA performed as expected. The high-fidelity power management CA sought to find the optimal percentage of endurance power the fuel cell handled. A MC parametric study that searched for the maximum endurance over a wide range of potential power differentials verified that an optimal split was found. An example that provides verification of the high-fidelity power management CA is shown in Figure 42. The results indicated that endurance durations increased as the fuel cell took more of the power load; however, at percentages over 14.3%, the fuel cell was unable to handle the

power demands. Further results of the optimal percentage are included in the mission simulations later in this chapter.

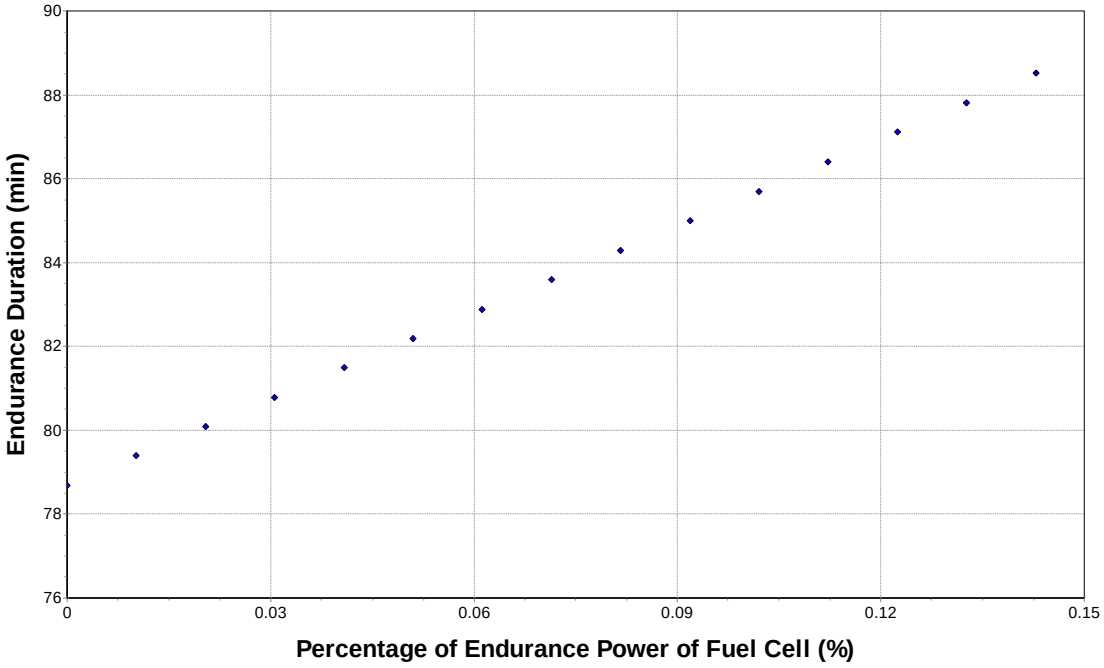

Figure 42. High-fidelity power management CA verification

IV.1.4. Power Source CA

The power source CA's V&V was critical to the validity of the model's results. Examining the effect on endurance duration as electric power required changed provided verification for both levels of fidelity. Validation, on the other hand, required published results or experimental results for comparison. A comparison of this kind was only available by taking the results of the low- and high-fidelity power source CA and comparing them against each other.

IV.1.4.1. Specific Power and Energy Code

The specific power and energy code used equations based on specific energy and specific power to calculate endurance duration. The most direct way to verify that these equations worked as expected was to modify the electric power required and view the response of the endurance duration. For this examination, only the power required during the climb segment was increased. As expected, increased power demands led to lower endurance durations (Figure 43).

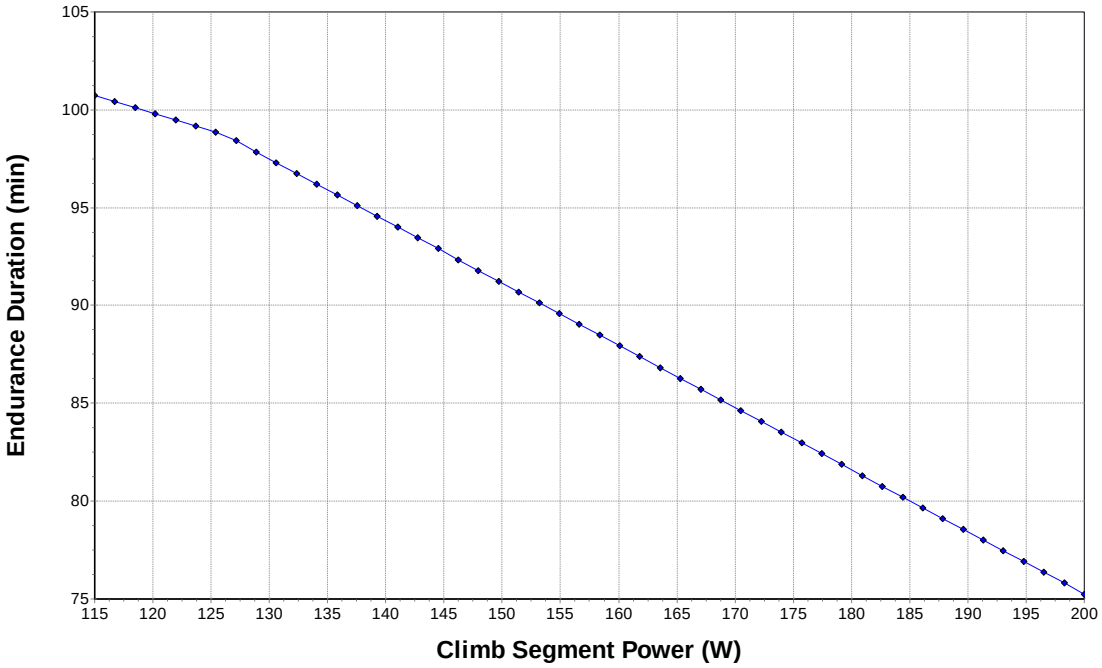

Figure 43. Verification of low-fidelity power source CA

Validation of the specific power and energy code was available only through comparison to the high-fidelity polarization curve results, which are presented in the simulation results later in this chapter. Further validation for the specific power and

energy code would come from future flight-tests through AFRL/RWAV or a test vehicle developed by AFIT.

IV.1.4.2. Ragone Plot and Polarization Curve Code

The Ragone plot and polarization code was a novel approach for dealing with the efficiencies of fuel cells and batteries that can be found with Ragone plots and polarization curves. Again, verification came from modifying the electric power required in the climb segment to see the changes of endurance duration. As expected, increased power demands led to lower endurance durations (Figure 44). This finding provided a basic verification for the code. It should be noted that the endurance durations shown in the plot were extremely high and not meant to serve as an indication for the capabilities of the GenMAV configuration. The values for power during climb were reduced to values below the actual power required for climb only to show that the high-fidelity power source code behaved as expected. The magnitude of the endurance durations also displayed the capabilities of hydrogen as a fuel and how having a high mass of hydrogen fuel vastly increased endurance durations. The significance of the endurance duration found in the high-fidelity power source CA is discussed later in this chapter. Validation for this code was available by comparing the results from the two different levels of fidelity of the power source CA. A further comparison was made between the predicted endurance durations and the results of current fuel-cell powered RPA flight shown in Table 1. The results of the mission simulation show this comparison later in Chapter 4.

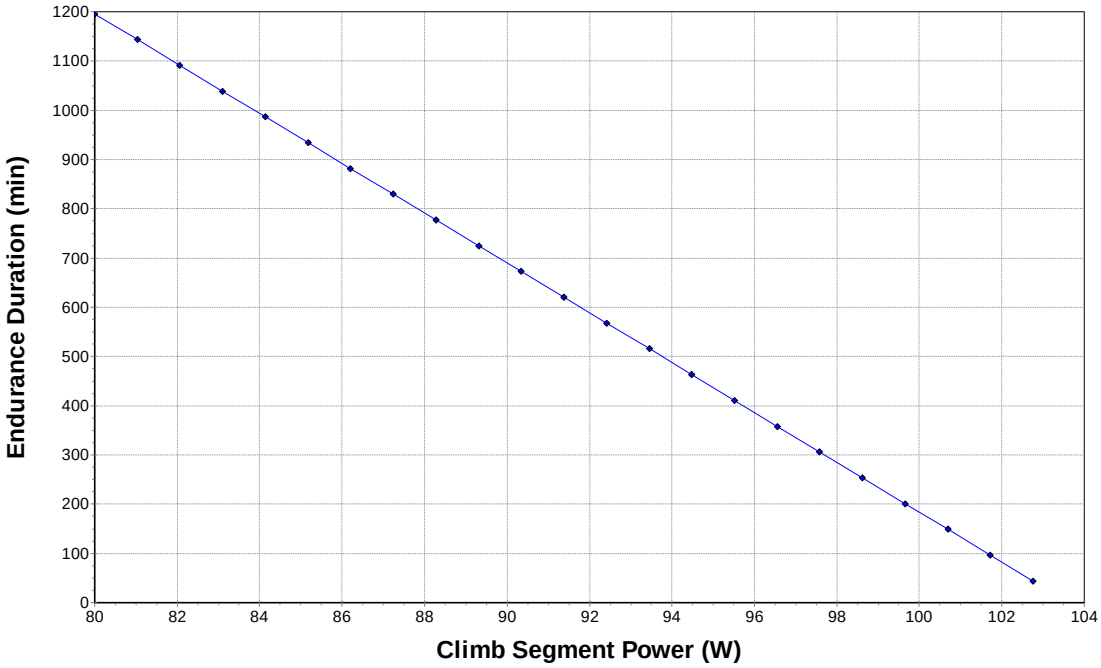

Figure 44. Verification of high-fidelity power source CA

IV.2. Design of Experiments Analysis

MC Design of Experiments (DOE) allowed for an exploration of the design space that was necessary to understand before finding solutions, particularly solutions that involved optimization. Overall, DOE gave the user hints as to where maximums or minimums would occur and also where feasible designs were located. Two different DOE were examined that looked at the two levels of fidelity for the power source CA. These were chosen because their analysis produced the desired calculation of the entire model: endurance duration. The first DOE explored the design space by running a "full-factorial" DOE study. A full-factorial DOE required intensive data collection but allowed for separation of the individual effects of the variables on the outcome. The second DOE utilized a "design explorer orthogonal array." This method required less

iteration to explore the design space when compared to a full-factorial DOE and was preferred due to the greater number of variables being manipulated in the second DOE.

Both techniques tested a specified range of given inputs to determine if they yielded valid design points. A valid design point meant that the resulting endurance duration was greater than zero and that the battery and fuel cell were able to handle the power and energy demands placed on them by the power management CA. The results of the DOE not only indicated what variables had the greatest affect on endurance duration but also showed where optimal solutions would likely come from. Both DOE used the electric power required that resulted from the low-fidelity aerodynamic and propulsion CAs and the mission segment information from Figure 30.

The first DOE (DOE #1) explored the changes to endurance energy from the low-fidelity power source CA over the ranges of inputs specified in Table 5. The values chosen were intended to reflect technology that ranged from current day to twenty-five years into the future. More importantly, the ranges covered the spectrum of feasible designs. The results of DOE #1 are shown in a glyph plot in Figure 45. A glyph plot was used because it was a useful tool for visualizing numerous variables effects on one plot. Each point or "glyph" on a glyph plot represented more than its three-space location by varying its characteristics by changes including size, orientation, and color. A glyph plot was a complex tool that required detailed explanation of its contents, but displaying several variables simultaneously to determine the effects on endurance energy was worthwhile. Overall, the results indicated where the best designs existed. By interpreting the values at these design points, the validity of current or future technology could be examined in the mission simulations.

Table 5. Variable ranges for DOE #1

	Minimum	Maximum	Units
SP_{batt}	800	2,500	W/kg
SE_{batt}	100	300	W-hr/kg
SP_{fc}	25	300	W/kg
SE_{fc}	600	1,200	W-hr/kg
$\%P_{fc,end}$	0	300	%

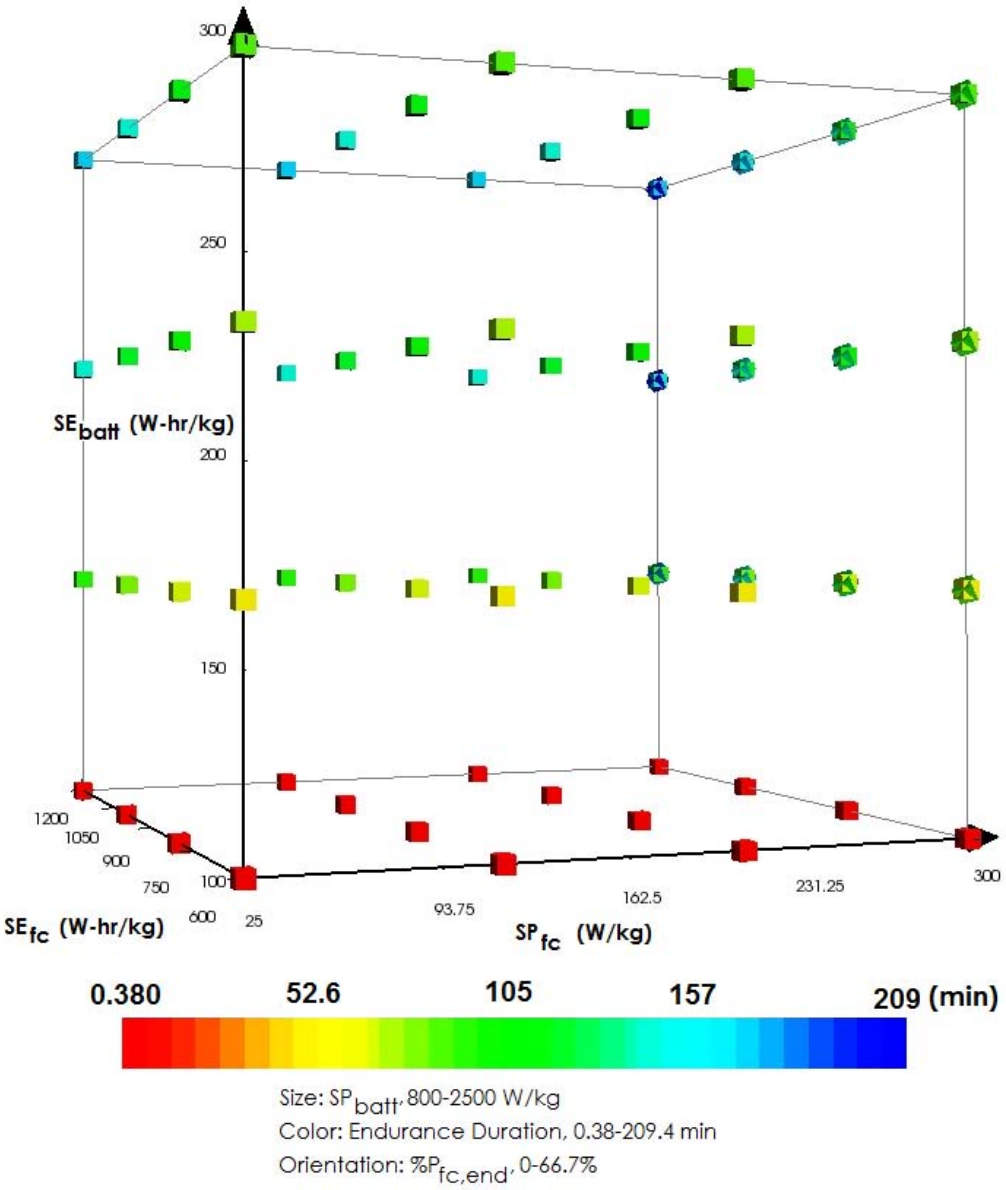

Figure 45. Glyph plot showing results of DOE #1

The glyph plot in Figure 45 indicated several different things. First and foremost, each of the points (squares) shown were feasible design points made up of each of the variables from Table 5 within the ranges specified. Results of the DOE that were not feasible were removed from the plot to reduce clutter. The traditional X, Y, and Z axis of the plot represented the fuel cell's specific power, specific energy, and the battery's specific energy. Size, color, and orientation were used beyond the X,Y, and Z coordinates to communicate multi-variable effects. The battery's specific power is shown by the size of the shape and because low specific power of the battery led to infeasible cases, only the largest size is shown in the glyph plot (2,500 W/kg). Endurance duration is represented by the color of the shape and ranged from 0.38 min to 209 min. The percentage of endurance power taken by the fuel cell is shown by the shape's orientation (seen on the right side of the plot).

Each of the points shown represented a feasible design point and an examination of the results indicated where maximum endurance duration values were likely to be found by searching for the darkest blue glyph. The maximum endurance durations were found in the back right of the plot, which represented the maximum specific energy and specific power of both the fuel cell and battery, or the most advanced technology. This was expected because higher specific energy and specific power values represent better or future ESDs. In a way, this conclusion served as further V&V for the model. Furthermore, the percentage of endurance power taken by the fuel cell was equal to 67% (shown by the orientation of the square). Percentages higher than this value led to infeasible solutions because the fuel cell was unable to handle the power demands. The DOE results suggested that while future technology provided the longest endurance

durations, current day technology still provided feasible results for the low-fidelity power source CA. Additionally, the designs that maximized endurance duration used ESDs with the highest specific energy and specific power, as well as the highest percent of endurance power taken by the fuel cell, provided the fuel cell could handle the power demands.

The second DOE (DOE #2) explored the resulting endurance durations from the high-fidelity power source CA over the ranges of inputs specified in Table 6. The values chosen again reflected current technology to twenty-five years into the future and attempted to explore all feasible design points. The results of DOE #2 are shown in glyph plots in Figure 46 and Figure 47.

Table 6. Variable ranges for DOE #2

	Minimum	**Maximum**	**Units**
$SP_{batt,initial}$	250	1,050	W/kg
$V_{initial}$	0.1	1.2	V
m_{casing}	0.02	0.08	kg
m_{cell}	0.01	0.05	kg
A_{fc}	10	80	cm^2
$f_{bop,tank}$	1	2	
$\%P_{fc,end}$	0	200	%

The data presented in Figure 46 shows the impact of the initial guesses for the battery's initial specific power and the fuel cell's starting voltage discussed in Chapter 3. These two variables along with the percentage of endurance power of the fuel cell are shown on the X, Y, and Z axis. The size and color of the design point both indicated endurance duration to increase the clarity of the plot. The wide range of endurance durations (4.63 min to 1,876 min) accounted for the minimum and maximum feasible design points as defined by the ranges in Table 6; however, the values used for the higher

values of endurance durations represent an extremely futuristic configuration. The results were still helpful to determine what locations to explore for optimizations in later mission simulations. The most interesting result shown in Figure 46 was the location of where to begin initial guesses for starting voltage of the fuel cell and initial specific power of the battery. The highest endurance durations came from starting voltages around 0.65 V, with other voltages significantly lowering the outcome of endurance duration. The initial specific power of the battery had less of an impact on the endurance duration, though values over 650 W/kg led to increased endurance durations.

The results from DOE #2 shown in the glyph plot in Figure 47 communicated the effect that the various fuel cell mass components had on endurance duration. The fuel cell casing mass, the mass per cell, and the area per cell are shown on the standard X, Y, and Z axis. The size of the glyph represents endurance duration. The color of the glyph indicates the weight factor of the fuel cell's BOP and fuel tank. The results of the DOE showed that the highest endurance durations occurred when the casing mass, the mass per cell, and fuel cell weight factor were at a minimum and the area per cell was at a maximum. This was expected because it left the most mass to be dedicated to hydrogen fuel. The results shown in Figure 47 also provided bench marks for technology to aim for to maximize endurance duration. For example, if the mass per cell was greater than 0.03 kg (0.066 lbs), very few feasible designs existed. This indicated that future fuel cell designs for a configuration like the one examined in this research should aim for a mass per cell of less than 0.03 kg.

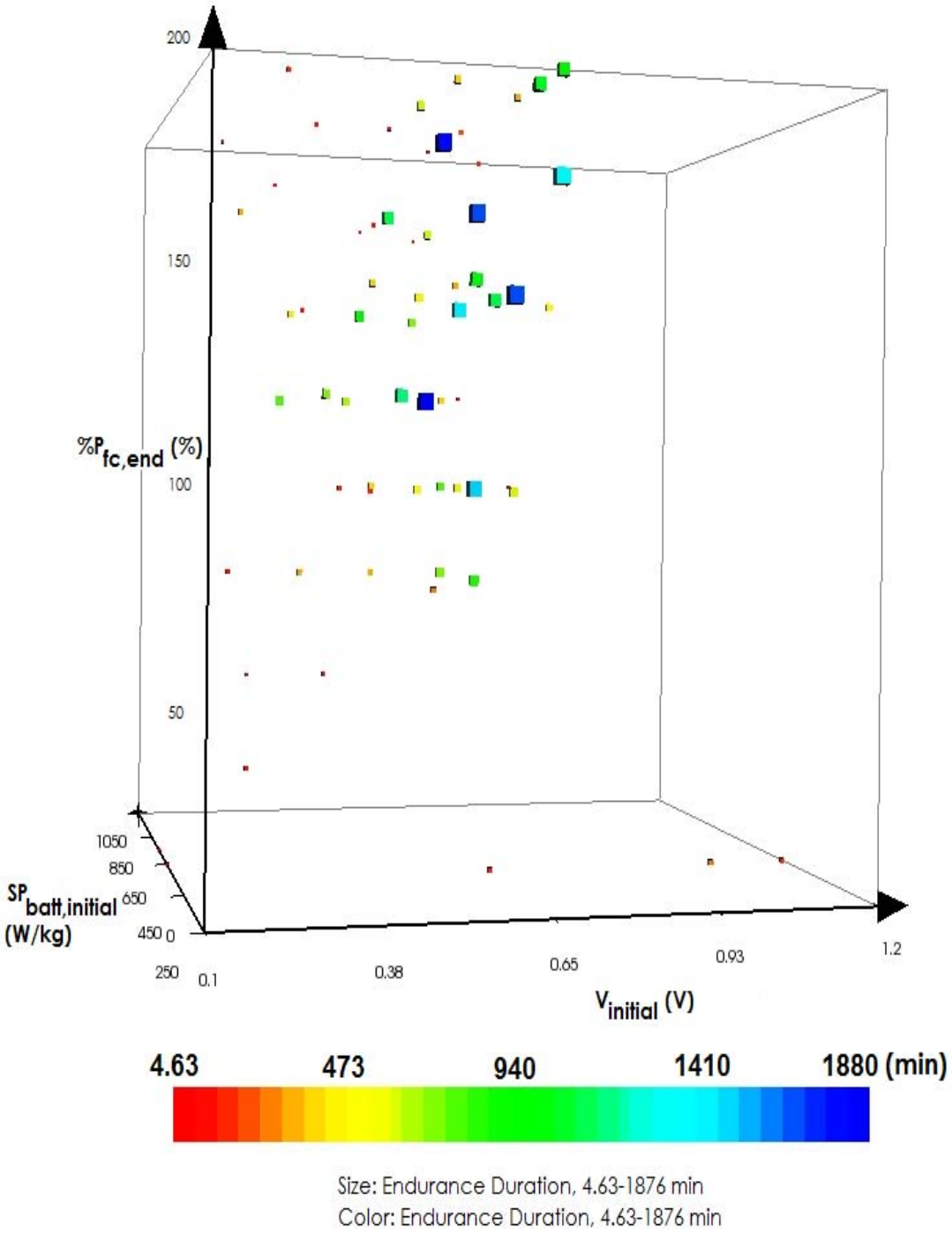

Figure 46. Glyph plot showing results of DOE #2 (1)

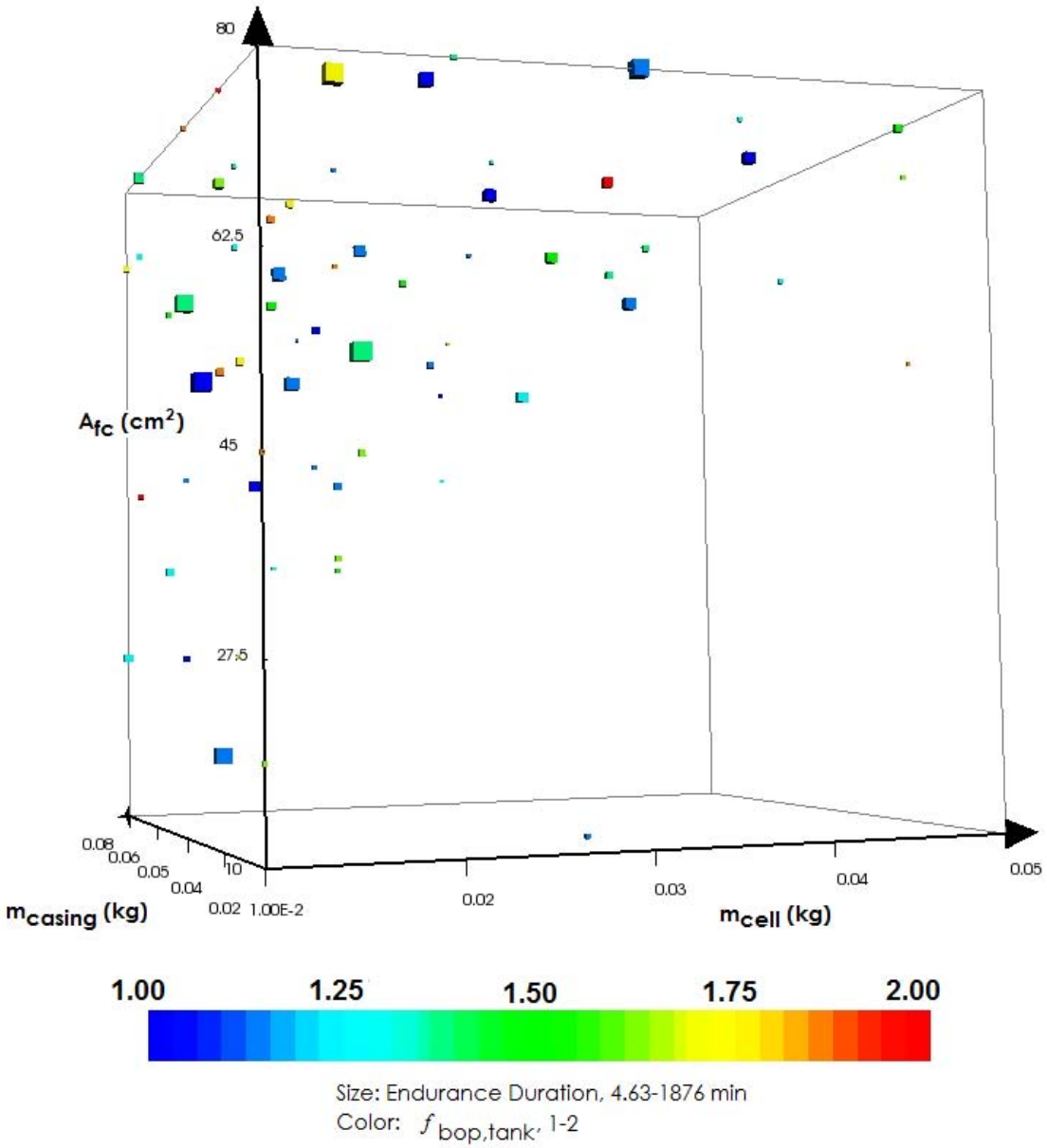

Figure 47. Glyph plot showing results of DOE #2 (2)

IV.3. Mission Simulations and Results

The goal of the mission simulations were to not only present the results of the model in terms of endurance duration, but also to show the key results from each CA. Numerous different simulations were examined to address the central questions of this

investigation. The mission simulations fell into three different categories: fidelity selection, total mass of the ESDs, and current versus future ESD technology. Each of the levels of fidelity needed to be explored to see how fidelity selection effected endurance duration. Table 7 shows the different simulations based on fidelity selection.

Table 7. Fidelity selection for mission simulations

Simulation	Aerodynamic CA	Propulsion CA	Power Management CA	Power Source CA
1	Low	Low	Low	Low
2	High	Low	Low	Low
3	High	High	Low	Low
4	High	High	High	Low
5	Low	High	Low	Low
6	Low	High	High	Low
7	Low	Low	High	Low
8	High	Low	High	Low
9	Low	Low	Low	High
10	High	Low	Low	High
11	High	High	Low	High
12	High	High	High	High
13	Low	High	Low	High
14	Low	High	High	High
15	Low	Low	High	High
16	High	Low	High	High

In total, there were sixteen different simulations to account for the different options of fidelity selection. In addition to these simulations, two categories were created for the total mass of the ESD based on a percentage of the gross take-off weight of the MAV. A conservative assumption for this percentage was around 25% according to guidance from AFRL/RZPS's. To account for an extreme case where the MAV integrated parts of the ESD for structure as well as carrying a reduced payload, a 40% ESD allowance was also investigated. Altogether, this brought the total simulations up to

thirty-two, with sixteen simulations at 25% and 40% of the gross take-off weight of the MAV, respectively.

The last category of mission simulations was current or future ESD technology. The current ESD technology provided guidance as to what the current picture of an EPMAV was while the future technology was intended to show the capabilities of an EPMAV in five years. The future technology simulations only investigated a 25% allowance for the power source mass. This brought the total number of simulations to forty-eight.

IV.3.1. Current Technology

The current ESD technology used for this analysis is shown in Table 8, Figure 48, and Figure 49. The literature review provided the specifications for the specific energy and specific power values shown in Table 8. No a priori information was found in the literature for fuel cell mass components of the magnitude required for this research; however, estimates were made using values from pieces of manufacturer's data from smaller fuel cells and a larger fuel cell with some details on component mass.[106,107,108] The approximations used provided adequate fidelity for the conceptual design stage and could be adjusted by the user for future examinations. The Ragone plot data came from the 1500 mAh LiPo battery shown in Figure 12. Finally, the polarization curve from the fuel cell came from suggested text book values for a PEMFC.[98]

Table 8. Current ESD technology values

	Value	Units
SP_{batt}	1,700	W/kg
SE_{batt}	190	W-hr/kg
SP_{fc}	80	W/kg
SE_{fc}	800	W-hr/kg
m_{casing}	0.063	kg
m_{cell}	0.02	kg
A_{fc}	20	cm^2
$f_{bop,tank}$	2	

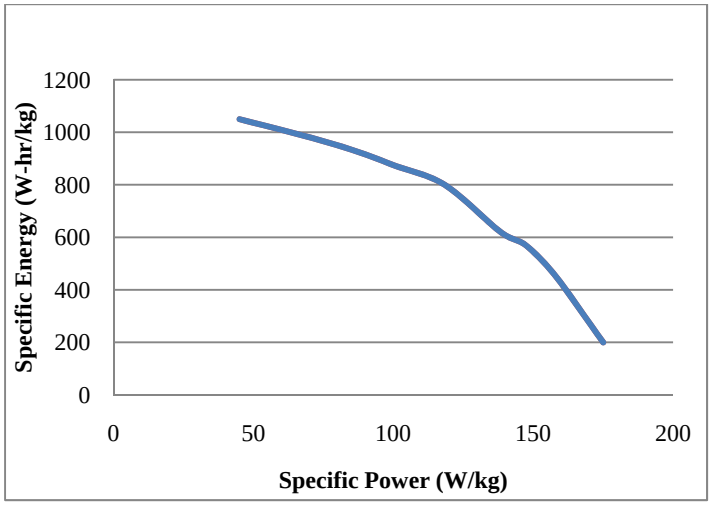

Figure 48. Current technology Ragone plot (LiPo)

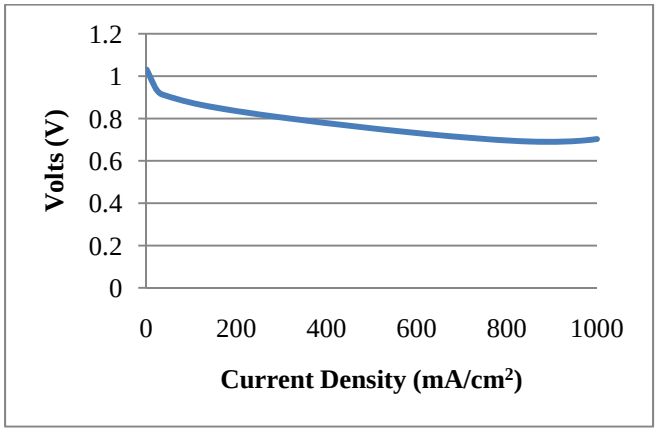

Figure 49. Current technology polarization curve (PEMFC)

IV.3.1.1. Current Technology, 25% ESD Allowance

The sixteen different fidelity configurations were investigated using current ESD technology and an ESD mass of 25% of the MAV's gross take-off mass. These results most accurately indicated the abilities of an EPMAV today. Table 9 shows the results from the aerodynamic and propulsion CAs (mission analysis) and Table 10 shows the results of the power management and power source CAs (post-processing).

Table 9. Mission analysis for current technology, 25% ESD allowance

	Climb			Ingress			Endurance			Egress			Descent		
	e	P_{req}	P_{elec}	e	P_{req}	P_{elec}	e	P_{req}	P_{elec}	E	P_{req}	P_{elec}	E	P_{req}	P_{elec}
	(%)	(W)	(W)	(%)	(W)	(W)	(%)	(W)	(W)	(%)	(W)	(W)	(%)	(W)	(W)
1	93.6	51.6	114.60	93.6	35.4	73.85	93.6	32.8	70.05	93.6	32.8	70.06	93.6	14.2	29.89
2	94.8	51.4	114.20	94.4	35.3	73.58	94.8	32.6	69.62	94.8	32.6	69.63	94.8	14.0	29.54
3	94.8	51.4	93.93	94.4	35.3	69.68	94.8	32.6	63.65	94.8	32.6	63.67	94.8	14.0	37.17
4	94.8	51.4	93.93	94.4	35.3	69.68	94.8	32.6	63.65	94.8	32.6	63.67	94.8	14.0	37.17
5	93.6	51.6	94.22	93.6	35.4	69.86	93.6	32.8	63.95	93.6	32.8	63.95	93.6	14.2	37.40
6	93.6	51.6	94.22	93.6	35.4	69.86	93.6	32.8	63.95	93.6	32.8	63.95	93.6	14.2	37.40
7	93.6	51.6	114.60	93.6	35.4	73.85	93.6	32.8	70.05	93.6	32.8	70.06	93.6	14.2	29.89
8	94.8	51.4	114.20	94.4	35.3	73.58	94.8	32.6	69.62	94.8	32.6	69.63	94.8	14.0	29.54
9	93.6	51.6	114.60	93.6	35.4	73.85	93.6	32.8	70.05	93.6	32.8	70.06	93.6	14.2	29.89
10	94.8	51.4	114.20	94.4	35.3	73.58	94.8	32.6	69.62	94.8	32.6	69.63	94.8	14.0	29.54
11	94.8	51.4	93.93	94.4	35.3	69.68	94.8	32.6	63.65	94.8	32.6	63.67	94.8	14.0	37.17
12	94.8	51.4	93.93	94.4	35.3	69.68	94.8	32.6	63.65	94.8	32.6	63.67	94.8	14.0	37.17
13	93.6	51.6	94.22	93.6	35.4	69.86	93.6	32.8	63.95	93.6	32.8	63.95	93.6	14.2	37.40
14	93.6	51.6	94.22	93.6	35.4	69.86	93.6	32.8	63.95	93.6	32.8	63.95	93.6	14.2	37.40
15	93.6	51.6	114.60	93.6	35.4	73.85	93.6	32.8	70.05	93.6	32.8	70.06	93.6	14.2	29.89
16	94.8	51.4	114.20	94.4	35.3	73.58	94.8	32.6	69.62	94.8	32.6	69.63	94.8	14.0	29.54

Several important conclusions came from the mission analysis in Table 9. Overall, the mission analysis yielded the same results for simulations 1-8 and 9-16 because the only difference between the two sets of simulations was the power source CA's fidelity, whose results are shown in Table 10. Both levels of fidelity for the aerodynamic CA predicted a highly efficient wing for the GenMAV. This corresponded to the results found in the V&V for the aerodynamic CA earlier in this chapter. The

maximum percent error between the two aerodynamic CAs for span efficiency factor was 1.27% and occurred in the endurance segment. It should be noted that the accuracy used in Table 9 was not high enough to show that the endurance segment had a slightly higher span efficiency factor than other segments. The reason the span efficiency factor was so close for each of the mission segments was the tightness of the range of velocities used throughout the mission. In addition to the velocities shown in Figure 30, the endurance velocity was equal to 15.93 m/s (35.6 mph), which was essentially the same as the segments that had a velocity of 16 m/s (35.8 mph). The similarity between the low- and high-fidelity results was expected due to the drag polar data coming directly from a drag polar created through AVL in Hrad's analysis.[24] The standard deviation of all span efficiency factors was only 0.18, which was also expected because span efficiency factor was constant for the low-fidelity analysis and near-constant for the high-fidelity analysis as shown earlier in Figure 34. Graphical results for the aerodynamic CA are shown in Figure 50.

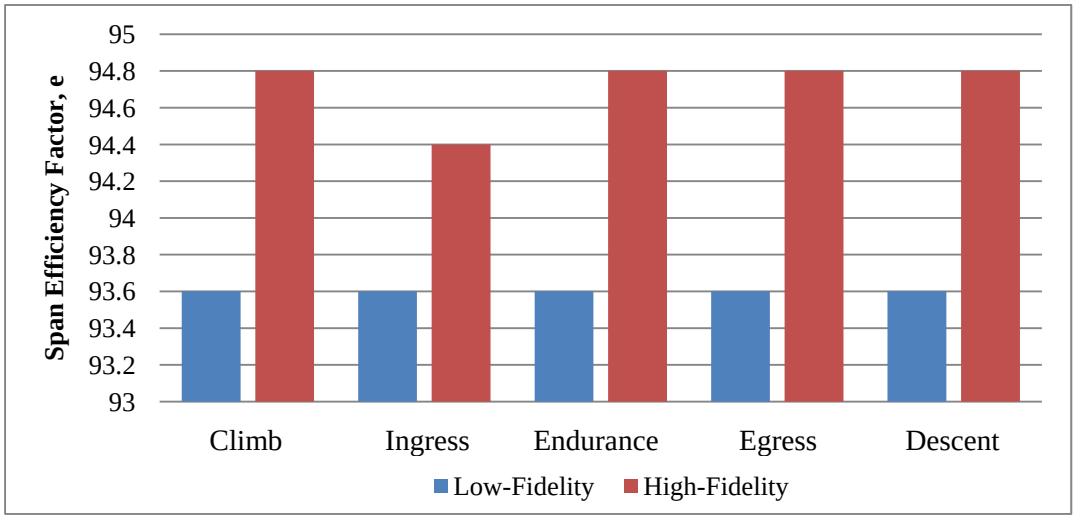

Figure 50. Aerodynamic CA results, simulations 1-16

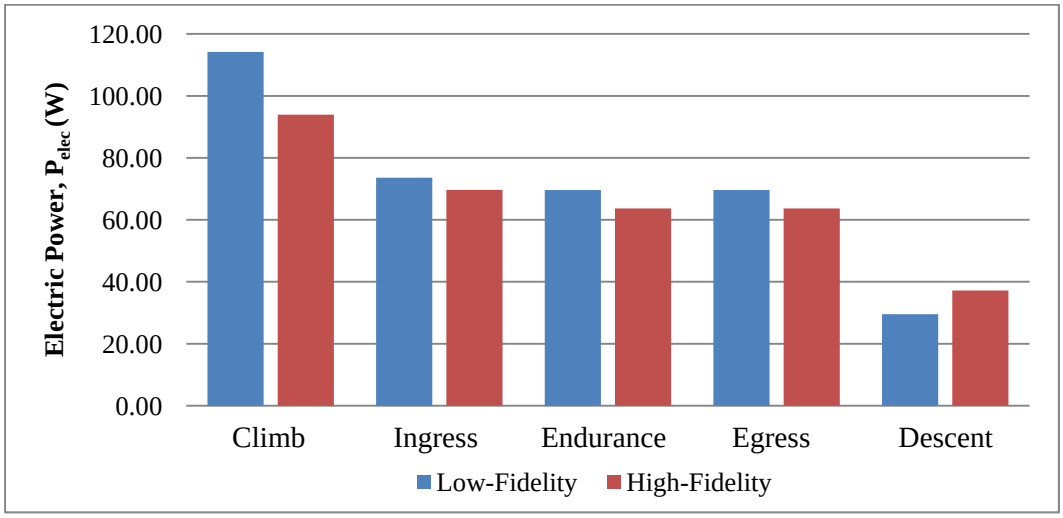

Figure 51. Propulsion CA results, simulations 1-16

The results of the propulsion CA were reflected in the values for aircraft power required and electric power. For each simulation, the climb segment required the most power, followed by the ingress, the egress, the endurance, and finally the descent segments. This result was expected because climbing aircraft and aircraft at higher velocities require greater power.[25] The values for power required and electric power in the endurance and egress segments were very similar due to the closeness of their velocities. The percent error of electric power values between the low- and high-fidelity propulsion CA was 21.6% for the climb segment, 20.5% for the descent segment, and less than 10% for the remaining segments. The highest errors came from the extremes of aircraft power required being fed into the two different fidelities of propulsion CA (i.e. both high and low values for power required). The errors were a result of the trends seen in Figure 40, which compared the electric power results of QPROP and the experimental propeller and motor CA. This plot shows that the two different fidelities predicted very similar results for electric power when its magnitude was approximately 85 W, with

values higher or lower than that diverging. The low percent error for the ingress, egress, and endurance legs were a result of operation nearest to an electric power of 85 W. Graphical results for the propulsion CA are shown in Figure 51, and assume that the high-fidelity aerodynamic CA was used.

Table 10. Post-processing for current technology, 25% ESD allowance

	$\%P_{fc,end}$ (%)	m_{fc} (kg)	m_{batt} (kg)	m_{fuel} (kg)	$SP_{batt,\ initial}$ (W/kg)	$V_{fc,\ initial}$ (V)	t_{end} (min)
1	100.0	–	–	–	–	–	Infeasible
2	100.0	–	–	–	–	–	Infeasible
3	100.0	–	–	–	–	–	Infeasible
4	18.2	0.145	0.109	–	–	–	107.3
5	100.0	–	–	–	–	–	Infeasible
6	18.1	0.145	0.110	–	–	–	106.5
7	14.3	0.132	0.123	–	–	–	88.5
8	15.3	0.134	0.121	–	–	–	90.2
9	100.0	–	–	–	–	–	Infeasible
10	100.0	–	–	–	–	–	Infeasible
11	100.0	–	–	–	–	–	Infeasible
12	–	–	–	–	–	–	Infeasible
13	100.0	–	–	–	–	–	Infeasible
14	–	–	–	–	–	–	Infeasible
15	–	–	–	–	–	–	Infeasible
16	–	–	–	–	–	–	Infeasible

The post-processing results, while seemingly mundane, presented valuable information to the user. The main take away from Table 10 was that current ESD technology barely makes the idea of an EPMAV feasible. Simulations 1-8 represented the low-fidelity power source CA and only the simulations that used the high-fidelity power management CA (simulations 4, 6, 7, and 8) were found to be feasible. The reason for this was that the low-fidelity power management CA assigned too much power to the fuel cell. This result was reasonable due to the small size of the ESDs being used and the low value of current fuel cells' specific power. The optimal percentage of endurance power taken by the fuel cell ($\%P_{fc,end}$) ranged from 14.3% to 18.2%. This value was

limited by the amount of power the fuel cell could provide. Expectations prior to the analysis were that the fuel cell would be utilized as much as possible to take advantage of its high specific energy and these results confirmed those expectations. The higher percentages came from the simulations that used the experimental propeller and motor code for the propulsion CA. The lower electric powers from the propulsion CA led to higher values for $\%P_{fc,end}$.

The highest endurance duration came from simulation 4 at 107.3 min. The percent error between the endurance durations was 17.5%. This error corresponded to the percent error in electric power from the mission analysis between the low- and high-fidelity propulsion CA. An endurance duration of over an hour and a half was higher than expectations, but two key assumptions of the low-fidelity analysis led to values for endurance duration that were likely inflated. First, the low-fidelity analysis assumed that the values for the specific energy and specific power for a battery and a fuel cell scaled evenly with ESD size. In reality, some types of losses would occur from scaling down these ESDs. Second, specific energy and specific power values for a fuel cell were misleading because a fuel cell operates more like an ICE than a battery. Similar to an ICE, a fuel cell would have limitless energy capabilities if fuel were to be continually supplied to it. A comparison to a battery-only MAV also provided prospective on the feasibility of the results. The endurance duration of the WASP III, a MAV with a total mass of approximately half the GenMAV, had an endurance duration of 45 min. Therefore, an estimate of slightly more than double this length was feasible when considering the additional mass the GenMAV could use for ESDs as well as the

endurance capabilities of fuel cells. Altogether, the low-fidelity results provided a benchmark for endurance duration and were correctly classified as low-fidelity in nature.

The high-fidelity power source CA always yielded an infeasible result. The results were infeasible because the fuel cell required a mass greater than the allowable power source mass set by the 25% ESD allowance. Given that the smallest RPA to fly from fuel cell-powered flight was approximately twice the mass of the GenMAV with a larger wingspan (Table 1), the results found from the high-fidelity CA provided a conservative estimate when compared to the low-fidelity CA.

IV.3.1.2. Current Technology, 40% ESD Allowance

The sixteen different fidelity configurations were again examined with current ESD technology, but this time an ESD mass of 40% of the MAV's gross take-off mass was used. These results indicated the abilities of an EPMAV today that integrated the ESDs into its structure and carried a limited payload. The results in Table 11 are from the mission analysis and Table 12 shows the results from the post-processing.

The mission analysis from the second set of simulations at 40% ESD allowance was very similar to those at 25% ESD allowance. The main differences were the increases in power required and electric power as well as the similarity in electric power values for different propulsion fidelity options. The increase in electric power was expected due to the higher total weight of the MAV. Also, the similarities in electric power values were feasible because they were closer to the location where QPROP and the experimental propeller and motor code predicted similar results (Figure 40). Since the same trends occurred for both the 25% and 40% ESD allowance, the conclusions will not be repeated; however, the post-processing results were worth addressing in detail.

Table 11. Mission analysis for current technology, 40% ESD allowance

	Climb			Ingress			Endurance			Egress			Descent		
	E	P_{req}	P_{elec}	e	P_{req}	P_{elec}	e	P_{req}	P_{elec}	e	P_{req}	P_{elec}	e	P_{req}	P_{elec}
	(%)	(W)	(W)	(%)	(W)	(W)	(%)	(W)	(W)	(%)	(W)	(W)	(%)	(W)	(W)
17	93.6	59.4	130.90	93.6	39.1	82.03	93.6	38.9	81.77	93.6	38.9	81.77	93.6	17.5	36.03
18	94.8	59.2	130.30	94.8	38.9	81.54	94.8	38.7	81.27	94.8	38.7	81.27	94.8	17.2	35.59
19	94.8	59.2	107.43	94.8	38.9	75.02	94.8	38.7	74.59	94.8	38.7	74.59	94.8	17.2	43.47
20	94.8	59.2	107.43	94.8	38.9	75.02	94.8	38.7	74.59	94.8	38.7	74.59	94.8	17.2	43.47
21	93.6	59.4	107.81	93.6	39.1	75.35	93.6	38.9	74.93	93.6	38.9	74.93	93.6	17.5	43.77
22	93.6	59.4	107.81	93.6	39.1	75.35	93.6	38.9	74.93	93.6	38.9	74.93	93.6	17.5	43.77
23	93.6	59.4	130.90	93.6	39.1	82.03	93.6	38.9	81.77	93.6	38.9	81.77	93.6	17.5	36.03
24	94.8	59.2	130.30	94.8	38.9	81.54	94.8	38.7	81.27	94.8	38.7	81.27	94.8	17.2	35.59
25	93.6	59.4	130.90	93.6	39.1	82.03	93.6	38.9	81.77	93.6	38.9	81.77	93.6	17.5	36.03
26	94.8	59.2	130.30	94.8	38.9	81.54	94.8	38.7	81.27	94.8	38.7	81.27	94.8	17.2	35.59
27	94.8	59.2	107.43	94.8	38.9	75.02	94.8	38.7	74.59	94.8	38.7	74.59	94.8	17.2	43.47
28	94.8	59.2	107.43	94.8	38.9	75.02	94.8	38.7	74.59	94.8	38.7	74.59	94.8	17.2	43.47
29	93.6	59.4	107.81	93.6	39.1	75.35	93.6	38.9	74.93	93.6	38.9	74.93	93.6	17.5	43.77
30	93.6	59.4	107.81	93.6	39.1	75.35	93.6	38.9	74.93	93.6	38.9	74.93	93.6	17.5	43.77
31	93.6	59.4	130.90	93.6	39.1	82.03	93.6	38.9	81.77	93.6	38.9	81.77	93.6	17.5	36.03
32	94.8	59.2	130.30	94.8	38.9	81.54	94.8	38.7	81.27	94.8	38.7	81.27	94.8	17.2	35.59

Table 12. Post-processing for current technology, 40% ESD allowance

	$\%P_{fc,end}$	m_{fc}	m_{batt}	m_{fuel}	$SP_{batt,\ initial}$	$V_{fc,\ initial}$	t_{end}
	(%)	(kg)	(kg)	(kg)	(W/kg)	(V)	(min)
17	100.0	–	–	–	–	–	Infeasible
18	100.0	–	–	–	–	–	Infeasible
19	100.0	–	–	–	–	–	Infeasible
20	31.8	0.298	0.109	–	–	–	187
21	100.0	–	–	–	–	–	Infeasible
22	31.7	0.298	0.110	–	–	–	186
23	27.5	0.282	0.126	–	–	–	161
24	27.7	0.283	0.125	–	–	–	163
25	100.0	–	–	–	–	–	Infeasible
26	100.0	–	–	–	–	–	Infeasible
27	100.0	–	–	–	–	–	Infeasible
28	37.0	0.285	0.083	0.039	667	0.75	503
29	100.0	–	–	–	–	–	Infeasible
30	37.0	0.285	0.084	0.039	650	0.75	494
31	34.0	0.285	0.105	0.017	725	0.7	178
32	34.0	0.285	0.105	0.018	725	0.7	181

The post-processing results seen in Table 12 brought forth more interesting results than the first set of simulations for current technology with only a 25% ESD allowance.

Beginning with the low-fidelity power source CA, the highest endurance duration was obtained in simulation 20 with an endurance length of 187 min. The higher endurance duration was directly related to the increase in mass of the fuel cell when compared to simulation 8 from Table 10. In simulation 20, all of the additional ESD mass was added to the fuel cell to take advantage of its high specific energy. Additionally, a larger fuel cell meant increased power capabilities and a higher optimal percentage of endurance power was handled by the fuel cell. For simulation 20, the optimal percentage was found to be 31.8% or a 75% increase over the result in simulation 8. The percent error between the endurance duration results for the low-fidelity power source CA was 10%. This percent error was smaller than the first set of simulations due to the similarity in values for electric power shown in Table 11. The higher weight allowance also led to feasible simulations from the high-fidelity power source CA.

The 40% ESD allowance led to high-fidelity endurance durations that ranged from results similar to the low-fidelity durations to more than double their length. The maximum endurance duration found from the high-fidelity CA came from simulation 28 with an endurance duration of 503 min (8.4 hr); however, the results of simulation 28 and 30 were clearly outliers with values more than twice as much as low-fidelity predictions. The extreme endurance durations in these two simulations came from the reduced electric power from the high-fidelity propulsion CA. The reduced electric power allowed for a smaller battery size and therefore a greater amount of hydrogen fuel. Though it was a small increase in hydrogen fuel, it provided substantial endurance duration gains because of its high specific energy of 33,330 W-hr/kg.[110] With a value this high, one gram of hydrogen provided over 33 W-hr of energy in a perfectly efficient fuel cell system.

Simulations 31 and 32, which used the low-fidelity propulsion CA, had only a 3.2% error when compared to the highest low-fidelity power source CA endurance results for this set of simulations.

All the results of the high-fidelity power source CA were extremely sensitive to the values assigned to the variables in Eq. (74) that made up the mass of the fuel cell. A lighter fuel cell led to more mass left over for hydrogen fuel. Altogether, the similarity between simulations 31 and 32 to the low-fidelity results made for the most interesting conclusion in that both the low- and high-fidelity tracks for the power source CA predicted essential the same endurance duration. Therefore, it was useful to visualize what led to the results of these simulations in the high-fidelity power source CA. The operating points on the Ragone plot and polarization curve indicated how the endurance duration was found. The operating points for simulation 32 are shown in Figure 52.

The operating points for simulation 32 were located at the top left of the Ragone plot to harness the benefits of the battery's high specific energy. Additionally, the operating points aligned from left to right in order of electric power needed from the ESD for the given segment. This matched expectations because less electric power required meant that they could take advantage of the high specific energy and provide better energy capabilities. The operating points for egress, ingress, and endurance were all very close because of their similar power requirements. The polarization curve showed that all mission segments operated at 0.7 V. This was expected because the code was designed to keep the fuel cell operating at the same power demands for the entire mission.

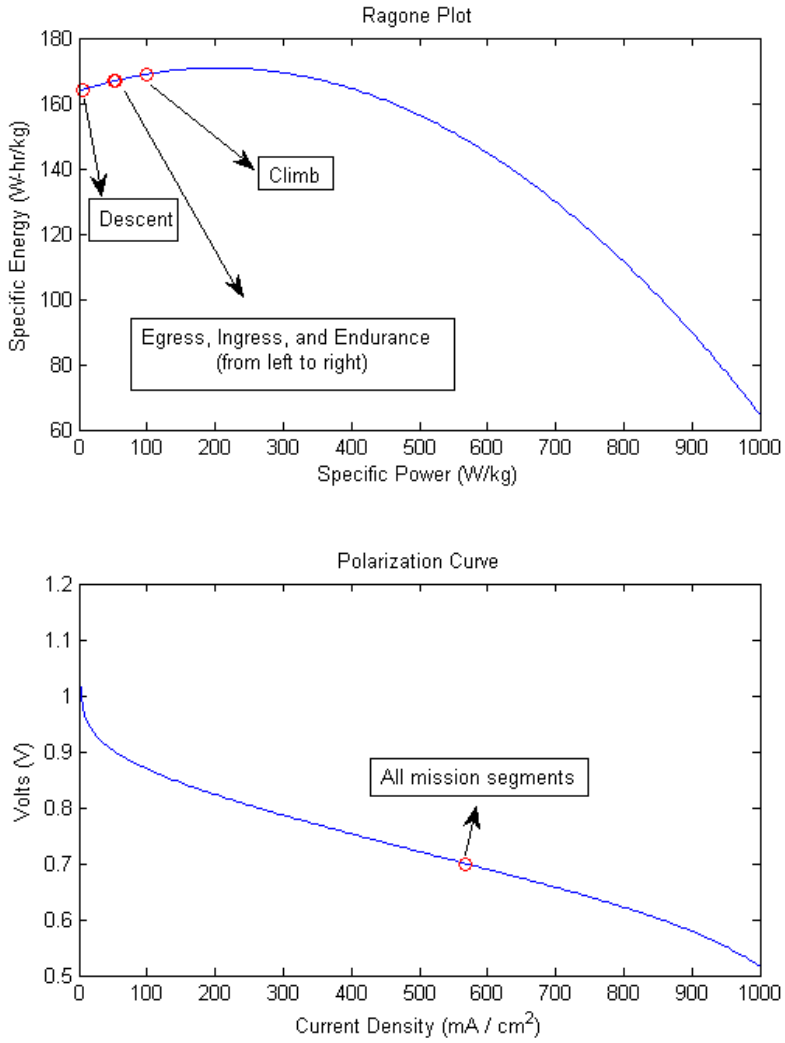

Figure 52. Operating points for simulation #32

IV.3.2. Future Technology

The future ESD technology used for this analysis is shown in Table 13, Figure 53, and Figure 54. The values used for future ESD technology represented an estimation of what ESD specifications could be five years from now. The literature review provided little guidance for future estimates and suggested only that advancements moved and will continue to move much slower than computing technology (i.e. Moore's Law).[109]

Therefore, it was assumed that the specifications would improve by 25% over the next five years. A 25% improvement implied either an increase in performance parameters or a decrease in mass. The area of the fuel cell was left the same due to space restrictions in the fuselage of the GenMAV. For the Ragone plot and polarization curve, the improvements shifted the operating lines to allow for better performance by the same margin.

Table 13. Future ESD technology values

	Value	Units
SP_{batt}	2,125	W/kg
SE_{batt}	237.5	W-hr/kg
SP_{fc}	125	W/kg
SE_{fc}	1,000	W-hr/kg
m_{casing}	0.047	Kg
m_{cell}	0.015	Kg
A_{fc}	20	cm^2
$f_{bop,tank}$	1.5	

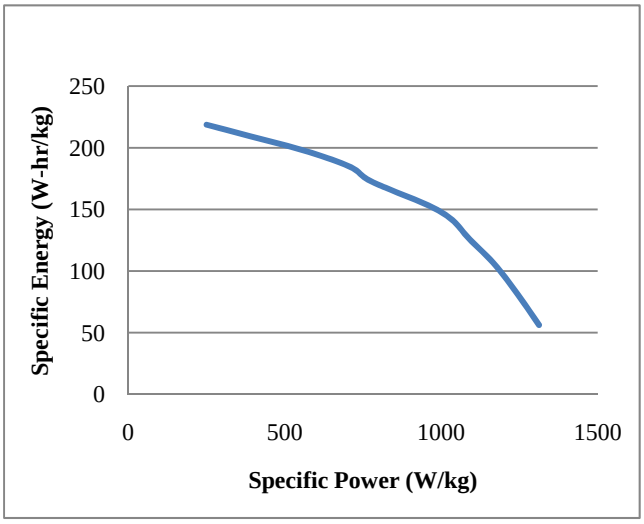

Figure 53. Future technology Ragone plot (LiPo)

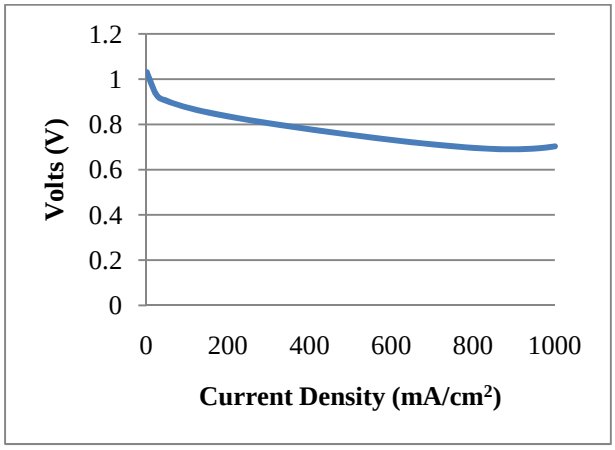

Figure 54. Future technology polarization curve (PEMFC)

IV.3.2.1. Future Technology, 25% ESD Allowance

The sixteen different fidelity configurations were investigated using future ESD technology and an ESD mass of 25% of the MAV's gross take-off mass. The mission analysis for the future technology was the same as the current technology for the same ESD allowance percentage (Table 9). This was because the advanced technology only improved values for the ESDs, which in turn only affected the post-processing results for these simulations. The post-processing results are shown in Table 14.

The post-processing results from the future ESD technology showed the potential for an EPMAV in the near future. Even with the improved fuel cell technology, the percent of endurance power handled by the fuel cell was limited by the fuel cell's capabilities; however, the highest optimal percentage of the endurance power that the fuel cell handled in the low-fidelity analysis was 35.8% or approximately twice what was found with the current technology simulations. This increase showed the benefits that a future fuel cell would provide in terms of power capabilities. The endurance duration found from the low-fidelity analysis with future technology was also almost double

current technology with a maximum endurance duration of 166 min. The gain in endurance duration came mainly from the fuel cell handling more power than before. The fuel cell's increased specific energy also provided endurance duration improvements. The percent error between the low-fidelity power source CA endurance duration results was 14.4%, which was a result of the different electric power values from the propulsion CA. The largest gains in endurance duration for the future simulations came from the high-fidelity power source CA (simulations 41-48).

Table 14. Post-processing for future technology, 25% ESD allowance

	$\%P_{fc,end}$ (%)	m_{fc} (kg)	m_{batt} (kg)	m_{fuel} (kg)	$SP_{batt,\ initial}$ (W/kg)	$V_{fc,\ initial}$ (V)	t_{end} (min)
33	100	–	–	–	–	–	Infeasible
34	100	–	–	–	–	–	Infeasible
35	100	–	–	–	–	–	Infeasible
36	35.8	0.182	0.072	–	–	–	166
37	100	–	–	–	–	–	Infeasible
38	35.5	0.182	0.073	–	–	–	165
39	30.5	0.171	0.083	–	–	–	142
40	30.7	0.172	0.083	–	–	–	143
41	100	–	–	–	–	–	Infeasible
42	100	–	–	–	–	–	Infeasible
43	100	–	–	–	–	–	Infeasible
44	60.5	0.186	0.019	0.050	1125	0.8	831
45	100	–	–	–	–	–	Infeasible
46	60.5	0.186	0.019	0.050	1125	0.8	820
47	56.0	0.186	0.034	0.035	1133	0.77	485
48	56.3	0.186	0.034	0.035	1133	0.78	495

The maximum endurance duration from the high-fidelity analysis was simulation 44 with an endurance duration of 831 min (13.85 hr). This value was close to double the endurance duration found with the current technology and a 40% ESD allowance. The impetus behind the increase in endurance duration was the reduced weight of the fuel cell (0.186 kg). The mass of the fuel cell was the same for all simulations because the same number of cells in the stack were required. A fuel cell mass of 0.186 g left 50 g of

hydrogen for the best-case future simulation compared to only 39 g in the current technology case with a 40% ESD allowance. The endurance duration for the simulations that used the high-fidelity propulsion CA (simulations 44 and 46) were nearly double the length of the simulations that used the low-fidelity power source CA (simulations 47 and 48). This was a result of the lower electric power in simulations 44 and 46. A lower electric power meant, a higher percentage of the endurance power taken by the fuel cell, a decreased battery size, and ultimately a greater mass for hydrogen fuel. At first glance, an endurance duration of 13.85 hr seemed unpractical; however, examples of current fuel cell-powered RPAs with endurance times close to 24 hrs (Table 1) suggested that this might be possible with the increases in technology proposed in Table 13.

IV.4. Chapter Four Summary

Chapter 4 provided validation and verification for the different tools that made up the four areas of CA. The mission simulations yielded a range of discoveries regarding the fidelity selection of the model, the ESD weight allowance of the aircraft, and the differences between current and future technology. Chapter 5 summarizes the main conclusions from the entire effort and suggests work that could be done in the future to continue what was accomplished in this endeavor.

V. Conclusion

V.1. Conclusions of Research

Altogether, this investigation satisfied the objectives laid out in Chapter 1. A conceptual design tool was created that calculated an EPMAV's endurance duration. This tool was unique to the MAV size and emphasized the propulsion and power source systems. The model consisted of four different areas of CAs and validation and verification were performed on each to give credence to the tool's predictions. The model then conducted a wide variety of mission simulations on the GenMAV configuration.

The mission simulations yielded important information about the fidelity selection of the simulation, the size of the ESD, and the capabilities of an EPMAV using today's technology versus five years from now. For the fidelity selection, it was found that the aerodynamic CAs led to similar results; however, the difference in these two options would increase if a drag polar was used from an independent source outside of AVL. The two CAs predicted a highly efficient wing for the GenMAV with span efficiency factors between 93.6%-94.8%. The propulsion CA resulted in the greatest discrepancy between CA selection. While they both followed the same trend of the climb segment requiring the most power and the descent requiring the least, QPROP predicted higher electric power values than the experimental propeller and motor code. The power management CA showed that the fuel cell's power capability was the limiting factor on hybridization of the battery and fuel cell. Furthermore, the level of hybridization varied depending on the selection of fidelity. For the inputs used in the entire set of mission

simulations, the percent of the endurance power taken by the battery ranged from 14.3% to 60.5%; however, the percentages fell into a much tighter range when the low- or high-fidelity power source CA's results were compared separately. The low-fidelity power management CA, which assigned the entire endurance power to the fuel cell, was found to be infeasible for all of the simulations. Lastly, the power source CA fidelity selection led to higher endurance durations from the high-fidelity analysis, especially those that came from the high-fidelity propulsion CA. This was largely due to the specific energy of hydrogen.

The different weight allowance between the current technology simulations showed that endurance duration increases by dedicating more mass to ESDs. A GenMAV with current technology had its endurance duration increase from 107.3 min to 187 min based upon the low-fidelity power source CA. The high-fidelity power source CA had even more dramatic gains that indicated the abilities of hydrogen as well as the gains from increased ESD mass. Altogether, the endurance capabilities from additional ESD mass outweighed the costs from the power required to move the extra mass through the air. Finally, the difference in current and future MAV analysis highlighted the potential of an EPMAV if ESD technology continues to progress. The current day technology showed that an EPMAV is both feasible and has the possibility to provide better endurance durations than a battery-only configuration.

The endeavor yielded additional conclusions that did not fall into the three specific categories the mission simulations addressed. The results showed that the best endurance times came from maximizing the mass of hydrogen and the fuel cell over the mass of the battery. The mass of hydrogen greatly affected endurance durations because

of its high specific energy. For the high-fidelity power source CA, the results indicated that the best guesses for starting fuel cell voltage and the battery's initial specific power were between 0.7 and 0.8 V and 650 and 1150 W/kg, respectively. These results were close to the expectations based upon the conclusions of the second DOE.

Overall, endurance durations ranged from 88.5 min to 831 min, although Chapter 4 showed that the spectrum was much tighter if the results were broken down by either current or future technology and a specific ESD mass allowance. To achieve an endurance duration of 88.5 minutes, the options included the low-fidelity CA for all CAs with the exception of the power management CA, current ESD technology, and a 25% ESD allowance. For an endurance duration of 831 minutes, the selections utilized included the high-fidelity CA for all CAs, future technology, and a 25% ESD allowance.

These conclusions provide assistance in the decision-making process that surrounds EPMAVs, as requested by the sponsor. The framework of the model allowed for future, user-friendly changes to investigate different missions, MAV platforms, motors, propellers, and ESDs. Furthermore, additional levels of fidelity could be added to the model to examine various aspects of MAV design as technology continues to change. Though the model satisfied the objectives of this research, several areas of research could be addressed in the future to increase the accuracy of the model or to ultimately get an EPMAV into the sky.

V.2. Recommendations for Future Research

The creation of a multi-fidelity model for the conceptual design of an EPMAV provided the foundation for several areas to be investigated in the future.

Recommendations for future research were based on improvements or changes that could be made to the model as well as follow on projects that stem from the model's creation such as flight-testing a physical EPMAV.

- A logical next step in the development of an AFIT EPMAV would be to perform dynamometer testing with the equipment recently acquired by AFIT for the examination of various ICE-battery hybrid configurations of small RPAs. These tests would provide validation for the propulsion CA of this effort and lead to more accurate predictions for future flight-testing.
- Along with the dynamometer tests, power source testing to obtain actual Ragone plots and polarization curves could be conducted by using ESDs and equipment from AFRL/RZPS. These tests would provide increased fidelity to the design of an EPMAV and would serve as further validation for this effort by using more accurate inputs.
- Flight-testing would serve as the ultimate validation for the model created in this effort and those before it. Flight-testing could be performed at AFIT with the BATMAV, a MAV owned and operated by AFIT, as well as ESDs from AFRL/RZPS. Flight-testing a different MAV configuration would require the creation of numerous files for programs like QPROP and AVL, but the easy access to the BATMAV still makes it advantageous. Another option for flight-testing would be the GenMAV configuration, which could be flown by working with AFRL/RWAV at Eglin AFB. Ideally, both flight-tests could be performed.
- Having completed a rubber endurance segment model, another model that prescribes the endurance duration and focuses on minimizing system mass would be interesting

to look at. A model of this type would be a transition from the framework created in this endeavor and would utilize mass feedback from the power sources to ensure that reductions in ESD weight were accounted for. Such a model would be similar to Hrad's effort and would provide a comparison.

- Additional levels of fidelity could be added to the model. In particular, a thesis could focus on each of the CAs presented. In the time allotted for a thesis, it was not possible to dig deep into any specific CA. While increased attention was given to the power source CA, a lot of time was still required by the other CAs to ensure the model ran successfully. Furthermore, it would be helpful to have students from different backgrounds, namely electrical engineering, help in the design. Increased fidelity of the model would be something that could be done in tandem with flight-testing and provide both modeled and experimental results for validation.
- If the fidelity of the power source CA were to be increased, several different areas could be addressed and the following are just a few examples. First, recharging could be added to the current battery model. Next, a DC-to-DC converter could be put into places so that the demands on the fuel cell and battery could be examined on a current and voltage basis instead of power alone. Finally, the various mission segments could be split into much smaller time increments to investigate the use of capacitors.
- The model could be modified to allow for different MAV configurations such as MAVs with rotary wings and flapping wings.

Appendix A: Software Versions

The analysis performed for this research depends on the model's ability to access several different pieces of software. The model will run only if the correct version of the software or an updated version of the software is used, provided the updated version of the software supports older versions. The following shows the software used in the model along with its version.

- Model Center Version 9.01
  - Optimization\Design Explorer Version: 2.2.6
  - Optimization\Gradient Optimizer Version: 2.2.6
  - Converger Version: 1.2.1
  - Design Explorer Version: 2.2.6
  - Gradient Optimizer Version: 2.2.6
  - MATLAB Plug-In Version: 1.6.7
- Analysis Server v.6.02 Build 33619
- Mathworks MATLAB R2009b
- Microsoft Excel 2007
- Athena Vortex Lattice (AVL) Version 3.26
- QPROP Version 1.21
- SolidWorks 2009 x64 Edition SP2.1
- XFOIL Version 6.96
- xflr5 Version 6.02
- All research was conducted on a HP d500t with an Intel Quad Core processer (2.67 GHz), 4 GB of RAM, a 32-bit operating system, and a Microsoft Windows version of Vista Home Premium, Service Pack 2

Appendix B: Software Tips and Tricks

Throughout the creation of the model, several challenges were encountered that are worth presenting to save future users time and energy. Some of the challenges were with particular software codes, while the majority came from working within MC or using MC to communicate with other programs. Overall, the best way to overcome these challenges and others like them was to become familiar with MC and the individual programs; however, the challenges in this effort are shown here so they can be avoided in the future.

- Decide on a naming convention for variables and use it throughout the creation of the model and all CAs. MC allows for variables with different names to be linked, but linkages in MC go far more smoothly if naming convention is the same. This is especially relevant when hundreds of variables are linked together. A proper naming convention can save days of work ensuring that the model's CAs are properly connected.
- Pay special attention to what language is being used for coding. Throughout the effort, the model crashed several times because of nuances between languages. For example, VBScript begins counting at zero for elements in an array and MATLAB begins at one. The difference is easy to account for, but it can be hard to find specific errors when MC crashes because the script files written in VBScript have to be tested in the MC environment. Another example of such an occurrence is that MATLAB has a stored value for pi and VBScript does not.
- For a variable-fidelity model using an if-block, linkages work very intuitively. For example, if you have power required on both branches of an if-block, link both results

to the component downstream that needs power required as an input. MC will automatically use the value for power required from the branch that was executed. This becomes slightly more complicated if the if-block occurs within a for-each loop. To store a value from an if-block for each iteration of a for-each loop, a quick script file (called a "collector" in this analysis) can be created to store the value of the branch that was executed. This is only necessary if the component that needs the data from the if-block is outside of the for-each loop.

- One general tip is to ensure that MATLAB and other codes work before integrating them into MC. The MC environment takes longer to run through the analysis and often makes it hard to find the specific error from the software being run. Furthermore, the time required to make small changes is greatly increased if debugging is performed within MC. Debugging can be performed outside of MATLAB by providing the specific code with the input variables necessary for execution. It is important that these test variables are commented out of the software's execution after debugging or else they will override the values MC feeds to it.
- Debugging the model in the MC environment for components such as the use of if-blocks and for-each loops works best with a "toy model." A toy model performs the same task as the real model, but the operations of the components within the toy model are simple so that the results are easy to confirm. Once a toy model works, it is easy to update the actual model.
- MC allows components from one model to be copied and pasted into another model. This increases the utility of the toy model discussed earlier. Furthermore, it might be

easier in future efforts to create a model for each of the CAs and then copy and paste them into the main model. This would allow for easier manipulation and debugging of individual CAs.

- MC did not always update to the latest version of updated MATLAB code. This was likely some kind of bug that will be fixed in future versions of the software, but the best way to get around this was to re-call the updated file in the MATLAB plug-in, save changes, and then restart MC.
- Even with a powerful PC, the size of DOE should be kept as small as possible to determine the results required. Running DOE with over 1,500 design points often crashed the PC used for analysis. Once completed, DOE of this size often crashed when the data was manipulated for post-processing analysis like glyph plots. Furthermore, even DOE with 64 design points could take longer than three hours to complete. To minimize computation costs, start with smaller DOE and determine if a larger sample is needed. Furthermore, make sure to plan so work in other areas can be completed while DOE are executed.
- MC requires a lot of RAM to conduct mission simulations or DOE. After running several of these studies, it was found that run time kept increasing. As such, occasionally closing MC and AS helped to free up RAM and increase run speed.
- MC would sometimes error from old links floating around from components deleted or replaced. For example, if a MATLAB plug-in is replaced with a script file that performs the same analysis but reduces computational costs, downstream components still thought the old component was there. This was not always the case, but when it

occurred, the link editor could be used to delete the corrupt linkages and change the links to the new code.

- Optimizations in MC were the best way to find out infeasible points of the model. In general, the use of a DOE or parametric study was much easier to find an optimal result. If an optimizer is desired, be sure to examine the design space with DOE and parametric studies to reduce the size of the design space that the optimizer iterates through.
- Running XFOIL in batch mode was complicated. This was solved by using the xflr5 GUI. With the GUI, XFOIL analysis was much more straightforward. It is highly recommended that future analysis with XFOIL be performed through xflr5.
- Finally, be sure to save work often. The use of MATLAB and MC on any PC is demanding and crashes did occur upon occasion. Additionally, be sure to create a naming convention for different versions of the model and code used for the model. Sometimes the changes that were made to the model or supporting codes led to errors and it was easiest to solve the errors by comparing the old and new versions of the code.

Appendix C: Software Files

The software used in the final model is presented in this section. The software is presented in order of the CA it fell into. The final section presents code that did not fall into a specific CA but was necessary for understanding the data flow through the model. Script files that only served MC-specific tasks such as "collectors" are not presented. The best way to understand how the model works is to run MC on a computer; however, the files are still included to give an idea of how each code affected the model.

C.1. Aerodynamic CA

a. drag_polar

File title: drag_polar
Parent program: MC
Description: This is a script file within MC. In addition to the code shown below, information on input and output variables had to be specified in a GUI within MC.
Code:

```
sub run
K=(CD_drag_polar-CD_0)/(CL_drag_polar)^2
velocity_endurance = sqr(2*mass_corrected*9.81*(sqr(K/(3*CD_0)))/(density*S_m2))
reset_to_stall_end = true
pi=4*Atn(1)
e =1/(pi*aspect_ratio*K)
end sub
```

b. run_AVL.fileWrapper

File title: run_AVL.fileWrapper
Parent program: MC
Description: This is the fileWrapper used to connect AVL to MC. It tells MC what are inputs and outputs and where to find them. In order for MC to access AVL, AS was required.
Code:

```
#
# Athena Vortex Lattice filewrapper
#
# @author: Paul Hrad; editted by Doug Pederson
# @version: 9 Nov 2010
# @helpURL: http://web.mit.edu/drela/Public/web/avl/
# @description: GenMAV AVL (Normal Dihedral - v2.2)
# @keywords: AVL, aero, vortex method

RunCommands
{
# Put ModelCenter values in the input files
```

```
# Geometry file
 generate inputFile1
# Constraint file
 generate inputFile2
# Mass file
 generate inputFile3

# Run the code
# This file transmits instruction to command line
 run "run_AVL_GenMAV.bat"

# Parse the standard output file
 parse outputfile
}

RowFieldInputFile inputFile1
{
# The template file is not changed. It is a template for the .avl file, which is changed by MS every iteration.
templateFile:                GenMAV.template
initializationFile:    GenMAV.initial
fileToGenerate:      GenMAV.avl

setDelimiters " ,"
setGroup "user_inputs.geometry_input_file"
variable: Mach       double 6 1          description="keep it zero for M<0.2"
variable: iYsym              double 7 1          description="Symm about y=0 and/or Z=0"
variable: iZsym              double 7 2          description="Symm about y=0 and/or Z=0"
variable: Zsym               double 7 3          description="Symm about y=0 and/or Z=0"
variable: S_ref_sqin         double 8 1          description="reference ares-> all coeffs"
variable: C_ref_in   double 8 2          description="-> Cm"
variable: b_ref_in   double 8 3          description="span-> Cl,Cn"
variable: X_origin_in        double 9 1          description="Global x Point of Origin"
variable: Y_origin_in        double 9 2          description="Global y Point of Origin"
variable: Z_origin_in        double 9 3          description="Global z Point of Origin"
variable: Cdp                double 10 1         description="Optional default profile drag added to geometry"

setGroup "user_inputs.fuselage"
variable: F_nodes    double 16 1         description="Source-Line node"
variable: F_space    double 16 2         description="Spacing, -3<range<3: 1=cosine"
variable: F_Trans_x          double 19 1         description="Translates fuselage x coordinates"
variable: F_Trans_y          double 19 2         description="Translates fuselage y coordinates"
variable: F_Trans_z          double 19 3         description="Translates fuselage z coordinates"

setGroup "user_inputs.Wing"
variable: Nchord_w double 29 1         description="# chordwise segments, wing"
variable: Cspace_w double 29 2         description="Spacing, -3<range<3: 1=cosine"
variable: Nspan_w  double 29 3         description="# spanwise segments, wing"
variable: Sspace_w double 29 4         description="Spacing, -3<range<3: -2= -sine"
variable: Angle_w  double 31 1         description="Offset added to incidence angles for all sections, in deg"
variable: scale_x_w double 33 1        description="Scale factor of x coordinates for wing"
variable: scale_y_w double 33 2        description="Scale factor of y coordinates for wing"
variable: scale_z_w double 33 3        description="Scale factor of z coordinates for wing"
variable: W_Trans_x          double 35 1         description="Translates wing x coordinates"
variable: W_Trans_y          double 35 2         description="Translates wing y coordinates"
variable: W_Trans_z          double 35 3         description="Translates wing z coordinates"
variable: W_yduplicate       double 37 1         description="y position of duplication"

setGroup "user_inputs.Wing.Section_1"
variable: Xle1                       double 43 1         description="Leading Edge Location,x"
variable: Yle1                       double 43 2         description="Leading Edge Location,y"
```

```
variable: Zle1                  double 43 3         description="Leading Edge Location,z"
variable: Chord1            double 43 4         description="Chord length"
variable: Ainc1                 double 43 5         description="Incidence angle about spanwise axis projected
on y-z plane"

setGroup "user_inputs.Wing.Section_2"
variable: Xle12                 double 49 1         description="Leading Edge Location,x"
variable: Yle12                 double 49 2         description="Leading Edge Location,y"
variable: Zle12                 double 49 3         description="Leading Edge Location,z"
variable: Chord2            double 49 4         description="Chord length"
variable: Ainc2                 double 49 5         description="Incidence angle about spanwise axis projected
on y-z plane"

setGroup "user_inputs.Wing.Section_3"
variable: Xle3                  double 54 1         description="Leading Edge Location,x"
variable: Yle3                  double 54 2         description="Leading Edge Location,y"
variable: Zle3                  double 54 3         description="Leading Edge Location,z"
variable: Chord3            double 54 4         description="Chord length"
variable: Ainc3                 double 54 5         description="Incidence angle about spanwise axis projected
on y-z plane"

setGroup "user_inputs.Wing.Section_4"
variable: Xle4                  double 59 1         description="Leading Edge Location,x"
variable: Yle4                  double 59 2         description="Leading Edge Location,y"
variable: Zle4                  double 59 3         description="Leading Edge Location,z"
variable: Chord4            double 59 4         description="Chord length"
variable: Ainc4                 double 59 5         description="Incidence angle about spanwise axis projected
on y-z plane"

setGroup "user_inputs.Wing.Section_5"
variable: Xle5                  double 64 1         description="Leading Edge Location,x"
variable: Yle5                  double 64 2         description="Leading Edge Location,y"
variable: Zle5                  double 64 3         description="Leading Edge Location,z"
variable: Chord5            double 64 4         description="Chord length"
variable: Ainc5                 double 64 5         description="Incidence angle about spanwise axis projected
on y-z plane"

setGroup "user_inputs.Wing.Section_6"
variable: Xle6                  double 69 1         description="Leading Edge Location,x"
variable: Yle6                  double 69 2         description="Leading Edge Location,y"
variable: Zle6                  double 69 3         description="Leading Edge Location,z"
variable: Chord6            double 69 4         description="Chord length"
variable: Ainc6                 double 69 5         description="Incidence angle about spanwise axis projected
on y-z plane"

setGroup "user_inputs.Wing.Section_7"
variable: Xle7                  double 74 1         description="Leading Edge Location,x"
variable: Yle7                  double 74 2         description="Leading Edge Location,y"
variable: Zle7                  double 74 3         description="Leading Edge Location,z"
variable: Chord7            double 74 4         description="Chord length"
variable: Ainc7                 double 74 5         description="Incidence angle about spanwise axis projected
on y-z plane"

setGroup "user_inputs.Wing.Section_8"
variable: Xle8                  double 79 1         description="Leading Edge Location,x"
variable: Yle8                  double 79 2         description="Leading Edge Location,y"
variable: Zle8                  double 79 3         description="Leading Edge Location,z"
variable: Chord8            double 79 4         description="Chord length"
variable: Ainc8                 double 79 5         description="Incidence angle about spanwise axis projected
on y-z plane"
```

```
setGroup "user_inputs.Wing.Section_9"
variable: Xle9                  double 84 1         description="Leading Edge Location,x"
variable: Yle9                  double 84 2         description="Leading Edge Location,y"
variable: Zle9                  double 84 3         description="Leading Edge Location,z"
variable: Chord9            double 84 4         description="Chord length"
variable: Ainc9                 double 84 5         description="Incidence angle about spanwise axis projected
on y-z plane"

setGroup "user_inputs.Wing.Section_10"
variable: Xle10                 double 89 1         description="Leading Edge Location,x"
variable: Yle10                 double 89 2         description="Leading Edge Location,y"
variable: Zle10                 double 89 3         description="Leading Edge Location,z"
variable: Chord10           double 89 4         description="Chord length"
variable: Ainc10            double 89 5         description="Incidence angle about spanwise axis projected on y-z
plane"

setGroup "user_inputs.Wing.Section_11"
variable: Xle11                 double 94 1         description="Leading Edge Location,x"
variable: Yle11                 double 94 2         description="Leading Edge Location,y"
variable: Zle11                 double 94 3         description="Leading Edge Location,z"
variable: Chord11           double 94 4         description="Chord length"
variable: Ainc11            double 94 5         description="Incidence angle about spanwise axis projected on y-z
plane"

setGroup "user_inputs.Wing.Section_12"
variable: Xle12                 double 99 1         description="Leading Edge Location,x"
variable: Yle12                 double 99 2         description="Leading Edge Location,y"
variable: Zle12                 double 99 3         description="Leading Edge Location,z"
variable: Chord12           double 99 4         description="Chord length"
variable: Ainc12            double 99 5         description="Incidence angle about spanwise axis projected on y-z
plane"

setGroup "user_inputs.Wing.Section_13"
variable: Xle13                 double 104 1        description="Leading Edge Location,x"
variable: Yle13                 double 104 2        description="Leading Edge Location,y"
variable: Zle13                 double 104 3        description="Leading Edge Location,z"
variable: Chord13           double 104 4        description="Chord length"
variable: Ainc13            double 104 5        description="Incidence angle about spanwise axis projected on y-z
plane"

setGroup "user_inputs.Wing.Section_14"
variable: Xle14                 double 109 1        description="Leading Edge Location,x"
variable: Yle14                 double 109 2        description="Leading Edge Location,y"
variable: Zle14                 double 109 3        description="Leading Edge Location,z"
variable: Chord14           double 109 4        description="Chord length"
variable: Ainc14            double 109 5        description="Incidence angle about spanwise axis projected on y-z
plane"

setGroup "user_inputs.Horizontal_Tail"
variable: Nchord_HT         double 119 1        description="# chordwise segments,HT"
variable: Cspace_HT         double 119 2        description="Spacing, -3<range<3: 1=cosine"
variable: Nspan_HT          double 119 3        description="# spanwise segments,HT"
variable: Sspace_HT         double 119 4        description="Spacing, -3<range<3: -2= -sine"
variable: Angle_HT          double 121 1        description="Offset added to incidence angles for all sections, in deg"
variable: HT_Trans_x        double 123 1        description="Translates HT x coordinates"
variable: HT_Trans_y        double 123 2        description="Translates HT y coordinates"
variable: HT_Trans_z        double 123 3        description="Translates HT z coordinates"
#variable: Y_duplicate   double 125 1    description="Geometric surface reflection about x-z axis"
```

```
setGroup "user_inputs.Horizontal_Tail.Left_tip"
variable: Xle1                    double 127 1        description="Leading Edge Location,x"
variable: Yle1                    double 127 2        description="Leading Edge Location,y"
variable: Zle1                    double 127 3        description="Leading Edge Location,z"
variable: Chord1          double 127 4        description="Chord Length"
variable: Ainc1                   double 127 5        description="Incidence angle about spanwise axis projected
on y-z plane"
variable: L_Elevon_gain1  double 130 2        description="Control deflection gain, units"
variable: L_Elevon_Xhinge1 double 130 3       description="Location of elevator as chord fraction"
#variable: SgnDup         double 130 7   description="Control surface duplication (+1 for elevator)"

setGroup "user_inputs.Horizontal_Tail.Center"
variable: Xle2                    double 133 1        description="Leading Edge Location,x"
variable: Yle2                    double 133 2        description="Leading Edge Location,y"
variable: Zle2                    double 133 3        description="Leading Edge Location,z"
variable: Chord2          double 133 4        description="Chord Length"
variable: Ainc2                   double 133 5        description="Incidence angle about spanwise axis projected
on y-z plane"
variable: L_Elevon_gain2  double 136 2        description="Control deflection gain, units"
variable: L_Elevon_Xhinge2 double 136 3       description="Location of elevator as chord fraction"
variable: R_Elevon_gain2  double 139 2        description="Control deflection gain, units"
variable: R_Elevon_Xhinge2 double 139 3       description="Location of elevator as chord fraction"

setGroup "user_inputs.Horizontal_Tail.Right_tip"
variable: Xle3                    double 142 1        description="Leading Edge Location,x"
variable: Yle3                    double 142 2        description="Leading Edge Location,y"
variable: Zle3                    double 142 3        description="Leading Edge Location,z"
variable: Chord3          double 142 4        description="Chord Length"
variable: Ainc3                   double 142 5        description="Incidence angle about spanwise axis projected
on y-z plane"
variable: R_Elevon_gain3  double 145 2        description="Control deflection gain, units"
variable: R_Elevon_Xhinge3 double 145 3       description="Location of elevator as chord fraction"


setGroup "user_inputs.Vertical_Tail"
variable: Nchord_VT       double 149 1        description="# chordwise segments,VT"
variable: Cspace_VT       double 149 2        description="Spacing, -3<range<3: 1=cosine"
variable: Angle_VT        double 151 1        description="Offset added to incidence angles for all sections, in deg"
variable: VT_Trans_x      double 153 1        description="Translates VT x coordinates"
variable: VT_Trans_y      double 153 2        description="Translates VT y coordinates"
variable: VT_Trans_z      double 153 3        description="Translates VT z coordinates"

setGroup "user_inputs.Vertical_Tail.VT_Root"
variable: Xle1                    double 157 1        description="Leading Edge Location,x"
variable: Yle1                    double 157 2        description="Leading Edge Location,y"
variable: Zle1                    double 157 3        description="Leading Edge Location,z"
variable: Chord1          double 157 4        description="Chord Length"
variable: Ainc1                   double 157 5        description="Incidence angle about spanwise axis projected
on y-z plane"
variable: Nspan1          double 157 6        description="# spanwise segments,VT"
variable: Sspace1         double 157 7        description="Spacing, -3<range<3: -2= -sine"

setGroup "user_inputs.Vertical_Tail.VT_Tip"
variable: Xle2                    double 161 1        description="Leading Edge Location,x"
variable: Yle2                    double 161 2        description="Leading Edge Location,y"
variable: Zle2                    double 161 3        description="Leading Edge Location,z"
variable: Chord2          double 161 4        description="Chord Length"
variable: Ainc2                   double 161 5        description="Incidence angle about spanwise axis projected
on y-z plane"
variable: Nspan2          double 161 6        description="# spanwise segments,VT"
```

```
variable: Sspace2                double 161 7          description="Spacing, -3<range<3: -2= -sine"
}

RowFieldInputFile inputFile2
{
# The template file is not changed. It is a template for the batch file, which is changed by MS every iteration.
templateFile:                    GenMAV_constraints.template
fileToGenerate:      GenMAV_constraints.batch

setDelimiters "= ,"
setGroup user_inputs.run_constraints
variable: density      double 4 2 description="Air Density" units="kg/m^3)"
variable: velocity      double 5 2 description="Velocity" units="m/s"
variable: mass_total    double 3 2 description="Unit Mass" Units="kg"
variable: PitchMoment   double 7 3 description="Set Pitch Moment"
variable: RollMoment    double 8 3 description="Set Roll Moment"
# The output file is named within this input file.
}

RowFieldInputFile inputFile3
{
# The template file is not changed. It is a template for the batch file, which is changed by MS every iteration.
templateFile:                    GenMAV_mass.template
fileToGenerate:      GenMAV.mass

setDelimiters "= ,"
setGroup user_inputs.total_mass
markAsBeginning "Battery"
variable: powersource_mass               double 1 1 description="Mass of fuel cell, battery, fuel, and tank" units="kg"
# The output file is named within this input file.
}

RowFieldOutputFile outputFile
{
# This routine parses the program output file.
# Other variables can be extracted as desired.
 fileToParse: results_GenMAV.txt

 setDelimiters "= ,"

setGroup Results.Ref_values
 markAsBeginning "Sref"
variable: Sref_sqin        double 1 2
variable: Cref_in                double 1 4
variable: bref_in                double 1 6
variable: Xref_CG_in                     double 2 2
variable: Yref_CG_in                     double 2 4
variable: Zref_CG_in                     double 2 6

setGroup Results.Other
 markAsBeginning "Alpha"
 variable: Alpha       double 1 2      description="Angle of Attack"
 variable: Beta              double 2 2      description="Slide slip angle"
 variable: L_Elevondouble 15 2            description="Left Elevon deflection"
 variable: R_Elevondouble 16 2            description="Right Elevon deflection"

setGroup Results.aero_coeff
 markAsBeginning "CLtot"
 variable: CL_tot    double 1 2           description="Total Lift Coef"
 variable: CD_tot    double 2 2           description="Total Drag Coef"
```

```
variable: CD_ind   double 3 4          description="Induced Drag Coef"
variable: e        double 5 4          description="Span Efficiency Factor"

setGroup Results.Other
markAsBeginning "Neutral"
variable: Xnp      double 1 4          description="neutral point"

}
```

c. run_AVL_GenMAV.bat

File title: run_AVL_GenMAV.bat
Parent program: AVL
Description: This file is the command line execution information. It tells MC to run AVL with the specified ".avl" file and the commands listed in the ".batch" file. ("%" is not a comment designator)
Code:

```
% avl GenMAV.avl GenMAV.run < GenMAV_constraints.batch
```

d. GenMAV_constraints.batch

Filename: GenMAV_constraints.batch
Parent program: AVL
Description: This file lists the commands passed to AVL to conduct aerodynamic analysis. This file will change depending on the values passed to it from MC for mass, density, and velocity
Code:

```
OPER
C1
M 1.4252
D 1.19586793456957
V 16.7261267661681
D1 PM 0.0
D2 RM 0.0
X
ST
results_GenMAV.txt
Y
QUIT
```

e. GenMAV_constraints.template

Filename: GenMAV_constraints.template
Parent program: MC
Description: This file is the same exact format as "GenMAV_constraints.batch", but serves as a template for the values passed to AVL from MC. Therefore, this file does not change when MC is ran.
Code: See code for "GenMAV_constraints.batch"

f. GenMAV.avl

Filename: GenMAV.avl
Parent program: AVL
Description: This file contains the geometry of the GenMAV for AVL.
Code:

```
GenMAV ! (Normal Dihedral - v2.2)
```

```
# Units in inches, sq-in, deg
#=============================================
# HEADER DATA
#=============================================
0.0                             Mach  !Default Mach for Prandtl-Glauert compressibility correction
0.0       0.0       0.0         iYsym  iZsym  Zsym  !Symm about y=0 and/or z=Zsym
111.68  4.7757  24.0            Sref   Cref   Bref  !Sref -> all coeffs | Cref -> Cm | Bref -> Cl,Cn
0.0       0.0       0.0         Xref   Yref   Zref  !Point of Origin
0.102                           CDp !Optional - default profile drag coeff added to geometry
#=============================================
# FUSELAGE DATA
#=============================================
BODY
Fuselage  !body name string
    37.0  1.0  !15 source-line nodes with cosine spacing (1.0)

TRANSLATE
    0.0  0.0  0.0
BFILE
            Fuselage_v2pt2.dat

#=============================================
# WING DATA
#=============================================
SURFACE
Right Wing  !surface name string
    7.0  1.0  25.0  -2.0  !Nchord Cspace Nspan Sspace
ANGLE
    9.0  !Offset added to incidence angles for all sections, in deg
SCALE
    1.0  1.0  1.0
TRANSLATE
    5.75  0.0  1.578
YDUPLICATE
    0.0

#------------------------------------------------------
#    Xle         Yle         Zle       Chord      Ainc
#------------------------------------------------------
SECTION
    0.0         0.0         0.0          5.0         0.0
AFILE
    GenMAVA0.dat
#----------------------------
SECTION

    0.0         1.5         0.02498    5.0         0.0
AFILE
    GenMAVA0.dat
#----------------------------
SECTION
    0.007623    7.11    0.25615    4.9619      0.0
AFILE
    GenMAVA1.dat
#----------------------------
SECTION
    0.024782    8.23    0.41519    4.8761      0.0
AFILE
    GenMAVA2.dat
#----------------------------
```

```
SECTION
    0.047308    8.91     0.54277    4.7635      0.0
AFILE
    GenMAVA3.dat
#----------------------------
SECTION
    0.087735    9.6        0.69949    4.5613      0.0
AFILE
    GenMAVA4.dat
#----------------------------
SECTION
    0.147058    10.2       0.86023    4.2647      0.0
AFILE
    GenMAVA5.dat#----------------------------
SECTION
    0.249591    10.82      1.05224    3.752      0.0
AFILE
    GenMAVA6.dat
#----------------------------
SECTION
    0.408039    11.37      1.24622    2.9598      0.0
AFILE
    GenMAVA7.dat
#----------------------------
SECTION
    0.512614    11.6       1.33428    2.4369      0.0
AFILE       GenMAVA8.dat
#----------------------------
SECTION
    0.671564    11.83      1.42659    1.6422      0.0AFILE
    GenMAVA9.dat
#----------------------------
SECTION
    0.745531    11.9       1.45554    1.2723      0.0
AFILE
    GenMAVA10.dat
#----------------------------
SECTION
    0.818751    11.95      1.47646    0.9062      0.0
AFILE
    GenMAVA11.dat
#----------------------------
SECTION
    1.0    12.0         1.4976    0.0      0.0
AFILE
    GenMAVA11.dat


#============================================
# TAIL DATA
#============================================
SURFACE
Horizontal Tail
    9.0  -2.0   20.0   1.0 !Nchord Cspace Nspan Sspace
ANGLE
    1.5  !Offset added to incidence angles for all sections, in deg
TRANSLATE
    14.75   0.0  0.0#----------------------------
SECTION  !Horizontal tail fin tip
#    Xle     Yle     Zle     Chord   Ainc
```

```
   1.5    -6.0      0.0   2.375   0.0
CONTROL
#   Cname     Cgain   Xhinge  HingeVec
   L_Elevon  1.0     0.5     0.0  0.0  0.0
#----------------------------
SECTION  !Horizontal tail fin root
   0.0   0.0   0.0   3.875  0.0
CONTROL
#   Cname     Cgain   Xhinge   HingeVec
   L_Elevon  1.0     0.5      0.0  0.0  0.0
CONTROL
#   Cname     Cgain   Xhinge   HingeVec
   R_Elevon  1.0     0.5      0.0  0.0  0.0
#----------------------------
SECTION  !Horizontal tail fin tip
   1.5      6.0       0.0   2.375   0.0
CONTROL
#   Cname     Cgain   Xhinge  HingeVec
   R_Elevon  1.0     0.5     0.0  0.0  0.0
#============================================
SURFACE
Vertical Tail Fin
   9.0  -2.0  !Nchord Cspace Nspan Sspace
ANGLE
   0.0  !Offset added to incidence angles for all sections, in deg
TRANSLATE
   14.75   0.0  0.0
#----------------------------
SECTION  !Vertical tail fin root
#   Xle     Yle     Zle     Chord   Ainc    Nspan   Sspace
   0.0   0.0   0.0   3.278   0.0     11.0     -2.0

#----------------------------
SECTION  !Vertical tail fin tip
   1.593   0.0   4.625   2.25   0.0     1.0     1.0
#============================================
# END genmav_2pt2.avl
```

g. GenMAV.template

Filename: GenMAV.template
Parent program: MC
Description: The template file for ".avl" information from MC. This file does not change when MC is ran.
Code: See GenMAV.avl

h. GenMAV.initial

Filename: GenMAV.initial
Parent program: AVL
Description: This is an optional file that has the same format as the ".avl" file used to set initial values in AVL.
Code: See GenMAV.avl

i. GenMAV.mass

Filename: GenMAV.mass
Parent program: AVL

Description: This file provides the GenMAV's mass, coordinates, and units, etc. This information was helpful to determine the mass of the ESD and sensors currently on the GeMAV. The detail of this file is really only necessary for eigenmode analysis, which this effort did not explore.
Code:

```
#
#  GenMAV - version 2.2 - cg 6.4 in
#  0-deg Dihedral (Baseline)
#  Mass & Inertia Breakdown
#
#   x back
#   y right
#   z up
#
#========================================
# UNIT DATA
# - Scales the mass, xyz, and inertia table data
# - LUNIT also scales all lengths / areas in AVL input file
#========================================
Lunit = 0.0254 m
Munit = 0.001 kg
Tunit = 1.0 s
#========================================
# CONSTANTS
# - Gravity and density to be used in trim setup
# - Must be in unit names given above
#========================================
g   = 9.81
rho = 1.225
#========================================
# MASS, POSITION, INERTIA DATA
# - x,y,z is location of item's own cg
# - Ixx...Iyz are item's inertias about item's own cg
# - Must use same point of origin as AVL input file
#========================================
#  Mass    x        y        z       Ixx       Iyy       Izz
*  1       1        1        1        1         1         1
+  0       0        0        0        0         0         0
   452.00  7.3160  0.000  0.123  141.86   1453.55  1420.45   ! Fuselage
   24.450  7.9870 -5.036  1.505  293.40   37.37    330.77    ! Left Wing
   24.450  7.9870  5.036  1.505  293.40   37.37    330.77    ! Right Wing
   8.3945  17.033 -2.760  0.000  25.180   6.830    32.010    ! Left Horizontal Tail
   8.3945  17.033  2.760  0.000  25.180   6.830    32.010    ! Right Horizontal Tail
   5.1766  16.816  0.000  2.235  9.2300   11.92    2.7000    ! Vertical Tail
   15.200 -0.3750  0.000  0.000  57.480   28.74    28.740    ! Propeller
   44.500  0.5000  0.000  0.000  5.5600   5.620    5.6200    ! Motor
   142.50  3.0000  0.000  0.750  25.110   21.45    7.5700    ! Battery
   91.000  5.2500 -0.563  0.000  81.050   81.05    25.590    ! Left Shock
   91.000  5.1250  0.563  0.000  81.050   81.05    25.590    ! Right Shock
   24.600  7.0000  0.000 -0.500  0.4600   0.980    1.4200    ! Spd Cntrl
   44.600  7.5000  0.000  2.240  1.1600   1.160    1.8600    ! AP / Modem
   16.000  9.8750  0.000  0.750  0.3000   1.030    1.1700    ! GPS
   9.3000  14.625  0.000  0.250  0.1500   0.240    0.1600    ! Servo 1
   9.3000  15.438  0.000  0.188  0.1500   0.240    0.1600    ! Servo 2
   7.1000  17.000  0.000  1.500  0.0700   0.070    0.0700    ! Camera
```

j. GenMAV.run

Filename: GenMAV.run

Parent program: AVL
Description: This optional file allows for the input of individual flight conditions that could otherwise be entered into the AVL user interface in MS DOS. For this analysis, a ".run" file was not used. Instead the desired flight conditions came from the run_AVL_GenMAV.batch file.
Code:

```
---------------------------------------------
 Run case  1:  Base Run

 alpha        ->  alpha       =   0.00000
 beta         ->  beta        =   0.00000
 pb/2V        ->  pb/2V       =   0.00000
 qc/2V        ->  qc/2V       =   0.00000
 rb/2V        ->  rb/2V       =   0.00000
 L_Elevon     ->  Cm pitchmom =   0.00000
 R_Elevon     ->  Cl roll mom =   0.00000

 alpha     =   0.00000     deg
 beta      =   0.00000     deg
 pb/2V     = -0.365837E-15
 qc/2V     =   0.00000
 rb/2V     =   0.00000
 CL        =  0.553571
 CDo       =  0.102
 bank      =   0.00000     deg
 elevation =   0.00000     deg
 heading   =   0.00000     deg
 Mach      =  0.400000E-01
 velocity  =   13.4100     m/s
 density   =   1.22500     kg/m^3
 grav.acc. =   9.81000     m/s^2
 turn_rad. =   0.00000     m
 load_fac. =   1.00000
 X_cg      =   6.40844     m
 Y_cg      =  0.409869E-09 m
 Z_cg      =  0.355575     m
 mass      =   1.01797     kg
 Ixx       =  0.181759E-02 kg-m^2
 Iyy       =  0.754403E-02 kg-m^2
 Izz       =  0.854157E-02 kg-m^2
 Ixy       =  0.413171E-05 kg-m^2
 Iyz       = -0.268490E-11 kg-m^2
 Izx       = -0.137953E-03 kg-m^2
 visc CL_a =   0.00000
 visc CL_u =   0.00000
 visc CM_a =   0.00000
 visc CM_u =   0.00000
```

k. GenMAV Airfoil Data Files

Filename: GenMAVA0.dat through GenMAVA11.dat
Parent program: AVL
Description: Airfoil data from root to tip. Each file is a separate airfoil. The actual code of each file is stored as a single column but was split into two columns to reduce wasted space.
Code:

GenMAVA0.dat	GenMAVA1.dat	GenMAVA2.dat	GenMAVA3.dat
MAV - v2.0 - Root Airfoil	MAV - v2.0 - Airfoil Cross Section - Chord 4.96188	MAV - v2.0 - Airfoil Cross Section - Chord 4.96188	MAV - v2.0 - Airfoil Cross Section - Chord 4.76346

1	0.00363	1	-0.00236	1	-0.00236	1	-0.00745
0.98248	0.00465	0.98849	-0.0017	0.98849	-0.0017	0.98432	-0.0068
0.96489	0.00549	0.97076	-0.00085	0.97076	-0.00085	0.96569	-0.00606
0.94721	0.00622	0.95295	-0.00012	0.95295	-0.00012	0.947	-0.0053
0.92947	0.00692	0.93507	0.00059	0.93507	0.00059	0.92826	-0.00447
0.91166	0.00765	0.91713	0.00132	0.91713	0.00132	0.90947	-0.00353
0.89381	0.00844	0.89914	0.00212	0.89914	0.00212	0.89065	-0.00246
0.87591	0.00933	0.8811	0.00302	0.8811	0.00302	0.8718	-0.00124
0.85797	0.01035	0.86303	0.00405	0.86303	0.00405	0.85294	0.00012
0.84002	0.01151	0.84493	0.00521	0.84493	0.00521	0.83409	0.00164
0.82205	0.01281	0.82683	0.00653	0.82683	0.00653	0.81527	0.00331
0.80409	0.01426	0.80873	0.00799	0.80873	0.00799	0.79649	0.00511
0.78616	0.01585	0.79066	0.00959	0.79066	0.00959	0.77777	0.00703
0.76827	0.01756	0.77264	0.01131	0.77264	0.01131	0.75916	0.00904
0.75044	0.01939	0.75466	0.01315	0.75466	0.01315	0.74056	0.01114
0.73271	0.02131	0.7368	0.01509	0.7368	0.01509	0.72199	0.01331
0.71498	0.02331	0.71894	0.0171	0.71894	0.0171	0.70352	0.01552
0.69729	0.02537	0.70111	0.01918	0.70111	0.01918	0.68505	0.01777
0.6797	0.02748	0.68338	0.02131	0.68338	0.02131	0.66659	0.02003
0.6621	0.02962	0.66565	0.02346	0.66565	0.02346	0.64815	0.02229
0.64452	0.03177	0.64794	0.02564	0.64794	0.02564	0.62971	0.02455
0.62695	0.03393	0.63023	0.02781	0.63023	0.02781	0.61122	0.02678
0.60938	0.03608	0.61252	0.02997	0.61252	0.02997	0.59273	0.02898
0.59177	0.03821	0.59478	0.03212	0.59478	0.03212	0.57423	0.03114
0.57415	0.0403	0.57703	0.03423	0.57703	0.03423	0.5557	0.03325
0.55653	0.04236	0.55927	0.0363	0.55927	0.0363	0.53718	0.0353
0.53888	0.04437	0.54148	0.03833	0.54148	0.03833	0.51863	0.0373
0.52122	0.04633	0.52369	0.0403	0.52369	0.0403	0.50007	0.03923
0.50356	0.04823	0.50589	0.04221	0.50589	0.04221	0.48151	0.0411
0.48588	0.05007	0.48807	0.04407	0.48807	0.04407	0.46292	0.04291
0.4682	0.05185	0.47026	0.04586	0.47026	0.04586	0.44432	0.04466
0.45048	0.05358	0.45241	0.0476	0.45241	0.0476	0.42571	0.04635
0.43276	0.05524	0.43455	0.04928	0.43455	0.04928	0.40705	0.04798
0.41503	0.05685	0.41668	0.0509	0.41668	0.0509	0.38839	0.04955
0.39725	0.0584	0.39877	0.05247	0.39877	0.05247	0.3697	0.05105
0.37948	0.0599	0.38086	0.05397	0.38086	0.05397	0.35097	0.05248
0.36167	0.06133	0.36291	0.05542	0.36291	0.05542	0.33225	0.05383
0.34383	0.06269	0.34494	0.05679	0.34494	0.05679	0.31347	0.05508
0.32599	0.06398	0.32696	0.05808	0.32696	0.05808	0.29467	0.05621
0.3081	0.06517	0.30893	0.05929	0.30893	0.05929	0.27588	0.0572
0.2902	0.06625	0.29089	0.06037	0.29089	0.06037	0.25703	0.05799
0.27229	0.06718	0.27284	0.06132	0.27284	0.06132	0.23818	0.05856
0.25433	0.06794	0.25475	0.06208	0.25475	0.06208	0.21933	0.05883
0.23637	0.06848	0.23665	0.06262	0.23665	0.06262	0.20048	0.05873
0.21842	0.06874	0.21856	0.06288	0.21856	0.06288	0.18163	0.05818
0.20046	0.06865	0.20046	0.06279	0.20046	0.06279	0.16286	0.05709

0.1825	0.06812	0.18236	0.06226	0.18236	0.06226	0.14412	0.05532
0.16462	0.06708	0.16434	0.06121	0.16434	0.06121	0.1254	0.05275
0.14677	0.0654	0.14636	0.05952	0.14636	0.05952	0.10703	0.0493
0.12893	0.06295	0.12838	0.05705	0.12838	0.05705	0.08867	0.04475
0.11143	0.05966	0.11075	0.05374	0.11075	0.05374	0.07065	0.03902
0.09394	0.05532	0.09312	0.04937	0.09312	0.04937	0.05324	0.03211
0.07677	0.04986	0.07582	0.04386	0.07582	0.04386	0.03584	0.02363
0.06019	0.04328	0.05911	0.03723	0.05911	0.03723	0.02006	0.0144
0.04361	0.0352	0.04241	0.02909	0.04241	0.02909	0.00506	0.00406
0.02857	0.02641	0.02726	0.02023	0.02726	0.02023	0	0
0.01429	0.01656	0.01286	0.0103	0.01286	0.0103	0	-0.0042
0	0.00511	0	0	0	0	0.00506	-0.00014
0	0.00111	0	-0.00403	0	-0.00403	0.02006	0.0102
0.01429	0.01256	0.01286	0.00627	0.01286	0.00627	0.03584	0.01943
0.02857	0.02241	0.02726	0.0162	0.02726	0.0162	0.05324	0.02791
0.04361	0.0312	0.04241	0.02506	0.04241	0.02506	0.07065	0.03482
0.06019	0.03928	0.05911	0.0332	0.05911	0.0332	0.08867	0.04055
0.07677	0.04586	0.07582	0.03983	0.07582	0.03983	0.10703	0.0451
0.09394	0.05132	0.09312	0.04533	0.09312	0.04533	0.1254	0.04855
0.11143	0.05566	0.11075	0.04971	0.11075	0.04971	0.14412	0.05112
0.12893	0.05895	0.12838	0.05302	0.12838	0.05302	0.16286	0.05289
0.14677	0.0614	0.14636	0.05549	0.14636	0.05549	0.18163	0.05398
0.16462	0.06308	0.16434	0.05718	0.16434	0.05718	0.20048	0.05453
0.1825	0.06412	0.18236	0.05823	0.18236	0.05823	0.21933	0.05463
0.20046	0.06465	0.20046	0.05876	0.20046	0.05876	0.23818	0.05436
0.21842	0.06474	0.21856	0.05885	0.21856	0.05885	0.25703	0.0538
0.23637	0.06448	0.23665	0.05859	0.23665	0.05859	0.27588	0.053
0.25433	0.06394	0.25475	0.05805	0.25475	0.05805	0.29467	0.05201
0.27229	0.06318	0.27284	0.05729	0.27284	0.05729	0.31347	0.05088
0.2902	0.06225	0.29089	0.05634	0.29089	0.05634	0.33225	0.04963
0.3081	0.06117	0.30893	0.05526	0.30893	0.05526	0.35097	0.04828
0.32599	0.05998	0.32696	0.05405	0.32696	0.05405	0.3697	0.04685
0.34383	0.05869	0.34494	0.05276	0.34494	0.05276	0.38839	0.04535
0.36167	0.05733	0.36291	0.05138	0.36291	0.05138	0.40705	0.04378
0.37948	0.0559	0.38086	0.04994	0.38086	0.04994	0.42571	0.04215
0.39725	0.0544	0.39877	0.04844	0.39877	0.04844	0.44432	0.04046
0.41503	0.05285	0.41668	0.04687	0.41668	0.04687	0.46292	0.03871
0.43276	0.05124	0.43455	0.04525	0.43455	0.04525	0.48151	0.0369
0.45048	0.04958	0.45241	0.04357	0.45241	0.04357	0.50007	0.03503
0.4682	0.04785	0.47026	0.04183	0.47026	0.04183	0.51863	0.0331
0.48588	0.04607	0.48807	0.04004	0.48807	0.04004	0.53718	0.0311
0.50356	0.04423	0.50589	0.03818	0.50589	0.03818	0.5557	0.02905
0.52122	0.04233	0.52369	0.03627	0.52369	0.03627	0.57423	0.02694
0.53888	0.04037	0.54148	0.0343	0.54148	0.0343	0.59273	0.02478
0.55653	0.03836	0.55927	0.03227	0.55927	0.03227	0.61122	0.02258
0.57415	0.0363	0.57703	0.0302	0.57703	0.0302	0.62971	0.02035

0.59177	0.03421	0.59478	0.02809	0.59478	0.02809	0.64815	0.0181
0.60938	0.03208	0.61252	0.02594	0.61252	0.02594	0.66659	0.01583
0.62695	0.02993	0.63023	0.02378	0.63023	0.02378	0.68505	0.01357
0.64452	0.02777	0.64794	0.0216	0.64794	0.0216	0.70352	0.01132
0.6621	0.02562	0.66565	0.01943	0.66565	0.01943	0.72199	0.00911
0.6797	0.02348	0.68338	0.01728	0.68338	0.01728	0.74056	0.00694
0.69729	0.02137	0.70111	0.01515	0.70111	0.01515	0.75916	0.00484
0.71498	0.01931	0.71894	0.01307	0.71894	0.01307	0.77777	0.00283
0.73271	0.01731	0.7368	0.01106	0.7368	0.01106	0.79649	0.00091
0.75044	0.01539	0.75466	0.00912	0.75466	0.00912	0.81527	-0.00089
0.76827	0.01356	0.77264	0.00728	0.77264	0.00728	0.83409	-0.00255
0.78616	0.01185	0.79066	0.00556	0.79066	0.00556	0.85294	-0.00407
0.80409	0.01026	0.80873	0.00396	0.80873	0.00396	0.8718	-0.00544
0.82205	0.00881	0.82683	0.0025	0.82683	0.0025	0.89065	-0.00666
0.84002	0.00751	0.84493	0.00118	0.84493	0.00118	0.90947	-0.00773
0.85797	0.00635	0.86303	0.00002	0.86303	0.00002	0.92826	-0.00866
0.87591	0.00533	0.8811	-0.00101	0.8811	-0.00101	0.947	-0.0095
0.89381	0.00444	0.89914	-0.00191	0.89914	-0.00191	0.96569	-0.01026
0.91166	0.00365	0.91713	-0.00271	0.91713	-0.00271	0.98432	-0.01099
0.92947	0.00292	0.93507	-0.00344	0.93507	-0.00344		
0.94721	0.00222	0.95295	-0.00415	0.95295	-0.00415		
0.96489	0.00149	0.97076	-0.00489	0.97076	-0.00489		
0.98248	0.00065	0.98849	-0.00573	0.98849	-0.00573		

GenMAVA4.dat		GenMAVA5.dat		GenMAVA6.dat		GenMAVA7.dat	
MAV - v2.0 - Airfoil Cross Section - Chord 4.56133		MAV - v2.0 - Airfoil Cross Section - Chord 4.26471		MAV - v2.0 - Airfoil Cross Section - Chord 3.75205		MAV - v2.0 - Airfoil Cross Section - Chord 2.95981	
1	-0.01304	1	-0.02097	1	-0.03156	1	-0.03916
0.99962	-0.01303	0.99244	-0.02059	0.98112	-0.02989	0.98063	-0.0368
0.98011	-0.01223	0.97142	-0.0194	0.95728	-0.02761	0.95093	-0.03316
0.96053	-0.01136	0.95036	-0.01804	0.93352	-0.02517	0.92125	-0.02951
0.94091	-0.01038	0.9293	-0.01652	0.90989	-0.02262	0.89156	-0.02589
0.92125	-0.00927	0.90825	-0.01482	0.88627	-0.01995	0.86181	-0.02229
0.90157	-0.008	0.88722	-0.01296	0.8627	-0.0172	0.83205	-0.01875
0.88187	-0.00657	0.86625	-0.01095	0.83925	-0.01439	0.80228	-0.01528
0.86219	-0.00498	0.84534	-0.00881	0.8158	-0.01154	0.77246	-0.01188
0.84253	-0.00324	0.82455	-0.00656	0.79237	-0.00867	0.74264	-0.00858
0.82293	-0.00137	0.80377	-0.00421	0.76896	-0.00579	0.7128	-0.00537
0.80337	0.00064	0.78303	-0.00179	0.74554	-0.00293	0.68293	-0.00226
0.78394	0.00274	0.7624	0.00068	0.72207	-0.00009	0.65306	0.00075
0.76451	0.00493	0.74177	0.00319	0.6986	0.0027	0.62314	0.00367
0.74512	0.0072	0.72116	0.00572	0.67511	0.00544	0.5932	0.00648
0.72583	0.0095	0.70056	0.00825	0.65159	0.00812	0.56325	0.0092
0.70654	0.01185	0.67996	0.01076	0.62807	0.01073	0.53322	0.01182

0.68727	0.01421	0.65931	0.01326	0.60452	0.01326	0.50319	0.01435
0.66801	0.01658	0.63866	0.01572	0.58096	0.01571	0.47311	0.01676
0.64875	0.01893	0.618	0.01813	0.5574	0.01809	0.44297	0.01907
0.62944	0.02127	0.5973	0.02048	0.53379	0.02039	0.41284	0.02124
0.61013	0.02356	0.57661	0.02278	0.51018	0.02261	0.38261	0.02325
0.59082	0.02582	0.5559	0.025	0.48655	0.02475	0.35237	0.02508
0.57147	0.02802	0.53517	0.02716	0.46286	0.02682	0.32211	0.02666
0.55212	0.03017	0.51444	0.02925	0.43917	0.02881	0.29178	0.02794
0.53275	0.03225	0.49367	0.03128	0.41544	0.03072	0.26145	0.02885
0.51337	0.03427	0.47289	0.03323	0.39167	0.03253	0.23111	0.02928
0.49399	0.03622	0.4521	0.03512	0.3679	0.03425	0.20077	0.02913
0.47457	0.03811	0.43126	0.03694	0.34406	0.03584	0.17043	0.02825
0.45514	0.03994	0.41042	0.03869	0.3202	0.03727	0.14023	0.02648
0.43571	0.0417	0.38955	0.04036	0.29633	0.03852	0.11007	0.02364
0.41622	0.0434	0.36863	0.04196	0.2724	0.03954	0.07994	0.01951
0.39674	0.04504	0.34771	0.04347	0.24847	0.04025	0.05038	0.01395
0.37722	0.04661	0.32674	0.04487	0.22454	0.04059	0.02083	0.00662
0.35766	0.0481	0.30575	0.04613	0.20061	0.04047	0	0
0.33811	0.04951	0.28475	0.04723	0.17668	0.03977	0	-0.00676
0.3185	0.05082	0.2637	0.04812	0.15285	0.03838	0.02083	-0.00013
0.29887	0.052	0.24265	0.04875	0.12906	0.03614	0.05038	0.0072
0.27924	0.05303	0.22159	0.04905	0.10529	0.03288	0.07994	0.01275
0.25956	0.05386	0.20054	0.04895	0.08197	0.0285	0.11007	0.01688
0.23987	0.05445	0.17948	0.04833	0.05866	0.02272	0.14023	0.01972
0.22019	0.05473	0.15852	0.04711	0.03578	0.01544	0.17043	0.02149
0.2005	0.05463	0.13759	0.04514	0.01368	0.00667	0.20077	0.02237
0.18081	0.05406	0.11667	0.04227	0	0	0.23111	0.02253
0.16121	0.05291	0.09616	0.03841	0	-0.00533	0.26145	0.02209
0.14165	0.05107	0.07565	0.03333	0.01368	0.00134	0.29178	0.02119
0.12209	0.04839	0.05552	0.02692	0.03578	0.01011	0.32211	0.0199
0.10291	0.04478	0.03608	0.01921	0.05866	0.01739	0.35237	0.01832
0.08374	0.04003	0.01664	0.00973	0.08197	0.02317	0.38261	0.0165
0.06491	0.03404	0	0	0.10529	0.02755	0.41284	0.01448
0.04674	0.02683	0	-0.00469	0.12906	0.03081	0.44297	0.01231
0.02857	0.01797	0.01664	0.00505	0.15285	0.03305	0.47311	0.01001
0.01209	0.00833	0.03608	0.01452	0.17668	0.03444	0.50319	0.00759
0	0	0.05552	0.02223	0.20061	0.03514	0.53322	0.00507
0	-0.00438	0.07565	0.02864	0.22454	0.03526	0.56325	0.00245
0.01209	0.00395	0.09616	0.03372	0.24847	0.03492	0.5932	-0.00027
0.02857	0.01359	0.11667	0.03758	0.2724	0.0342	0.62314	-0.00309
0.04674	0.02244	0.13759	0.04045	0.29633	0.03319	0.65306	-0.006
0.06491	0.02966	0.15852	0.04242	0.3202	0.03194	0.68293	-0.00901
0.08374	0.03564	0.17948	0.04364	0.34406	0.03051	0.7128	-0.01213
0.10291	0.0404	0.20054	0.04426	0.3679	0.02892	0.74264	-0.01533
0.12209	0.044	0.22159	0.04436	0.39167	0.0272	0.77246	-0.01864
0.14165	0.04669	0.24265	0.04406	0.41544	0.02539	0.80228	-0.02203

0.16121	0.04853	0.2637	0.04343	0.43917	0.02348	0.83205	-0.02551
0.18081	0.04967	0.28475	0.04254	0.46286	0.02149	0.86181	-0.02905
0.2005	0.05025	0.30575	0.04144	0.48655	0.01942	0.89156	-0.03265
0.22019	0.05035	0.32674	0.04018	0.51018	0.01728	0.92125	-0.03627
0.23987	0.05007	0.34771	0.03878	0.53379	0.01506	0.95093	-0.03992
0.25956	0.04948	0.36863	0.03727	0.5574	0.01276	0.98063	-0.04356
0.27924	0.04865	0.38955	0.03567	0.58096	0.01038		
0.29887	0.04762	0.41042	0.034	0.60452	0.00793		
0.3185	0.04644	0.43126	0.03225	0.62807	0.0054		
0.33811	0.04513	0.4521	0.03043	0.65159	0.00279		
0.35766	0.04372	0.47289	0.02854	0.67511	0.00011		
0.37722	0.04222	0.49367	0.02659	0.6986	-0.00263		
0.39674	0.04066	0.51444	0.02456	0.72207	-0.00542		
0.41622	0.03902	0.53517	0.02247	0.74554	-0.00826		
0.43571	0.03732	0.5559	0.02031	0.76896	-0.01112		
0.45514	0.03555	0.57661	0.01809	0.79237	-0.014		
0.47457	0.03373	0.5973	0.01579	0.8158	-0.01687		
0.49399	0.03184	0.618	0.01344	0.83925	-0.01972		
0.51337	0.02988	0.63866	0.01103	0.8627	-0.02253		
0.53275	0.02786	0.65931	0.00857	0.88627	-0.02528		
0.55212	0.02578	0.67996	0.00607	0.90989	-0.02795		
0.57147	0.02364	0.70056	0.00356	0.93352	-0.0305		
0.59082	0.02143	0.72116	0.00103	0.95728	-0.03294		
0.61013	0.01918	0.74177	-0.0015	0.98112	-0.03522		
0.62944	0.01688	0.7624	-0.00401				
0.64875	0.01455	0.78303	-0.00648				
0.66801	0.0122	0.80377	-0.0089				
0.68727	0.00983	0.82455	-0.01125				
0.70654	0.00747	0.84534	-0.0135				
0.72583	0.00512	0.86625	-0.01564				
0.74512	0.00281	0.88722	-0.01765				
0.76451	0.00055	0.90825	-0.01951				
0.78394	-0.00165	0.9293	-0.02121				
0.80337	-0.00375	0.95036	-0.02273				
0.82293	-0.00575	0.97142	-0.02409				
0.84253	-0.00763	0.99244	-0.02528				
0.86219	-0.00937						
0.88187	-0.01096						
0.90157	-0.01238						
0.92125	-0.01365						
0.94091	-0.01477						
0.96053	-0.01575						
0.98011	-0.01662						
0.99962	-0.01741						

GenMAVA8.dat		GenMAVA9.dat		GenMAVA10.dat		GenMAVA11.dat	
MAV - v2.0 - Airfoil Cross Section - Chord 2.43693		MAV - v2.0 - Airfoil Cross Section - Chord 1.64218		MAV - v2.0 - Airfoil Cross Section - Chord 1.27234		MAV - v2.0 - Airfoil Cross Section - Chord 0.90625	
1	-0.03903	1	-0.03443	1	-0.03052	1	-0.02225
0.96767	-0.03519	0.96265	-0.03079	0.97516	-0.02835	0.99356	-0.02376
0.93151	-0.03097	0.90869	-0.02572	0.9053	-0.02248	0.89513	-0.01667
0.89529	-0.02684	0.85471	-0.02082	0.83533	-0.01686	0.79642	-0.01009
0.85908	-0.02283	0.80058	-0.01609	0.76522	-0.0115	0.69763	-0.00414
0.82283	-0.01893	0.74646	-0.01155	0.69512	-0.00645	0.59882	0.00104
0.78655	-0.01515	0.69225	-0.00719	0.62481	-0.00176	0.49975	0.00523
0.75027	-0.0115	0.63793	-0.00304	0.55445	0.00247	0.40069	0.00819
0.71393	-0.00796	0.58361	0.00087	0.48407	0.00616	0.30161	0.00961
0.67757	-0.00454	0.52914	0.00451	0.4135	0.00914	0.20252	0.0091
0.64119	-0.00123	0.47462	0.00779	0.34294	0.01125	0.10343	0.00622
0.60472	0.00195	0.42009	0.01064	0.27237	0.01226	0.00478	0.00045
0.56824	0.00501	0.36542	0.01296	0.2018	0.0119	0	0
0.53171	0.00795	0.31075	0.01459	0.13122	0.00985	0	-0.02207
0.49511	0.01075	0.25607	0.01537	0.06095	0.00574	0.00478	-0.02162
0.4585	0.01338	0.20139	0.01509	0	0	0.10343	-0.01585
0.4218	0.01583	0.14671	0.0135	0	-0.01572	0.20252	-0.01297
0.38506	0.01804	0.09227	0.01032	0.06095	-0.00998	0.30161	-0.01246
0.34831	0.01997	0.03792	0.0052	0.13122	-0.00587	0.40069	-0.01388
0.31147	0.02153	0	0	0.2018	-0.00382	0.49975	-0.01684
0.27463	0.02263	0	-0.01055	0.27237	-0.00346	0.59882	-0.02103
0.23779	0.02315	0.03792	-0.00698	0.34294	-0.00446	0.69763	-0.0262
0.20094	0.02297	0.09227	-0.00186	0.4135	-0.00657	0.79642	-0.03216
0.16409	0.02189	0.14671	0.00132	0.48407	-0.00956	0.89513	-0.03874
0.1274	0.01975	0.20139	0.00292	0.55445	-0.01324	0.99356	-0.04583
0.09078	0.0163	0.25607	0.0032	0.62481	-0.01748		
0.05418	0.01128	0.31075	0.00241	0.69512	-0.02217		
0.01828	0.00453	0.36542	0.00078	0.76522	-0.02722		
0	0	0.42009	-0.00154	0.83533	-0.03258		
0	-0.00821	0.47462	-0.00439	0.9053	-0.0382		
0.01828	-0.00367	0.52914	-0.00767	0.97516	-0.04407		
0.05418	0.00307	0.58361	-0.01131				
0.09078	0.00809	0.63793	-0.01522				
0.1274	0.01154	0.69225	-0.01937				
0.16409	0.01369	0.74646	-0.02373				
0.20094	0.01476	0.80058	-0.02827				
0.23779	0.01495	0.85471	-0.033				
0.27463	0.01442	0.90869	-0.0379				
0.31147	0.01332	0.96265	-0.04297				
0.34831	0.01176						
0.38506	0.00984						
0.4218	0.00762						
0.4585	0.00517						

0.49511	0.00254						
0.53171	-0.00026						
0.56824	-0.00319						
0.60472	-0.00626						
0.64119	-0.00944						
0.67757	-0.01274						
0.71393	-0.01616						
0.75027	-0.0197						
0.78655	-0.02336						
0.82283	-0.02714						
0.85908	-0.03104						
0.89529	-0.03505						
0.93151	-0.03917						
0.96767	-0.04339						

l. Fuselage_v2pt2.dat

Filename: Fuselage_v2pt2.dat
Parent program: AVL
Description: This file contains the geometry of the fuselage for AVL.
Code:

```
BATCAM-Like Fuselage
   16.5    0.797885
   15       0.797885
   14       0.797885
   13       0.909318
   12       1.064884
   11       1.180087
   10       1.371137
   9        1.512565
   8        1.586391
   7        1.639581
   6        1.691099
   5        1.724589
   4        1.686682
   3        1.596548
   2        1.44186
   1        1.286937
   0        1.055502
   0       -1.055502
   1       -1.286937
   2       -1.44186
   3       -1.596548
   4       -1.686682
   5       -1.724589
   6       -1.691099
   7       -1.639581
   8       -1.586391
   9       -1.512565
   10      -1.371137
   11      -1.180087
   12      -1.064884
   13      -0.909318
   14      -0.797885
```

```
 15        -0.797885
 16.5      -0.797885
```

m. results_GenMAV.txt

```
Filename: results_GenMAV.txt
Parent program: AVL
Description: This file contains the results of the AVL analysis.  These results are then passed into MC through the
".fileWrapper" file.
Code:
 ---------------------------------------------------------------
 Vortex Lattice Output -- Total Forces

 Configuration: GenMAV
    # Surfaces =   4
    # Strips   =  81
    # Vortices = 629

  Sref =  111.68       Cref =  4.7757       Bref =  24.000
  Xref =  6.4084       Yref = 0.40987E-09   Zref = 0.35557

 Standard axis orientation,  X fwd, Z down

 Run case: Base Run

  Alpha =   8.51756     pb/2V =   0.00000     p'b/2V =   0.00000
  Beta  =   0.00000     qc/2V =   0.00000
  Mach  =     0.040     rb/2V =   0.00000     r'b/2V =   0.00000

  CXtot =  -0.01625     Cltot =   0.00000     Cl'tot =   0.00000
  CYtot =   0.00000     Cmtot =   0.00000
  CZtot =  -1.17537     Cntot =   0.00000     Cn'tot =   0.00000

  CLtot =   1.16000
  CDtot =   0.19016
  CDvis =   0.10200     CDind =   0.08816
  CLff  =   1.13036     CDff  =   0.08318    | Trefftz
  CYff  =   0.00000       e   =     0.9481   | Plane

  L_Elevon       =  -6.71732
  R_Elevon       =  -6.71719

 ---------------------------------------------------------------

 Derivatives...
                      alpha              beta
               ----------------    ----------------
 z force    |    CLa =   4.941830    CLb =  -0.000007
 y force    |    CYa =   0.000000    CYb =  -0.465485
 roll  x mom.|    Cla =  -0.000002    Clb =  -0.195926
 pitch y mom.|    Cma =  -2.049888    Cmb =   0.000013
 yaw   z mom.|    Cna =   0.000000    Cnb =   0.046396

                  roll rate  p       pitch rate  q        yaw rate  r
               ----------------    ----------------    ----------------
 z force    |    CLp =   0.000002    CLq =   9.684513    CLr =   0.000005
 y force    |    CYp =   0.011938    CYq =   0.000002    CYr =   0.272264
 roll  x mom.|    Clp =  -0.424554    Clq =  -0.000015    Clr =   0.316637
 pitch y mom.|    Cmp =  -0.000005    Cmq = -12.263052    Cmr =  -0.000009
```

```
yaw   z mom.|    Cnp =  -0.080907    Cnq =  -0.000002    Cnr =  -0.151682

             L_Elevon     d1     R_Elevon     d2
             ----------------    ----------------
z force     |  CLd1 =   0.009120   CLd2 =   0.009120
y force     |  CYd1 =  -0.000371   CYd2 =   0.000371
roll  x mom.|  Cld1 =   0.000676   Cld2 =  -0.000676
pitch y mom.|  Cmd1 =  -0.017649   Cmd2 =  -0.017650
yaw   z mom.|  Cnd1 =   0.000089   Cnd2 =  -0.000089
Trefftz drag| CDffd1 =   0.000728 CDffd2 =   0.000728
span eff.   |    ed1 =   0.007412    ed2 =   0.007411



Neutral point  Xnp =   8.389417

Clb Cnr / Clr Cnb  =   2.022934    (  > 1 if spirally stable)
```

C.2. Propulsion CA

a. qprop2.fileWrapper

```
Filename: qprop2.fileWrapper
Parent program: MC
Description: This is “fileWrapper” file for MC to communicate with qprop.
Code:
#
# Basic QPROP filewrapper
#
# @author: Doug Pederson (modified from Paul Hrad's work)
# @version: 4 Feb 2011
# @description: MAV QPROP analysis
#

RunCommands
{
# Put ModelCenter values in the input file
 generate inputFile1

 generate inputFile2

 generate inputFile3

 generate inputfile4

# Run the code
 run "qprop_batch.bat"
# Parse the standard output file
 parse outputfile
}

RowFieldInputFile inputFile1
{
templateFile:                    qcon.template
fileToGenerate:      qcon.def

setDelimiters "= ,"
```

```
setGroup Flight_conditions
variable: density                   double 1 1      description="Density (kg/m^3)"
variable: dynamic_viscosity             double 2 1      description="Dynamic Viscosity (kg/m-s)"
variable: speed_of_sound            double 3 1      description="Speed of Sound (m/s)"

}

RowFieldInputFile inputFile2
{
templateFile:                   qprop_batch.template
fileToGenerate:         qprop_batch.bat

setDelimiters "= ,"

variable: velocity double 1 4 default=1.0 description="flight velocity"
variable: airframeThrustRqd   double 1 8 default=1.0 description="thrust required"

}

RowFieldInputFile inputFile3
 {
 templateFile:                  motor.template
 fileToGenerate:     motor

 setDelimiters " ,"
 setGroup inputs_motor
 variable: Rmotor    double 6 1                  description="Rmotor(ohms)"
 variable: Io                   double 7 1                      description="Io (amps)"
 variable: Kv                   double 8 1                  description="Kv (rpm/volts)"

 }

RowFieldInputFile inputFile4
 {
 templateFile:                  prop.template
 fileToGenerate:     prop

 setDelimiters " ,"
 markAsBeginning "prop"
 setGroup inputs_prop
 variable: blade_number         double 4 1                  description="number of blades"
 variable: tip_radiusdouble 4 2                 description="radius of blade"

 setGroup radius
 variable: r1                   double 17 1             description="radius 1 "
 variable: r2                   double 18 1             description="radius 2 "
 variable: r3                   double 19 1             description="radius 3 "
 variable: r4                   double 20 1             description="radius 4 "
 variable: r5                   double 21 1             description="radius 5 "
 variable: r6                   double 22 1             description="radius 6 "
 variable: r7                   double 23 1             description="radius 7 "
 variable: r8                   double 24 1             description="radius 8 "
 variable: r9                   double 25 1             description="radius 9 "
 variable: r10                  double 26 1             description="radius 10 "

 setGroup chord
 variable: c1                   double 17 2             description="chord 1 "
 variable: c2                   double 18 2             description="chord 2 "
 variable: c3                   double 19 2             description="chord 3 "
 variable: c4                   double 20 2             description="chord 4 "
```

```
variable: c5                    double 21 2             description="chord 5 "
variable: c6                    double 22 2             description="chord 6 "
variable: c7                    double 23 2             description="chord 7 "
variable: c8                    double 24 2             description="chord 8 "
variable: c9                    double 25 2             description="chord 9 "
variable: c10                   double 26 2             description="chord 10 "

setGroup beta
variable: b1                    double 17 3             description="beta 1 "
variable: b2                    double 18 3             description="beta 2 "
variable: b3                    double 19 3             description="beta 3 "
variable: b4                    double 20 3             description="beta 4 "
variable: b5                    double 21 3             description="beta 5 "
variable: b6                    double 22 3             description="beta 6 "
variable: b7                    double 23 3             description="beta 7 "
variable: b8                    double 24 3             description="beta 8 "
variable: b9                    double 25 3             description="beta 9 "
variable: b10                   double 26 3             description="beta 10 "

setGroup aero_coeff
variable: CL_a_prop                     double 6 2
variable: CL_0_prop                     double 6 1
variable: CL_min_prop                   double 7 1
variable: CL_max_prop                   double 7 2
variable: CD_0_prop                     double 9 1
variable: CD2u_prop                     double 9 2
variable: CD2l_prop                     double 9 3
variable: CLCD0_prop                    double 9 4
variable: REref_prop                    double 10 1
variable: REexp_prop                    double 10 2
variable: Rfac_prop                     double 13 1
variable: Cfac_prop                     double 13 2
variable: Bfac_prop                     double 13 3
variable: Radd_prop                     double 14 1
variable: Cadd_prop                     double 14 2
variable: Badd_prop                     double 14 3
}

RowFieldOutputFile outputFile
{
# This routine parses the program output file.
# Other variables can be extracted as desired.

fileToParse: Qprop.dat

setDelimiters "= "

markAsBeginning "V(m/s)"
        setGroup Qprop_outputs
variable: RPM                   double 2  3             description="RPM"
variable: Dbeta         double 2 4      description="pitch change in degrees"
variable: thrust_prop  double 2             5             description="Prop Thrust"
variable: Q                     double 2        6description="Prop Torque"
variable: Pshaft        double 2  7       description="Shaft power"
variable: Volts         double 2  8       description="motor voltage"
variable: Amps                  double 2  9       description="motor current"
variable: eff_mot    double 2  10      description="Efficiency of Motor"
variable: eff_prop   double 2  11      description="Efficiency of propeller"
variable: adv_ratio double 2  12      description="J"
variable: CT                    double 2  13      description="Torque coeff"
```

```
variable: CP                double 2  14     description="Power coeff"
variable: DV                double 2  15     description="slipstream velocity increment"
variable: eff_total   double 2            16     description="Total Eff"
variable: Pelec      double 2  17     description="Electrical power"
variable: Pprop      double 2  18     description="Propeller power"
variable: cl_avg     double 2  19     description="power-weighted average of local cl(r)"
variable: cd_avg     double 2  20     description="power-weighted average of local cd(r)"

}
```

b. motor

```
Filename: motor
Parent Program: QPROP
Description: This is the input motor file for the GenMAV motor.  This file will change based upon the inputs fed to it through the ".fileWrapper" file.  Note that there is no file extension for this file.
Code:
AXI 2808/20 Motor     ! name

 1       ! motor type  (1 = permanent-magnet brushed or brushless DC motor)

 0.105    ! Rmotor (Ohms)
 1.1     ! Io     (Amps)
 1300.0     ! Kv     (rpm/Volt)
```

c. motor.template

```
Filename: motor.template
Parent program: MC
Description: This is the template MC uses for the "motor" file.  This file does not change when MC executes.
Code:  See code for "motor."
```

d. prop

```
Filename: prop
Parent Program: QPROP
Description: This is the input propeller file for the GenMAV propeller.  This file will change based upon the inputs fed to it through the ".fileWrapper" file.  Note that there is no file extension for this file.
Code:
prop Graupner 8x4.5 CAM Folding Prop template-data is overridden

 2.0     0.0  ! Nblades   R

 0.21  0.188   ! CL0     CL_a
-0.46  1.0   ! CLmin   CLmax

 0.0185  0.0366  0.089  -0.03   !  CD0    CD2u  CD2l    CLCD0
 50000.0   -0.05       !  REref  REexp

 0.0254  0.0254   1.0  !  Rfac   Cfac   Bfac
 0.0     0.0      4.0  !  Radd   Cadd   Badd

#  r    chord    beta
 0.89    0.51    20.3
 1.11    0.83    20.3
 1.33    0.88    17.9
 1.78    0.88    13.1
```

```
 2.22    0.85     21.1
 2.67   0.73    8.76
 3.11    0.69     6.25
 3.55    0.56     4.14
 3.78    0.47     3.18
 4.0    0.01     1.56
```

e. prop.template

Filename: prop.template
Parent program: MC
Description: This is the template MC uses for the "prop" file. This file does not change when MC executes.
Code: See code for "prop"

f. qcon.def

Filename: qcon.def
Parent program: QPROP
Description: Input conditions for the air density, viscosity, and speed of sound used by QPROP.
Code:

```
1.19586793456957    ! rho  kg/m^3
1.80392605149236E-5  ! mu   kg/m-s
339.33323631572    ! a    m/s
```

g. qcon.template

Filename: qcon.template
Parent program: MC
Description: This is the template MC uses for the "qcon.def" file. This file does not change when MC executes.
Code: See code for "qcon.def"

h. Qprop.dat

Filename: Qprop.dat
Parent program: QPROP
Description: This is the file that holds the results from the QPROP analysis. MC retrieves information from this file through the ".fileWrapper."
Code:

```
# QPROP Version 1.22
#
# prop Graupner 8x4.5 CAM Folding Prop template-data is overridden
#
# AXI 2808/20 Motor
#   0.10500      Rmotor (Ohms)
#    1.1000      Io     (Amps)
#    1300.0      Kv     (rpm/Volt)
#
#   rho =  1.1959     kg/m^3
#   mu  = 0.18039E-04 kg/m-s
#   a   =  339.33     m/s
#
# 1       2       3       4       5       6       7       8     9      10      11      12      13      14      15     16
17         18     19
#
# V(m/s)   rpm     Dbeta     T(N)     Q(N-m)   Pshaft(W)   Volts    Amps   effmot   effprop   adv      CT         CP
DV(m/s)   eff     Pelec      Pprop      cl_avg  cd_avg
```

```
# 16.000   7783.      0.000  0.8858      0.2584E-01   21.06       6.472    4.6180   0.7047   0.6729   0.19323  0.6662E-02
0.1913E-02   1.3689   0.4742   29.89       14.17       0.1996  0.2016E-01
#
# radius   chord   beta      Cl       Cd       Re     Mach     effi     effp    Wa(m/s)     Aswirl      adv_wake
  0.0242  0.0161  24.547   0.1606  0.02045    27076  0.075    0.9760   0.7754   16.23      0.6824      0.1980
  0.0273  0.0204  24.457   0.1708  0.02028    37061  0.081    0.9677   0.7861   16.34      0.8954      0.1997
  0.0305  0.0221  23.591   0.1773  0.02022    43368  0.087    0.9630   0.7892   16.42      0.9906      0.2006
  0.0337  0.0224  21.974   0.1803  0.02018    47059  0.094    0.9609   0.7870   16.48      1.005       0.2011
  0.0368  0.0223  19.767   0.1804  0.02011    50337  0.100    0.9595   0.7813   16.52      0.9949      0.2014
  0.0400  0.0223  17.718   0.1801  0.02004    53730  0.107    0.9579   0.7748   16.56      0.9869      0.2017
  0.0431  0.0223  16.733   0.1825  0.02002    57209  0.114    0.9556   0.7704   16.61      0.9962      0.2022
  0.0463  0.0224  17.703   0.1907  0.02009    60739  0.121    0.9517   0.7708   16.68      1.038       0.2030
  0.0495  0.0223  20.518   0.2043  0.02026    64175  0.128    0.9462   0.7752   16.77      1.107       0.2042
  0.0526  0.0221  23.567   0.2183  0.02045    67184  0.135    0.9407   0.7789   16.87      1.173       0.2054
  0.0558  0.0217  25.118   0.2272  0.02058    69353  0.142    0.9368   0.7783   16.95      1.201       0.2063
  0.0589  0.0209  23.731   0.2261  0.02055    70301  0.149    0.9362   0.7708   16.97      1.163       0.2064
  0.0621  0.0200  20.066   0.2174  0.02039    70352  0.156    0.9380   0.7576   16.95      1.082       0.2060
  0.0653  0.0191  15.707   0.2061  0.02019    70267  0.164    0.9404   0.7415   16.92      0.9957      0.2055
  0.0684  0.0185  12.237   0.1974  0.02004    70958  0.171    0.9414   0.7270   16.91      0.9403      0.2052
  0.0716  0.0182  10.584   0.1945  0.01996    72912  0.178    0.9397   0.7176   16.95      0.9328      0.2056
  0.0747  0.0180  10.181   0.1954  0.01995    75297  0.186    0.9362   0.7122   17.01      0.9544      0.2064
  0.0779  0.0177  10.255   0.1977  0.01996    76924  0.193    0.9323   0.7082   17.08      0.9811      0.2073
  0.0811  0.0170  10.077   0.1992  0.01999    76543  0.200    0.9296   0.7030   17.14      0.9888      0.2079
  0.0842  0.0159   9.497   0.1992  0.02002    74402  0.208    0.9279   0.6962   17.17      0.9803      0.2082
  0.0874  0.0149   8.749   0.1986  0.02004    71959  0.215    0.9256   0.6890   17.21      0.9810      0.2088
  0.0905  0.0142   8.072   0.1979  0.02005    70916  0.222    0.9202   0.6827   17.32      1.025       0.2100
  0.0937  0.0135   7.576   0.1976  0.02006    69971  0.230    0.9109   0.6777   17.49      1.121       0.2121
  0.0969  0.0109   6.999   0.1973  0.02024    58254  0.237    0.9075   0.6696   17.55      1.133       0.2129
  0.1000  0.0047   6.120   0.1969  0.02106    26072  0.245    0.9280   0.6491   17.19      0.8375      0.2082
```

i. qprop_batch.bat

Filename: qprop_batch.bat
Parent program: QPROP
Description: Provides the inputs for QPROP in batch mode. It provides the parameters QPROP needs from the ".fileWrapper" file and tells QPROP to save the data to the ".dat" file.
Code:

```
qprop prop motor 16.7237715232997  0 0  0 3.55128337633925 0 0 0  > Qprop.dat 2>&1

REM notes http://web.mit.edu/drela/Public/web/qprop/qprop_doc.txt
REM Below lists the required inputs. In brackets are optional]
REM qprop propfile motorfile Vel Rpm [ Volt dBeta Thrust Torque Amps Pele ]   (single-point)
REM "dBeta", which is the pitch-change angle in degrees, (assumed zero if omitted)
```

j. qprop_batch.template

Filename: qprop_batch.template
Parent program: MC
Description: This is the template MC uses for the "qprop_batch.bat" file. This file does not change when MC executes.
Code: See code for "qprop_batch.bat"

k. exp_prop_motor.m

Filename: exp_prop_motor.m
Parent program: MC
Description: This is the code for the high-fidelity propulsion CA written by Todd Rotramel. Data obtained for the Graupner 8x4.5 is not included at the request of WSU. They can be contacted for further details.

Code: See Reference 97 for code beyond MC setup.

```
% setGroup mission_data
% variable: airframePwrRqd        double        input      matlabName="Pend"
% variable: velocity              double        input      matlabName="Vend"
% variable: altitude_initial      double        input      matlabName="h_TO"
% variable: altitude_final        double        input      matlabName="h_AGL"
% setGroup motor_data
% variable: Io                    double        input      matlabName="I0"
% variable: Rmotor                double        input      matlabName="R"
% variable: Kv                    double        input      matlabName="Kvmax_N"
% setGroup dc_dc
% variable: Imax                  double        input
% variable: Vmax                  double        input
% setGroup outputs
% variable: Pelec                 double        output     matlabName="Pin_EM"
% variable: Volts                 double        output     matlabName="V"
% variable: Amps                  double        output     matlabName="I"
% variable: eff_motor             double        output     matlabName="EM_Eff"
% variable: eff_prop              double        output     matlabName="Prop_Eff_End"
% variable: RPM                   double        output     matlabName="N_Prop_End"
% variable: Q                     double        output     matlabName="Q_Shaft_End"
% variable: Pshaft                double        output     matlabName="P_Shaft_End"
% variable: adv_ratio             double        output     matlabName="Prop_J_End"
% variable: Pprop                 double        output     matlabName="Prop_P_End"
% variable: thrust_prop           double        output     matlabName="Prop_T_End"
```

C.3. Power Managment CA

a. end_percent

Filename: end_percent
Parent program: MC
Description: This is script file for the low- and high-fidelity power management CA. If low-fidelity, the input variable for percent of endurance power that the fuel takes is equal to one. If high-fidelity, a parametric study is used to sweep through different percentages (typically ranging from 0%-200%).
Code: See end_percent in MC using a parametric study.

C.4. Power Source CA

a. specific_p_e_final.m

Filename: specifc_p_e_final.m
Parent program: MC/MATLAB plug-in
Description: This is the code for the low-fidelity power source CA in MATLAB. It communicates with MC via the MATLAB plug-in.
Code:

```
% variable: segment_power     double[]    input       description = "Array of Mission Power"                 units="W"
% variable: segment_duration                double[]    input       description = "Array of Mission Durations (Excluding
Endurance)"                    units="s"
% variable: endurance_percentage              double      input       description = "Split of average power between fc and
batt"
% variable: endurance_duration_initial        double      input       description = "Initial guess at end duratoin"
```

```
% variable: batt_se                    double      input       description = "Battery sepecifc energy"
units="W-hr/kg"
% variable: batt_sp                    double      input       description = "Battery sepecifc power"
units="W/kg"
% variable: powersource_mass           double      input       description = "Mass of battery and fuel cell"
units="kg"
% variable: fc_se                      double      input       description = "Fuel cell sepecifc energy"
units="W-hr/kg"
% variable: fc_sp                      double      input       description = "Fuel cell sepecifc power"
units="W/kg"
% variable: remaining_energy_batt      double      output      description = "Energy left in Battery"
units="W-hr"
% variable: remaining_energy_fc        double      output      description = "Energy left in FC"
units="W-hr"
% variable: endurance_duration         double      output      description = "Endurance Duration"
units="hr"
% variable: segment_mass_delta         double[]    output      description = "Array of fuel burn"
units="kg"
% variable: final_durations            double[]    output      description = "Array of Mission Durations"
units="s"
% variable: total_mission_duration     double      output      description = "Total mission duration"
units="hr"
% variable: batt_mass                  double      output      description = "battery mass"
units="kg"
% variable: fc_dry_mass                double      output      description = "dry fuel cell mass"
units="kg"
% variable: fuel_mass                  double      output      description = "fuel mass"
units="kg"
% variable: power_each_fc              double      output
% variable: energy_batt                double[]    output

%%Title: Specific Power and Energy
%%Author: Doug Pederson
%%Date: 5 Feb 2011
%%Description: Calculates the remaining energy for the endurance leg using
%%specific energy and power of the fuel cell and batter

% %%Code Testing Vars%%
% clc
% segment_power = [110;87;70;84;50];
% segment_duration = [333.333;300;0;300;500];
% batt_se = 200;
% batt_sp = 1700;
% fc_se = 900;
% fc_sp = 60;
% powersource_mass = .7371;
% endurance_percentage = .9;
% endurance_duration_initial = 300;

%%%Find the power that the power sources provide%%%
%Power that Fuel Cell Provides%
power_each_fc = endurance_percentage*segment_power(3)
for j = 1:1:5
   if segment_power(j) < power_each_fc
   power_fc(j) = segment_power(j)
   else power_fc(j) = power_each_fc
   end
end

%Power that Batt Provides%
```

```
segment_power = segment_power'
power_batt = segment_power-power_fc
for i = 1:1:5
if power_batt(i) < 0
   power_batt(i) = 0
end
end

%%%Calculate Batt Mass, Fuel Cell Mass, and Fuel Mass%%%
batt_mass_p = max(power_batt)/batt_sp    %mass required to satisify power
segment_duration = segment_duration'
segment_duration(3) = endurance_duration_initial %converging routine
energy_batt = (power_batt.*segment_duration)/3600 %W-hr (original endurance duration is a guess that convers
batt_mass_e = sum(energy_batt)/batt_se   %mass required to satisify energy
batt_mass_vec(1) = batt_mass_p
batt_mass_vec(2) = batt_mass_e
batt_mass = max(batt_mass_vec)           %select whichever mass is greater
fc_mass = powersource_mass-batt_mass
fc_dry_mass = fc_mass              %Dry and wet makes no diffference with lump calculations

%Energy for both fc and batt w/o endurance%
segment_duration(3) = 0 %back to zero once battery has been sized
energy_fc = (power_fc.*segment_duration)/3600  % W-hr,
energy_batt = (power_batt.*segment_duration)/3600 %W-hr

%%%Determine the remaining energy based upon mass and specific energy%%%
remaining_energy_batt = batt_mass*batt_se-sum(energy_batt)
remaining_energy_fc = fc_mass*fc_se - sum(energy_fc)
remaining_energy_total = remaining_energy_fc+remaining_energy_batt
endurance_duration = (remaining_energy_total/segment_power(3))*60      %Calculates the endurance duration in min
(Goal of thesis!)
segment_duration(3) = endurance_duration*60
final_durations = segment_duration'                              %sec
total_mission_duration = sum(final_durations)/3600               %hrs

%%Delta Mass Calculation%%
%At the lowest level of fidelity there is no need to adjust for the mass
%burn and no fuel
segment_mass_delta = [0;0;0;0;0]
fuel_mass = 0
```

b. polarization_ragone_comp_final.m

```
Filename: polarization_ragone_comp_final.m
Parent program: MC/MATLAB plug-in
Description: This is the code for the high-fidelity power source CA in MATLAB.  It communicates with MC via the
MATLAB plug-in.
Code:
% setGroup general_data
% variable: segment_power            double[]       input
% variable: segment_duration         double[]       input
% variable: endurance_percentage      double         input
% variable: endurance_duration_initial double        input
% variable: powersource_mass         double         input
% setGroup fc_data
% variable: fc_Eoc                   double         input
% variable: fc_A                     double         input
% variable: fc_r                     double         input
% variable: fc_m                     double         input
```

```
% variable: fc_n                    double          input
% variable: area_per_cell           double          input
% variable: fc_casing               double          input
% variable: mass_per_cell           double          input
% variable: fc_weight_factor        double          input
% variable: starting_voltage        double          input
% variable: hydrogen_se             double          input
% setGroup batt_data
% variable: batt_sp_points          double[]        input
% variable: batt_se_points          double[]        input
% variable: batt_sp_initial         double          input
% setGroup outputs
% variable: endurance_duration      double          output
% variable: endurance_duration_batt  double         output
% variable: endurance_duration_fc    double         output
% variable: segment_mass_delta      double[]        output
% variable: final_durations         double[]        output
% variable: total_mission_duration   double         output
% variable: batt_mass               double          output
% variable: fc_dry_mass             double          output
% variable: fuel_mass               double          output


%%Title: Polarization Curve
%%Author: Doug Pederson
%%Date: 5 Feb 2011
%%Description: This file creates a Ragone Plot and Polarization curve and
%%also calculates the endurance duration.

%Variables for testing code; comment out for Model Center
% close all; clear all; clc;
% segment_power = [110;87;70;84;50];
% segment_duration = [333.333;300;0;300;333.3];
% endurance_percentage = 1;
% endurance_duration_initial = 300;
% fc_Eoc = 1.031;               %Values for Eoc, A, r, m, and n come from p. 60 of Fuel Cell Systems Explained
% fc_A = 0.03;
% fc_r = 0.000245;
% fc_m = 2.11E-5;
% fc_n = 0.008;
% area_per_cell = 15;
% fc_casing = 0.05;
% mass_per_cell = 0.02;
% fc_weight_factor = 1.5;             %accounts for BOP and tank weight
% powersource_mass = .2572;
% batt_sp_points = [200; 325; 425; 500; 575; 620; 800; 875; 940; 1000; 1050];                 %be sure to include
max/min values
% batt_se_points = [175; 166.6666667; 160; 154.1666667; 146.6666667; 138.3333333; 118.3333333; 100;
83.33333333; 63.33333333; 45];    %be sure to include max/min values
% batt_sp_initial =250;
% starting_voltage = 0.7;
% hydrogen_se = 33300   ;                   %Whr/kg of hydrogen gas at 20 MPa
(http://hypertextbook.com/facts/2005/MichelleFung.shtml)

%%Find the power that the power sources provide%%
%Power that Fuel Cell Provides%
power_each_fc = endurance_percentage*segment_power(3);
for j = 1:1:5;
   if segment_power(j) < power_each_fc;
   power_fc(j) = segment_power(j);
```

```
   else power_fc(j) = power_each_fc;
   end
end

%Power that Batt Provides%
segment_power = segment_power';
power_batt = segment_power-power_fc;
for i = 1:1:5;
if power_batt(i) < 0;
  power_batt(i) = 0;
end
end

%%Battery Analysis%%
%Scale Specific Power for Optimzation%

%Determine Ragone Plot Curves Equations%
coeff_for_se = polyfit(batt_sp_points,batt_se_points,2);
coeff_for_sp = polyfit(batt_se_points,batt_sp_points,2);
%Determine Battery Size%
batt_mass_p = max(power_batt)/batt_sp_initial  ;          %Design variable in optimization (batt_sp_initial)
segment_duration = segment_duration';
segment_duration(3) = endurance_duration_initial %converging routine w/ initial guess on endurance duration
energy_batt = ((power_batt.*(segment_duration)))/3600;   %W-hr
batt_se_initial = polyval(coeff_for_se, batt_sp_initial);
batt_mass_e = sum(energy_batt)/batt_se_initial;          %mass required to satisify energy
batt_mass_vec(1) = batt_mass_p;
batt_mass_vec(2) = batt_mass_e;
batt_mass = max(batt_mass_vec)               %select whichever mass is greater

%Determine battery "burn" for each mission%
segment_duration(3)=0;  %back to zero once sizing is complete to allow for burn calc
batt_segment_sp = power_batt/batt_mass;
batt_segment_se = polyval(coeff_for_se, batt_segment_sp);
batt_operating_percentage = batt_segment_se/max(batt_se_points);
batt_energy_burn = ((batt_segment_sp.*segment_duration)/3600)/batt_operating_percentage;
batt_remaining_energy = batt_mass*max(batt_se_points)-sum(batt_energy_burn) ;
endurance_duration_batt = batt_remaining_energy/segment_power(3)          %Constraint for optimization, must be >=
0

%FC Analysis%%
%Create Voltage model in the form: V=Eoc-ir-A*ln(i)+m*exp(ni) (p. 60 of Fuel Cell Systems Explained)
format shortG                                %speeds up/cleans up file
syms polarization_curve_i
f = fc_Eoc-fc_r*polarization_curve_i-fc_A*log(polarization_curve_i)-fc_m*exp(fc_n*polarization_curve_i)-
starting_voltage; %Design variable in optimization (starting_voltage)
fc_current = double(solve(f,polarization_curve_i));
fc_power = fc_current*starting_voltage/1000;       %W/cm^2; convert to A from mA
total_area_required = power_each_fc/fc_power;
number_of_cells = ceil(total_area_required/area_per_cell)   %rounds up to the nearest whole number
fc_dry_mass = fc_weight_factor*(number_of_cells*mass_per_cell + fc_casing)
fuel_mass = powersource_mass-batt_mass-fc_dry_mass

%Determine fuel burn per segment
voltage_eff = starting_voltage/1.48;  %HHV, Fuel Cell Systems Explained p. 33
fuel_eff = 0.95 ;                        %Fuel Cell Systems Explained p. 33
fc_eff = voltage_eff*fuel_eff;              %Fuel Cell Systems Explained p. 33
fc_energy = (power_fc.*segment_duration)/3600;     %W-hr
hydrogen_energy = fc_energy/fc_eff;         %W-hr
segment_mass_delta = hydrogen_energy/hydrogen_se ; %kg
```

```
endurance_mass_delta = fuel_mass-sum(segment_mass_delta);
endurance_duration_fc = fc_eff*(hydrogen_se*endurance_mass_delta)/segment_power(3)   %Constraint for
optimization, must be >= 0

%%%Outputs%%%
%Total Endurance%
endurance_duration = (endurance_duration_batt + endurance_duration_fc)*60  %min, Objective function for
optimazation, max this
segment_duration(3) = endurance_duration*60;
final_durations = segment_duration;                          %sec
total_mission_duration = sum(final_durations)/3600;                %hrs

%Mass Burn%
segment_mass_delta(3) = endurance_mass_delta;

% %%Create Plots%%
% %Create Ragone Plot%
% format shortG
% ragone_plot_sp = linspace(1,1000,200);
% ragone_plot_se = polyval(coeff_for_se, ragone_plot_sp);
% subplot(2,1,1)
% plot(ragone_plot_sp, ragone_plot_se);
% xlabel('Specific Power (W/kg)')
% ylabel('Specific Energy (W-hr/kg)')
% title('Ragone Plot')
% hold on
% plot(batt_segment_sp, batt_segment_se, 'ro')
%
% %Create Polarization Curve for fuel Cell%%
% subplot(2,1,2)
% pol_curve_i = linspace(1,1000,200);
% pol_curve_v = fc_Eoc-fc_r*pol_curve_i-fc_A*log(pol_curve_i)-fc_m*exp(fc_n*pol_curve_i);
% plot(pol_curve_i,pol_curve_v);
% xlabel('Current Density (mA / cm^2)')
% ylabel('Volts (V)')
% title('Polarization Curve')
% hold on
% plot(fc_current, starting_voltage, 'ro')
```

C.5. Additional Model Center Script Files

a. thrust_power_rqd

Filename: thrust_power_rqd
Parent program: MC
Description: A script file that calculates the thrust and power required by the aircraft. Like all script files, the proper inputs and outputs had to be added into the GUI in the MC environment.
Code:

```
sub run
airframeThrustRqd = weight_total*((roc/velocity) + 0.5*density*velocity^2*(S_m2/weight_total)*CD_0 +
(2*weight_total*K/(S_m2*density*velocity^2)))
airframePwrRqd = velocity*airframeThrustRqd
end sub
```

Vita

Lt Pederson was a distinguished graduate from AFROT Detachment 695 at the University of Portland. There, he received a B.S. in Mechanical Engineering as well as the School of Engineering Dean's Award in 2009. His first assignment in the USAF was at the Air Force Institute of Technology where he worked under the direction of assistant professor of aeronautical engineering Lt Col Frederick G. Harmon. Following graduation, Lt Pederson will head to Los Angeles AFB to work with the Global Positioning Systems Directorate.

Bibliography

[1]Singer, P.W. *Wired for War: The Robotics Revolution and Conflict in the 21st Century*, Penguin Group Inc, New York, 2009.

[2]United States Air Force, "Air Force Basic Doctrine," URL: http://www.dtic.mil/doctrine/jel/service_pubs/afdd1.pdf, [cited 16 May 2010].

[3]Dickman, G. G., "Rapid Prototyping of Micro Air Vehicle Control Systems," AIAA 2005-7068, *Infotech@Aerospace Conference*, Arlington VA, 2005.

[4]McConnell, V. P., "Military UAVs Claiming the Skies with Fuel Cell Power," *Fuel Cells Bulletin*, Dec 07.

[5]Cox, T. H., Nady C.J., Skoog, M. A., Somers, I. A., and Warner, R., "Civil UAV Capability Assessment," NASA, Dec., 2004.

[6]Barnes, J. E., "Pentagon budget calls for more unmanned aircraft," URL: http://articles.latimes.com/2010/feb/02/nation/la-na-budget-pentagon2-2010feb02, [cited 16 May 2010].

[7]Admin, "U.S. Military UAV Market Forecast 2010-2015," URL: http://www.marketresearchmedia.com/2010/04/09/unmanned-aerial-vehicles-uav-market/, [cited 16 May 2010].

[8]Mueller, T. J., and DeLaurier, J. D., "An Overview of Micro Air Vehicle Aerodynamics," *Fixed and Flapping Wing Aerodynamics for Micro Air Vehicle Applications*, AIAA, Reston, VA, 2001.

[9]Babinsky, H., Cattafesta, L., Abate, G., "Design Considerations for a Micro Aerial Vehicle Aerodynamic Characterization Facility at the University of Florida Research and Engineering Education Facility," AIAA 2006-3309, *AIAA Aerodynamic Measurement Technology and Ground Testing Conference*, Reston, VA, 2006.

[10]Mueller, T. J., "On the Birth of Micro Air Vehicles," *International Journal of Micro Air Vehicles*, Vol.1, No.1, 2009.

[11]Kohout, L. L., and Schmitz, P. C., "Fuel Cell Propulsion Systems for an All-Electric Air Vehicle," AIAA 2003-2867, *AIAA/ICAS International Air and Space Symposium and Exposition: The Next 100 Y*, Dayton, OH, 2003.

[12]Bradley, T. H., Moffitt, B. A., Fuller, T. F., and Mavris, D., Parekh, D. E., "Design Studies for Hydrogen Fuel cell-powered Unmanned Aircraft Systems," AIAA 2008-6413, *AIAA Applied Aerodynamics Conference*, Honolulu, HI, 2008.

[13]AeroVironment, "UAS Advanced Development: Hornet," URL: http://www.avinc.com/ uas/adc/hornet/, [cited 2 June 2010].

[14]Popsci, "AeroVironment Global Observer" URL: http://www.popsci.com/military-aviation-space/article/2005-11/aerovironment-global-observer, [cited 28 Jan 2011].

[15]Parsch, A., "Directory of U.S. Military Rockets and Missiles: Spider-Lion," URL: http://www. designation-systems.net/dusrm/app4/spider-lion.html, [cited 2 June 2010].

[16]DTIC, "Solid Oxide Fuel Cell Power Systems for Small UAVs," URL: http://www.dtic. mil/ndia/2007power/NDIARegency/Thur/Session20AdaptiveMaterialsSession20SOFCsfor UAVPowerSources/AdaptiveMaterialsSession20SOFCforUAVPowerSources.pdf, [cited 28 Jan 2011].

[17]Multidisciplinary Flight Dynamics and Control Laboratory, "Fuel Cell Powered UAV: Environmentally Friendly" URL: http://www.calstatela.edu/centers/mfdclab/research/ fcuav.htm, [cited 28 Jan 2011].

[18]Newswise, "Hydrogen Fuel Cells Power Unmanned Aerial Vehicle," URL: http://www.newswise.com/articles/view/523053/ [cited 28 Jan 2011].

[19]DLR, "Successful First Flight of the "HyFish" - A Fuel Cell-Model Takes to the Sky," URL: http://www.dlr.de/desktopdefault.aspx/tabid-13/135_read-8329/, [cited 28 Jan 2011].

[20]Barnard Microsystems Limited, "Korean Scientists Build Fuel Cell-Powered Unmanned Aircraft," URL: http://www.barnardmicrosystems.com/L4E_fuel_cell_flight.htm, [cited 28 Jan 2011].

[21]AeroVironment, "UAS Advanced Development: Fuel Cell Puma," URL: http://www. avinc.com/ uas/adc/fuel_cell_puma/, [cited 2 June 2010].

[22]ScienceDaily, "Ion Tiger Fuel Cell Unmanned Air Vehicle Completes 23-hour Flight," URL: http://www.sciencedaily.com/releases/2009/10/091013123350.htm, [cited 16 Dec 2010].

[23]Moffitt, B. A., Bradley, T. H., Mavris, D., and Parakh, D. E., "Design Space Exploration of Small-Scale PEM Fuel Cell Long Endurance Aircraft," AIAA 2006-7701, AIAA *Aviation Technology, Integration and Operations Conference (ATIO)*, Wichita, KS, 2006.

[24]Hrad, P.M. “Conceptual Design Tool for Fuel-Cell Powered Micro Air Vehicles,” MS Thesis, Aeronautics and Astronautics Dept., Air Force Institute of Technology, Dayton, OH, 2010.

[25] Anderson, J. D., *Aircraft Performance and Design*, McGraw Hill, Boston, MA, 1999.

[26]Ofoma, U. C., Wu, C. C., “Design of a Fuel Cell-Powered UAS for Environmental Research,” AIAA 2004-6384, *AIAA “Unmanned Unlimited” Technical Conference*, Reston VA, 2004.

[27]Turan, M., “Tools For the Conceptual Design and Engineering Analysis of Micro Air Vehicles,” Aeronautics and Astronautics Dept., Air Force Institute of Technology, Dayton, OH, 2009.

[28]Tennekes, H., *The Simple Science of Flight: From Insects to Jumbo Jets*, The MIT Press, Cambridge MA, 2009.

[29]Jones, K. D., Lund, T.C., and Platzer, M. F., “Experimental and Computational Investigation of Flapping Wing Propulsion for Micro Air Vehicles,” *Fixed and Flapping Wing Aerodynamics for Micro Air Vehicle Applications*, AIAA, Reston, VA, 2001.

[30]Sibilski, K., Pietrucha, J., and Zlocka, M., “The Comparative Evaluation of Power Requirements for Fixed, Rotary, and Flapping Wings Micro Air Vehicles,” AIAA 2007-6498, *AIAA Atmospheric Flight Mechanics Conference and Exhibit*, Hilton Head, SC, 2007.

[31] Prior, S.D., Chen, S.T., Karamanoglu, M., Odedra, S., Erbil, M., Barlow, C., and Lewis, D., “The Future of Battlefield Micro Air Vehicle Systems,” URL: http://eprints.mdx.ac.uk/3861/1/The_Future_of_Battlefield_Micro_Air_Vehicle_Systems.pdf, [cited 18 May 2010].

[32]Schimmel, G., “Interview with Dr. Paul MacCready,” URL: http://www.modelaircraft.org/Mag/PaulMcCready/interview.htm, [cited 18 May 2010].

[33]AeroVironment, “Wasp III,” URL: http://avinc.com/downloads/Wasp_III.pdf. [cited May 18 2010].

[34]Grasmeyer, J. M., and Keennon, M. T., “Development of the Black Widow Micro Air Vehicle,” AIAA 2001-0127, *AIAA Aerospace Sciences Meeting & Exhibit*, Reno, NV, 2001.

[35]Air Force Special Operations Command, “Wasp III,” URL: http://www.af.mil/information/factsheets/factsheet.asp?id=10469, [cited 19 May 2010].

[36]Stewart, K., Wagener, J., Abate, G., and Salichon, M., “Design of the Air Force Research Laboratory Micro Aerial Vehicle Research Configuration,” AIAA 2007-0667, *AIAA Aerospace Sciences Meeting and Exhibit*, Reno, NV, 2007.

[37]Mueller, T. J., "Aerodynamic Measurements at Low Reynolds Numbers for Fixed Wing Micro-Air Vehicles," *RTO EN-9*, 1999.

[38]Electropaedia, "Battery and Energy Technologies: Performance Characteristics," URL: http://www.mpoweruk.com/performance.htm. [cited 28 May 2010].

[39]Winter, M., Brodd, R. J., "What Are Batteries, Fuel Cells, and Supercapacitors?" American Chemical Society, *Chemical Reviews*, Vol. 104, No. 10, 2004.

[40]Staniewicz, R.J., "Lithium Thionyl Chloride Cells and Batteries Technical Predictions Versus 1994 Realities," *Journal of Power Sources*, Vol. 54, 1995.

[41]GMB Power, "Why GMB Li-$SOCl_2$ Batteries?" URL: http://www.gmbattery.com/English/Li-socl2_battery.html, [cited 2 June 2010].

[42]Goldstein, J., Brown, I., Koretz, B., "New Developments in the Electric Fuel Ltd. Zinc/Air System," *Journal of Power Sources*, Vol. 80, 1999.

[43]Wang, X., Sebastian, P.J., Smit, M.A., Yang, H., Gamboa, S.A., "Studies on the Oxygen Reduction Catalyst for Zinc–Air Battery Electrode," *Journal of Power Sources*, Vol. 124, 2003.

[44]Georgi, D., "Metal Air Batteries, Half a Fuel Cell?" URL: http://www.batteriesdigest.com/metal_air.htm [cited 2 June 2010].

[45]B.W., "Ultimate Specific Energy for Batteries, Ultracapacitors," URL: http://nextbigfuture.com/2009/06/ultimate-specific-energy-for-batteries.html, [cited 2 June 2010].

[46]Buchmann, I., "The High-Power Lithium-Ion," URL: http://www.batteryuniversity.com/partone-5A.htm, [cited 2 June 2010].

[47]O'Hayre, R., Cha, S.W., Colella, W., Prinz, F.B., *Fuel Cell Fundamentals*, John Wiley & Sons, Hoboken, NJ, 2009.

[48]Aguiar, P., Brett, D.J.L., Brandon, N.P., "Solid Oxide Fuel Cell/Gas Turbine Hybrid System Analysis for High-Altitude Long-Endurance Unmanned Aerial Vehicles," International Journal of Hydrogen Energy, Vol. 33, 2008.

[49]Narayan, S.R., Valdez, T.I., "High-Energy Portable Fuel Cell Power Sources," *The Electrochemical Society Interface*, 2008.

[50]McGrath, K.M., Prakash, G.K., Olah, G.A., "Direct Methanol Fuel Cells," *Ind. Eng. Chem.*, Vol. 10, No. 7, 2004.

[51]Ha, S., Dunbar, Z., Masel, R.I., "Characterization of A High Performance Passive Direct Formic Acid Fuel Cell," *Journal of Power Sources*, Vol. 158, 2006.

[52]Parsch, A., "Directory of U.S. Military Rockets and Missiles: Wasp," URL: http://www.designation-systems.net/dusrm/app4/wasp.html, [cited 2 June 2010].

[53]Protonex, "Small Unmanned Aerial Vehicle Again SuRPAses Record Flight Time Using Protonex Fuel Cell System Technology," URL: http://www.protonex.com/_assets/pressrelease/a2dc527a-9f14-4a4e-8d6d-065e32f9a155.pdf, [cited 2 June 2010].

[54]Lupo, S., Nyberg, H., Karlsson, A., and Mohseni, K., "Xwing – A 3D Viscous Design Tool for Wings," AIAA 2008-173, *AIAA Aerospace Sciences Meeting and Exhibit*, Reno, NV, 2008.

[55]Pines, D. J., and Bohorquez, F., "Challenges Facing Future Micro-Air-Vehicle Development," *Journal of Aircraft*, Vol. 43, No. 2, 2006.

[56]Babinsky, H., Cattafesta, L., Abate, G., "Design Considerations for a Micro Aerial Vehicle Aerodynamic Characterization Facility at the University of Florida Research and Engineering Education Facility," AIAA 2006-3309, *AIAA Aerodynamic Measurement Technology and Ground Testing Conference*, San Francisco, CA, 2006.

[57]Morris, S.J., Holden, M., "Design of Micro Air Vehicles and Flight-test Validation," URL: http://www.spyplanes.com/pdf_new/notredame0600.pdf, [cited 2 June 2010].

[58]Khambatta, P., Ukeiley, L., Tinney, C., Stanford, B., and Ifju, P., "Flow Characteristics of a Three-Dimensional Fixed Micro Air vehicle Wing," AIAA 2008-3820, *Fluid Dynamics Conference and Exhibit*, Seattle, WA, 2008.

[59]Abate, G., "Micro Aerial Vehicle (MAV) Research at AFRL," *2008 International Symposium on Unmanned Aircraft Systems*, 2008.

[60]Krunz, P.J., and Kroo, I., "Analysis and Design of Airfoils for Use at Ultra-Low Reynolds Numbers," *Fixed and Flapping Wing Aerodynamics for Micro Air Vehicle Applications*, AIAA, Reston, VA, 2001.

[61]Pelletier, A., Mueller, T.J., "Low Reynolds Number Aerodynamics of Low-Aspect-Ratio, Thin/Flat/Cambered-Plate Wings," *Journal of Aircraft*, Vol. 37, No. 5, 2000.

[62]Mueller, T.J., DeLaurier J.D., "Aerodynamics of Small Vehicles," *Annual Rev. Fluid Mech*, 2003.

[63]Stewart, K., Abate, G., and Evers, J., "Flight Mechanics and Control Issues for Micro Air Vehicles," AIAA-2006-6638, *AIAA Atmospheric Flight Mechanics Conference and Exhibit*, Keystone, CO, 2006.

[64]Shields, M. C., Hatcher, C. M., Pitcairn, R. A., Aiken, C. W., Berman, D. B., Carnahan, C. M., Foley, W. A., Hammervold, S. P., Holway, W. E., and Marek, L. C., "Design and Development of a Reconnaissance Micro Air Vehicle and Launch System," http://www.colorado.edu/ASEN/SrProjects/Archive/AIAA_Paper_Awards/MARVLIS_AIAA_Final.pdf, [cited 2 June 2010].

[65]Drela, M., and Youngren, H., "AVL 3.26 User Primer," URL: http://web.mit.edu/drela/Public/web/avl/avl_doc.txt, [cited 2 June 2009].

[66]Gur, O., and Rosen, A., "Optimization of Propeller Based Propulsion System," *Journal of AircrafIt*, Vol. 46, No. 1, 2009.

[67]Lundstrom, D., Amadori, K., and Krus, P.,"Validation of a Small Scale Electric Propulsion System Models," AIAA-2010-483, *Aerospace Sciences Meeting Including the New Horizons Forum and Aerospace Exposition*, Orlando, FL, 2010.

[68]Esky Helicopters, "Brushed vs Brushless Motors," URL: http://www.eskyhelicopters.com/faq/ brushless-motors.php, [cited 2 June 2010].

[69]Ostler, J. N., Bowman, W. J., Snyder, D. O., and McLain, T. W., "Performance Flight-testing of Small, Electric Powered Unmanned Aerial Vehicles," *International Journal of Micro Air Vehicles*, Vol. 1, No. 3, 2009.

[70]Merchant, M.P., and Miller, L. S., "Propeller Performance Measurement for Low Reynolds Number UAV Applications," AIAA-2006-1127, *Aerospace Sciences Meeting and Exhibit*, Reno, NV, 2006.

[71]Deters, R.W., and Selig, M. S., "Static Testing of Micro Propellers," AIAA-2008-6246, *Applied Aerodynamics Conference*, Honolulu, HI, 2008.

[72]OL, M., Zeune, C., and Logan, M., "Analytical – Experimental Comparison for Small Electric Unmanned Air Vehicle Propellers," AIAA-2008-7345, *Applied Aerodynamics Conference*, Honolulu, HI, 2008.

[73]Drela, M., "DC Motor/Propeller Matching," URL: http://web.mit.edu/drela/Public/web/qprop/motorprop.pdf, [cited 2 June 20`0].

[74]Drela, M., "QPROP Formulation," URL: http://web.mit.edu/drela/Public/web/qprop/qprop_theory.pdf, [cited 2 June 2010].

[75]Day, D.A., "Aviation Fuel," URL: http://www.centennialofflight.gov/essay/Evolution_of_Technology/fuel/Tech21.htm, [cited 2 June 2010].

[76] Dell, R.M., Rand, D.A.J, *Understanding Batteries*, The Royal Society of Chemistry, Cambridge, UK, 2001.

[77] Fultz, B., "Types of Batteries, and Differences in Energy and Power," Lecture APh 150, *Topics in Applied Physics*, California Institute of Technology, 2007.

[78]Stux, A. M., and Swider-Lyons, K., "Survey of Commercial Small Lithium Polymer Batteries," *Chemical Dynamics and Diagnostics Branch*, NRL/MR/6110—07-9073, 2007.

[79]Mueller, T. J., Kellogg, J. C., Ifju, P. J., and Shkarayev, S. V., *Introduction to the Design of Fixed-Wing Micro Air Vehicles*, AIAA, Reston, VA, 2007.

[80]Haile, S. M., "Fuel Cell Materials and Components," *Acta Materialia*, Vol. 51, 2003.

[81]Mathworks, "Fuel Cell Stack," URL: http://www.mathworks.com/access/helpdesk/help/toolbox/physmod/powersys/ref/fcpolarisation_curve.gif, [cited 2 June 2010].

[82]U.S. Department of Energy, "Metal Hydrides," URL: http://www1.eere.energy.gov/hydrogenandfuelcells/storage/metal_hydrides.html, [cited 2 June 2010].

[83]Felley, C., Dyson, P.J., Laurenczy, G., "A Viable Hydrogen-Storage System Based On Selective Formic Acid Decomposition with a Ruthenium Catalyst," *Angewandte Chemie International Edition*, 2008, pp. 3966-3968.

[84]Gomadam, P. M., Merritt, D. R., Scott, E. R., Schmidt, C. L., Skarstad, P. M., and Weidner, J. W., "Modeling Li/CFx-SVO Hybrid-Cathode Batteries," *Journal of The Electrochemical Society*, Vol. 154, 2007.

[85]Bradley, T., Moffitt, B. A., Parekh, D. E., Fuller, T. F., and Mavris, D. N., "Energy Management for Fuel cell-powered Hybrid-Electric Aircraft," AIAA 2009-4590, *International Energy Conversion Engineering Conference*, Denver, CO, 2009.

[86]Bradley, T. H., Moffitt, B. A., Mavris, D., and Parekh, D. E., "Development and Experimental Characterization of a Fuel Cell-Powered Aircraft," *Journal of Power Sources*, Vol. 171, 2007.

[87]Dufresne, S., Johnson, C., and Mavris, D. N., "Variable Fidelity Conceptual Design Environment for Revolutionary Unmanned Aircraft Systems," *Journal of Aircraft*, Vol. 45, No. 4, 2008.

[88]Bradley, T. H., Moffitt, B. A., Fuller, T. F., and Mavris, D., Parekh, D. E., "Design Studies for Hydrogen Fuel cell-powered Unmanned Aircraft Systems," AIAA 2008-6413, *AIAA Applied Aerodynamics Conference*, Honolulu, HI, 2008.

[89]Moffitt, B. A., Bradley, T. H., Parekh, D. E., and Mavris, D., "Design and Performance Validation of a Fuel Cell Unmanned Aircraft System," AIAA 2006-823, *AIAA Aerospace Sciences Meeting and Exhibit*, Reno, NV, 2006.

[90]Moffitt, B. A., Bradley, T. H., Mavris, D., and Parekh, D. E., "Reducing Uncertainty of a Fuel Cell UAS through Variable Fidelity Optimization," AIAA 2007-7793, *AIAA Aviation Technology, Integration and Operations Conference (ATIO)*, Belfast, 2007.

[91]Bradley, T.H., Moffitt, B.A., Mavris, D.N., Fuller, T.F., Parekh, D.E. "Hardware-in-the-Loop Testing of a Fuel Cell Aircraft Powerplant," *Journal of Propulsion and Power* 2009, Vol 25, No 6. 2009.

[92]Kroo, I., and Shevell, R., "Aircraft Design: Synthesis and Analysis," URL: http://adg. stanford.edu/aa241/AircraftDesign.html, [cited 2 June 2010].

[93]Ostler, J. N., Bowman, W. J., Snyder, D. O., and McLain, T. W., "Performance Flight-testing of Small, Electric Powered Unmanned Aerial Vehicles," *International Journal of Micro Air Vehicles*, Vol. 1, No. 3, 2009.

[94]Drela, M., and Youngren, H., "*XFOIL*," Software Package, URL: http://web.mit.edu/ drela/Public/web/xfoil/, [cited 19 Jan 2011].

[95]Drela, M., "QPROP Users Guide," URL: http://web.mit.edu/drela/Public/web/ QPROP/QPROP_doc.txt , [cited 19 Jan 2011].

[96]Drela, M., "Propeller Characterization for QPROP," URL: http://web.mit.edu/drela/ Public/web/qprop/prop_measure.pdf, [cited 10 Feb 2011].

[97]Rotramel, Todd. "Optimization of Hybrid-Electric Propulsion Systems for Small Remotely-Piloted Aircraft" MS Thesis, Aeronautics and Astronautics Dept., Air Force Institute of Technology, Dayton, OH, 2011.

[98]Larminie, J., and Dicks, A., *Fuel Cell Systems Explained*, 2nd Edition, Wiley, New York, 2003.

[99]Stewart, K. C., Blackburn, K., Wagener, J., Czabaranek, J., and Abate, G., "Development and Initial Flight-tests of a Single-Jointed Articulated-Wing Micro Air Vehicle," AIAA 2008-6708, *AIAA Atmospheric Flight Mechanics Conference and Exhibit*, Reston VA, 2008.

[100]Hobby Lobby, "8x4.5 CAM Folding Prop," URL: http://www.hobbylobby.com/8x4.5 _cam_folding_ prop_3.2mm _38mm _spinner_414_prd1.htm, [cited 19 Jan 2011].

[101]ICARE, "AXI 2808/20 Gold Line," URL: http://www.icare-rc.com/catalog/280820-gold-line-p-568.html, [cited 19 Jan 2011].

[102]Raymer, D.P., *Aircraft Design: A Conceptual Approach*, AIAA Education Series, Reston, VA, 2006.

[103]Short, S. R., "Modeling and Analysis of Active Turbulators on Low Reynolds Number Unmanned Aerial Vehicles," Masters Thesis, North Carolina State University, Department of Aerospace Engineering, Urbana IL, 2008.

[104]John B. Brandtnd, J. B and Selig, M.S., "Propeller Performance Data at Low Reynolds Numbers," AIAA 2011-1255, *49th AIAA Aerospace Sciences Meeting*, Orlando, FL, 2011.

[105]Ananda, G., "UIUC Propeller Database," URL: http://www.ae.illinois.edu/m-selig/props /data/apce_9x4.5_jb1000_6917.txt , [cited 15 Feb 2011]

[106]Fuel Cell Store, "Fuel Cell Stacks 20 W < 100 W," URL: http://fuelcellstore.com/en/pc/ viewCategories.asp?idCategory=46, [cited 2 Feb 2011].

[107]Uniterm, "Fuel Cell," URL: http://www.uniterm.pl/ogniwa_paliwowe/fuelcell.html, [cited 2 Feb 2011].

[108]Murphy, O. J., Cisar, A., and Clarke, E., "Low-Cost Light Weight High Power Density PEM Fuel Cell Stack," *Electrochimica Acta*, Vol. 43, No. 24, 1998.

[109]Buchmann, I., "The Future Battery," URL: http://batteryuniversity.com/parttwo-54.htm, [cited 2 Feb 2011].

[110]Fung, M.,"Energy Desnity of Hydrogen," URL: http://hypertextbook.com/facts/2005/ MichelleFung.shtml, [cited 9 Feb 2011].

REPORT DOCUMENTATION PAGE

Form Approved
OMB No. 074-0188

PLEASE DO NOT RETURN YOUR FORM TO THE ABOVE ADDRESS.

1. REPORT DATE *(DD-MM-YYYY)*	**2. REPORT TYPE**	**3. DATES COVERED** *(From – To)*
24 Mar 2011	Master's Thesis	Aug 2009 – Mar 2011

4. TITLE AND SUBTITLE
5.
Conceptual Design Tool To Analyze Electrochemically-Powered Micro Air Vehicles

5a. CONTRACT NUMBER
5b. GRANT NUMBER
5c. PROGRAM ELEMENT NUMBER

6. AUTHOR(S)
Douglas J. Pederson, 2d Lt, USAF

5d. PROJECT NUMBER
5e. TASK NUMBER
5f. WORK UNIT NUMBER

7. PERFORMING ORGANIZATION NAMES(S) AND ADDRESS(S)
Air Force Institute of Technology
Graduate School of Engineering and Management (AFIT/EN)
2950 Hobson Way
WPAFB OH 45433-7765

8. PERFORMING ORGANIZATION REPORT NUMBER
AFIT/GAE/ENY/11-M25

9. SPONSORING/MONITORING AGENCY NAME(S) AND ADDRESS(ES)
Dr. Thomas Reitz
Air Force Research Laboratory, Propulsion Directorate
1950 Fifth Street, Bldg. 18G, Rm G33
Wright Patterson AFB, OH 45433-7251
DSN 785-4275, Thomas.Reitz@wpafb.af.mil

10. SPONSOR/MONITOR'S ACRONYM(S)
AFRL/RZPS

11. SPONSOR/MONITOR'S REPORT NUMBER(S)

12. DISTRIBUTION/AVAILABILITY STATEMENT
Approved for public release, distribution unlimited

13. SUPPLEMENTARY NOTES
This material is declared a work of the U.S. Government and is not subject to copyright protection on the United States

14. ABSTRACT

A multi-fidelity conceptual design tool was developed to assess electrochemically-powered micro air vehicles (MAVs). The tool utilizes four areas of contributing analyses (CAs): aerodynamics, propulsion, power management, and power sources to determine the endurance duration of a given mission. The low-fidelity aerodynamic CA consisted of drag polar calculations and the high-level CA used a vortex theory code called Athena Vortex Lattice (AVL). The propulsion CA employed QPROP and a MATLAB code that used experimental propeller data and motor constants to predict propeller-motor combination performance for the low- and high-fidelity tracks, respectively. The power management CA determined the percentage of required power the power sources needed to provide by a user-defined split or an optimization to maximize endurance duration for the two fidelity options. The power source CA used specific energy and specific power calculations for the low-fidelity track and polarization curves and Ragone plots for the high-fidelity track. Model Center software allowed for integration of each of these CAs into one model. Based on the current state of the art battery and fuel cell technology, the model predicted endurance durations ranging from 88.5 to 107.3 min. The mission simulations that led to these durations used a generic MAV (GenMAV) configuration and the complete spectrum of fidelity combinations.

15. SUBJECT TERMS
Micro Air Vehicles, Electrochemical Energy, Conceptual Design, Remotely-Piloted Aircraft, Fuel Cell, Battery

16. SECURITY CLASSIFICATION OF:			**17. LIMITATION OF ABSTRACT**	**18. NUMBER OF PAGES**	**19a. NAME OF RESPONSIBLE PERSON**
a. REPORT	**b. ABSTRACT**	**c. THIS PAGE**			Frederick G. Harmon, Lt Col, USAF
U	U	U	UU	193	**19b. TELEPHONE NUMBER** (937) 255-3636, ext 7478 frederick.harmon@afit.edu

Standard Form 298 (Rev. 8-98)
Prescribed by ANSI Std. Z39-18

Form Approved
OMB No. 074-0188